CZECH TECHNICAL UNIVERSITY IN PRAGUE

Faculty of Electrical Engineering

Department of Microelectronics

Gas sensors based on diamond and 2D layers

Dissertation thesis

Ing. Michal Kočí

Study programme:	**Electrical Engineering and Communications P0714D060004**
Study specialization:	**Electronics and Measuring Technique**
Supervisor:	**prof. Ing. Miroslav Husák, CSc.**
Supervisor specialist:	**prof. Ing. Alexander Kromka, DrSc.**

Prague 2024

Declaration

I hereby declare I have written this doctoral thesis independently and quoted all the sources of information used in accordance with methodological instructions on ethical principles for writing an academic thesis. All sources and other materials used have been quoted in the list of references. All the co-authors on the referred publications have been acknowledged. Moreover, I state that this thesis has neither been submitted nor accepted for any other degree.

In Prague on 9 September 2024

Michal Kočí

Digitálně podepsal Michal Kočí
Datum: 2024.09.09 13:46:03 +02'00'

Ing. Michal Kočí

Acknowledgment

In this section, I would like to thank my supervisor prof. Ing. Miroslav Husák, CSc. from the Department of Microelectronics, Czech Technical University in Prague and supervisor specialist prof. Ing. Alexander Kromka, DrSc. from the Institute of Physics of the Czech Academy of Sciences, for giving me the best possible support I could have asked for during my studies and for the opportunity for personal growth and expansion of my knowledge in scientific activities. I greatly appreciate their encouraging attitude, friendly manner, and positive and helpful approach.

Furthermore, I would like to express my gratitude to the Department of Microelectronics for its kindness and the many opportunities to gain valuable knowledge. In addition to my supervisor and other members of the department, I would like to thank by name: Ing. Václav Procházka, Ph.D.; Ing. Adam Bouřa, Ph.D.; Ing. Alexandr Pošta and Ing. Alexandr Laposa, Ph.D.

My thanks also belong to all my colleagues at the Institute of Physics of the Academy of Sciences of the Czech Republic, who participated in various parts of my research and provided me with technical assistance and valuable suggestions. I want to mention namely: Ing. Ondrej Szabó, Ph.D.; Ing. Rajisa Jackivová; Ing. Kateřina Aubrechtová Dragounová, Ph.D.; Ing. Štěpán Potocký, Ph.D.; Mgr. Jitka Libertínová and Mgr. Oleg Babčenko, Ph.D.

Finally, I would like to thank my family and friends, especially Ing. Lukáš Hliněný, who have always supported me and provided me with a great deal of understanding and patience.

Abstract

This dissertation thesis deals with nanocrystalline diamond (NCD) thin films and 2D layers based on transition metal dichalcogenide (TMD) and carbon for gas sensing applications. The research focuses on studying these materials and their combination as the active (sensing) layer in gas conductivity sensors with interdigital structure (IDT). The emphasis of the study is on improving the response to gases at room temperature. The measured characteristics and parameters are compared with laboratory and commercially available sensors. The presented studies range from basic materials to complex heterostructures combining two different materials to improve the gas response are presented in this work. Each sensing-structure is characterized, and a gas interaction model is provided to describe the differences in sensing principles for these conductivity sensors. This work is a commented collection of the author's publications with a linked text.

The first part of the study focuses on the characterization of hydrogen-terminated NCD (H-NCD) without modification and its comparison with commercial sensors, specifically the TGS 826 and the PY2055 at temperatures ranging from 40 °C to 125 °C. The part includes preparing the structure and H-NCD, describing the measuring apparatus and chambers, and a model of the material - gas molecule interactions. In addition, it contains a critical discussion between the gas sensing mechanisms for H NCD and TGS 826

The second part focuses on improving the H-NCD layer by comparing the responses of NCDs with their different grain sizes, different terminations (hydrogen and oxygen-terminated), and surface coverage with gold nanoparticles (Au NPs). The Au NPs improved the responses to both gases by reducing the nominal resistance, thereby increasing the relative response of the sensor, particularly at 125 °C. The gas-sensing enhancement is explained by reducing the barrier's resistance between the NCD grains via Au NPs electrically conductive islands.

The third part introduces a novel heterostructure consisting of H-NCD and the TMD material molybdenum disulfide (MoS_2). This material's combination significantly improves the gas response at room temperature, attributed to the formed p-n junction sensitive to gas molecules. This heterostructure operated at room temperature also reduces power consumption due to the absence of a heating element.

The last fourth part of the study describes a carbon-based heterostructure combining H-NCD and modified graphene oxide (GO), specifically reduced (rGO) and thiol-functionalized (SH-GO). The SH-GO / H-NCD heterostructure significantly improves the response to ethanol vapor at room temperature, achieving a 634 % response at 100 ppm concentration. Even though both materials exhibit p-type conductivity, the between them seems to be a key factor resulting in high sensitivity to gas presence.

Keywords

Gas sensors, nanocrystalline diamond, molybdenum disulfide, graphene oxide, heterostructure sensors

Abstrakt

Disertační práce se zabývá tenkými vrstvami nanokrystalického diamantu (NCD) a 2D vrstvami na bázi dichalkogenidu přechodných kovů (TMD) a uhlíku pro aplikace v oblasti detekce plynů. Práce se zaměřuje na výzkum těchto materiálů a jejich kombinace pro použití jako aktivní neboli snímací vrstvy ve vodivostních senzorech plynů s interdigitální strukturou (IDT). Důraz je kladen na zlepšení citlivosti při pokojové teplotě. Naměřené charakteristiky a parametry jsou porovnávány s jinými dostupnými senzory, komerčními i laboratorně připravenými. Materiálový výzkum zahrnuje základní materiály i složité heterostruktury kombinující dva různé materiály, které mají zlepšit citlivost na plyny. Každá struktura je charakterizována. Model interakce s plynem popisuje rozdíly v principech snímání těchto senzorů plynů. Práce je sepsána jako komentovaný soubor autorových publikací s doplňujícím textem.

První část práce je zaměřena na charakterizaci vodíkem zakončeným NCD (H-NCD) bez modifikace a jeho porovnání s komerčními senzory TGS 826 a PY2055. Práce obsahuje přípravu struktury, popis měřicí aparatury, popis komor a model interakce materiál – molekula plynu. Dále obsahuje kritickou diskusi mezi mechanismy snímání plynů pro H-NCD a TGS 826.

Druhá část se zaměřuje na zlepšení citlivosti H-NCD vrstvy porovnáním reakcí NCD s různou velikostí zrn, různým zakončením (H-NCD a O-NCD) a pokrytím povrchu nanočásticemi zlata (Au NPs). Au NPs zlepšily citlivost na oba plyny snížením jmenovitého odporu, čímž se zvýšila relativní odezva senzoru. Zlepšení detekce plynů se vysvětluje snížením odporu bariéry mezi zrny NCD prostřednictvím elektricky vodivých ostrůvků Au NPs.

Třetí část představuje novou heterostrukturu kombinující H-NCD a TMD materiál disulfid molybdenu (MoS_2). Kombinace těchto dvou materiálů výrazně zlepšuje citlivost na plyn při pokojové teplotě, zejména vytvořeným p-n přechodem citlivým na molekuly plynu. Tato heterostruktura také snižuje spotřebu energie kvůli absenci topného prvku.

Poslední čtvrtá část práce popisuje heterostrukturu na bázi uhlíku kombinující H-NCD a modifikovaný oxid grafenu (GO), konkrétně redukovaný (rGO) nebo funkcionalizovaný thiolovou skupinou (SH-GO). Heterostruktura SH-GO / H-NCD výrazně zlepšuje citlivost na výpary ethanolu při pokojové teplotě a dosahuje až 634 % pro koncentraci 100 ppm. Oba materiály vykazují vodivost typu p a klíčovým faktorem, který vede k vysoké citlivosti na přítomnost plynu, je přechodová mezivrstva mezi oběma materiály.

Klíčová slova

Senzory plynů, nanokrystalický diamant, sulfid molybdeničitý, grafén oxid, senzory na bázi heterostruktury

Contents

Acknowledgment i
Abstract ii
Abstrakt iii
Contents iv
List of physical quantities vii
List of acronyms viii
List of figures x
List of tables xi
List of graphs xii
1. Introduction 1
1.1 Gas sensors 1
1.1.1 Conductivity sensors 2
1.1.2 Optical infrared gas sensors 3
1.1.3 Mass sensitive gas sensors 4
1.2 Objectives of thesis 5
2. State of The Art 6
2.1 Conductivity gas sensors 6
2.1.1 3D nanocrystalline sensing layer 7
2.1.2 2D sensing monolayer 8
2.1.3 1D nanowire 10
2.2 New approach and materials for conductivity gas sensors 11
2.2.1 Carbon-based materials 11
2.2.2 TMD materials 13
2.2.3 Heterostructures and composites 14
2.3 Comparison of gas sensors 16
3. Experimental part 18
3.1 Experimental apparatus for gas sensor measurement 18
3.2 Measurement and results 21
3.2.1 Measurement at 125 °C 22
3.2.2 Measurement at 22°C (room temperature) 24
3.3 Gas interaction models 26
3.3.1 SnO_2 26
3.3.2 H-NCD 27
3.3.3 MoS_2 28
3.3.4 GOs 28
3.3.5 H-NCD with Au NPs 29
3.3.6 MoS_2 / H-NCD heterostructure 30

3.3.7 SH-GO / H-NCD heterostructures 32
4. Author's publication 34
4.1 Hydrogen-Terminated Diamond Surface as a Gas Sensor: A Comparative Study of its Sensitivities 34
4.1.1 Abstract 34
4.1.2 Summary 34
4.1.3 Author's contribution 35
4.1.4 Paper's contributions 35
4.2 Enhanced gas sensing capabilities of diamond layers using Au nanoparticles 36
4.2.1 Abstract 36
4.2.2 Summary 36
4.2.3 Author's contribution 37
4.2.4 Paper's contributions 37
4.3 Improved Gas Sensing Capabilities of MoS2/Diamond Heterostructures at Room Temperature 38
4.3.1 Abstract 38
4.3.2 Summary 38
4.3.3 Author's contribution 39
4.3.4 Paper's contributions 39
4.4 Gas sensors based on diamond heterostructures for air quality monitoring 40
4.4.1 Abstract 40
4.4.2 Summary 40
4.4.3 Author's contribution 41
4.4.4 Paper's contributions 41
4.5 Highly sensitive gas and ethanol vapor sensors based on carbon heterostructures for room temperature detection 42
4.5.1 Abstract 42
4.5.2 Summary 42
4.5.3 Author's contribution 43
4.5.4 Paper's contributions 43
5. Conclusion 44
5.1 My scientific contribution 46
5.2 Prospects and future work 47
6. References 48
7. List of publications and internships 58
7.1 Publications with DOI 58
7.1.1 Lead author 58
7.2 Conferences 59
7.2.1 Lead author 59
7.2.2 Co-author 60
7.3 Internships 61
7.3.1 Long-term internships 61

7.3.2 Short-term internships.....61

Appendix..... I

I. Hydrogen-Terminated Diamond Surface as a Gas Sensor: A Comparative Study of its Sensitivities..... II

II. Enhanced gas sensing capabilities of diamond layers using Au nanoparticles XVIII

III. Improved Gas Sensing Capabilities of MoS_2/Diamond Heterostructures at Room Temperature..... XXVIII

IV. Gas sensors based on diamond heterostructures for air quality monitoring XXXVIII

List of physical quantities

Symbol	**Unit**	**Physical quantities**
φ	°	Angle
S	m^2	Area
C	F	Capacitance
C_X	ppm	Concentration
V_0	V	Electric potential
E	eV	Energy
f	Hz	Frequency
Z	Ω	Impedance
l	m	Length
m	g	Mass
P_T		Probability
R	Ω	Resistance
ρ	Ω · m	Resistivity
T	°C	Temperature
t	s	Time
V	m^3	Volume
Ψ		Wave function
W	m	Width

List of acronyms

Acronym	Meaning
1D	One dimensional
2D	Two dimensional
2DEG	2D electron gas
2DHG	2D hole gas
3D	Three dimensional
Au NPs	Gold nanoparticles
CNT	Carbon nanotube
CVD	Chemical vapor deposition
DC	Direct current
GO	Graphene oxide
H-NCD	Hydrogen-terminated nanocrystalline diamond
HPHT	High pressure/high temperature
i.e.	Id est (that is)
IDT	Interdigital structure
IoT	Internet of Thinks
IR	Infrared
M	Metal
MEMS	Micro-electro-mechanical structure
MFC	Mass flow controller
MISFET	Metal-insulator-semiconductor field-effect transistor
MoS_2	Molybdenum disulfide
N_A	Concentration of free charge carriers (acceptor)
NCD	Nanocrystalline diamond
N_D	Concentration of free charge carriers (donor)
n-type	Negative type
O-NCD	Oxygen-terminated nanocrystalline diamond
PANI	Polyaniline
PC	Personal computer
PECVD	Plasma-enhanced chemical vapor deposition
p-n type	Positive - negative type
ppm	Parts per million
PRGO	Poly-reduced graphene oxide
p-type	Positive type
QCM	Quartz crystal microbalance
rGO	Reduced graphene oxide
RT	Room temperature
SCR	Space charge region
SEM	Scanning electron microscope
SH-GO	Thiol functionalized graphene oxide
SMU	Source measure unit

Acronym	**Meaning**
SWCNT	Single walled carbon nanotube
TMD	Transition metal dichalcogenide
UV	Ultraviolet
VOCs	Volatile organic compounds
WBG	Wide-bandgap
ZIF-8	Zeolitic imidazolate framework

List of figures

Figure 1-1 Principle schemes of conductivity sensors **a)** tubular, **b)** with IDT structure [1] 3
Figure 1-2 Principle scheme of infrared gas sensors [25] 3
Figure 1-3 Principle scheme of QCM sensor [1] 4
Figure 2-1 Energy band of n-type semiconductor during oxidation and reduction process [1]....6
Figure 2-2 SEM image of TGS sensor with SnO_2 active layer [1] 7
Figure 2-3 Tunnelling effect through a potential rectangular wall [2].....8
Figure 2-4 Electrical model representation of a nanocrystalline layer [4] 8
Figure 2-5 The schematic drawing of the crystal structure of graphene (gray–carbon) [40] 9
Figure 2-6 The schematic drawing of the crystal structure of MoS_2 (TMD) (blue–molybdenum, yellow–sulfur) [35].....9
Figure 2-7 Electrical model representation of TMD monolayer [4] 10
Figure 2-8 The schematic drawing of the crystal structure of (a) CNT (gray–carbon) [40] and (b) MoS_2 / SnO_2 nanotubes (light grey– SnO_2, black – MoS_2) [29].....10
Figure 2-9 Electrical model representation of nanotube [4].....11
Figure 2-10 Graphene / MoS_2 heterostructure: (a) schematic drawing and (b) SEM images [75] 15
Figure 2-11 Junction of two materials with slightly inconsistent lattice constants [2] 15
Figure 3-1 3D design of an experimental apparatus for gas sensor measurement.....18
Figure 3-2 Photograph of an experimental apparatus for gas sensor measurement.....19
Figure 3-3 3D design of testing chamber for IDT 6×10 mm sensors.....19
Figure 3-4 Photograph of a testing chamber for IDT 6×10 mm sensors.....20
Figure 3-5 Photograph of a testing chamber for larger sensors 21
Figure 3-6 Schematic time process of gas interaction between the SnO_2 material and oxidizing and reducing gases.....27
Figure 3-7 Schematic time process of gas interaction between the H-terminated NCD and oxidizing and reducing gases 27
Figure 3-8 Schematic illustration of the gas sensing mechanism between a layer of MoS_2 nanoflakes and (left) oxidizing and (right) reducing gases.....28
Figure 3-9 Schematic illustration of the gas sensing mechanism between a GO and NO_2 29
Figure 3-10 a) gas interaction model and b) substitute circuit diagram of the H-NCD layer with Au NPs.....30
Figure 3-11 Schematic illustration of the gas sensing mechanism and charge transport for two parallel connected layers represented by MoS_2 nanoflakes and H-NCD exposed to the (left) oxidizing and (right) reducing gas 31
Figure 3-12 Schematic illustration of two ways (I. and II.) for the current flow between IDT electrodes, I. - horizontal flow through H-NCD, and II. – combined horizontal / vertical flow, horizontal through H-NCD and MoS_2 and vertical through MoS_2 / H-NCD heterostructure.....32
Figure 3-13 Gas interactions between the oxidizing gas (NO_2) and SH-GO / H-NCD heterostructure.....33

List of tables

Table 2-1 Comparison of responses of various sensors for gas sensing at room temperature....17

Table 3-1 Responses of sensors at 125 °C / 0.1 V exposed to 100 ppm ethanol vapor, 100 ppm NH_3 and 100 ppm NO_2. The table highlights the best and the second-best values in dark green and light green. 22

Table 3-2 Responses of sensors at 22 °C / 0.1 V exposed to 100 ppm ethanol vapor, 100 ppm NH_3 and 100 ppm NO_2. The table highlights the best and the second-best values in dark green and light green. 24

List of graphs

Graph 3-1 Responses of measured sensors to 100 ppm ethanol C_2H_5OH at 125 °C 23

Graph 3-2 Responses of measured sensors to 100 ppm ammonia NH_3 at 125 °C 23

Graph 3-3 Responses of measured sensors to 100 ppm nitrogen dioxide NO_2 at 125 °C.....24

Graph 3-4 Responses of measured sensors to 100 ppm ethanol C_2H_5OH at 22 °C (room temperature) 25

Graph 3-5 Responses of measured sensors to 100 ppm ammonia NH_3 at 22 °C (room temperature) 25

Graph 3-6 Responses of measured sensors to 100 ppm nitrogen dioxide NO_2 at 22 °C (room temperature) 26

1. Introduction

Air cleanliness/quality is crucial for maintaining a high quality of life on Earth. However, it is essential to note that solutions are available to mitigate these negative impacts. Gas sensors have become an essential component of both industrial and everyday life due to the increasing number of harmful substances released into the air, primarily by heavy industry [1–11]. In the 21st century, industry has become one of the leading sources of air pollution, emitting harsh inorganic compounds, such as ammonia (NH_3), carbon oxides (CO_X), sulfur oxides (SO_X), and nitrogen oxides (NO_X) into the atmosphere. Furthermore, sectors such as polymers, paints, aerosols, and oil processing, which heavily rely on organic solvents, also contribute to pollution through volatile organic compounds (VOCs). Ethanol (C_2H_5OH), one of the most frequently used solvents in the mentioned industries [12, 13], is a significant component of VOCs. Additionally, according to the 2018 ERSO report for the European Commission [14], ethanol is a psychoactive substance associated with 25 % of fatal traffic accidents.

The demand for air quality monitoring and pollutant detection has significantly increased over the last 20 years. Advanced gas sensing technology enables effective monitoring and detection of pollutants, facilitating informed decision-making and necessary actions to mitigate potential harm. Acknowledging the risks associated with these substances and implementing appropriate measures to ensure the safety and well-being of individuals and the environment is crucial.

While conductivity-based metal oxide (MO_X) sensors, particularly SnO_2, are currently the most commonly used due to their low cost and flexible production, they have limitations. These sensors require a high operating temperature and cannot be reduced in size too much, making them unsuitable for use as sensor nodes in IoT applications with Energy-Harvesting supply. Consequently, there is a high demand for developing new high-accuracy sensors capable of detecting various gases with excellent reproducibility, sensitivity, and stability. New sensing materials, surface treatments, or manufacturing processes must be developed to achieve high-quality, smaller, more accurate, and cost-effective sensors. The main goal is to increase the sensor's performance while reducing production costs.

In accordance with this objective, great attention is focused on novel materials suitable for conductivity gas sensors. Gas sensors with wide-bandgap (WBG) semiconductors, such as diamond thin layers or 2D materials, show great potential for miniaturization and modification through material science or technological progress. These highly advanced materials have been extensively researched, making them a reliable choice for gas-sensing applications. It is important to note that using these materials is still in the experimental stage, but the initial results so far have been very promising.

1.1 Gas sensors

Gas sensors are designed to detect and measure the concentration of gases or gas mixtures. Their operation is based on a physical/chemical reaction of a substance, which is then

converted into an electrical signal. The output signal is typically analog, such as a change in resistance or frequency. Gas sensors are characterized by their high sensitivity, selectivity, excellent time stability, and wide measurement range [1]. It is important to mention that different gases may require different types of sensors, and consideration should be given to the specific application and environmental conditions.

The *sensitivity* indicates the conversion ratio between the change in concentration and the output signal, often defined as a change in the output signal divided by a change in concentration.

The *selectivity* is an essential parameter of gas sensors and indicates a gas's sensitivity in the mixture. Selectivity means the ability of a sensor to detect a specific gas from multiple analytes. It can be calculated using multiple times the sensor gives us higher values than a non-selective gas of the same concentration.

The *time stability* of the sensor refers to the percentage change in output at a constant gas concentration. Ideally, the change in output over time is zero.

The *measurement range* is the range of gas concentration that the sensor detects. The range is defined as the linear part of the sensor sensitivity curve, with a specific concentration that can be precisely determined [3].

The following subchapters describe the three most common physical principles employed in gas sensing.

1.1.1 Conductivity sensors

Conductivity sensors, also known as chemoresistive or solid-state semiconductor gas sensors, use a change in the active layer's conductivity due to a reaction with gases. These sensors are the most commonly used. They mostly consist of a substrate or base plate, conductive electrodes for connecting measuring wires, a heating element ensuring the correct temperature, and active layers reacting to gases. The active layer is often a chemically stable semiconductor with suitable parameters, especially with sufficient gas reaction intensity. A suitable and very often used material is SnO_2. Cheap silicon is unsuitable due to its tendency to form a non-conductive oxide layer. For proper function, it is necessary to ensure direct contact between gases and the active layer. Gas conductivity sensors use chemisorption, i.e., the binding (sorption) of gas molecules on a solid's surface by chemical bonding with electron transfer. The transfer of electrons between substances is called the oxidation-reduction process. The active layer chemisorbs a gas on its surface, mainly oxygen, and thus draws or receives electrons from the semiconductor's conduction band [1, 15–20]. Two main types of conductivity sensors exist: a) tubular type and b) thin films.

An older type of conductivity sensor is the tubular type with marking TGS from Figaro Engineering. This type was developed in Japan in the second half of the last century. The sensor consists of active material in a tube with conductive electrodes for measurement and a heating fiber ensuring the correct temperature (**Figure 1-1a**). The advantage of this arrangement is the action of gas from all sides of the active material and the heating of only the active material. The disadvantage is the larger dimensions [1, 21, 22].

A modern conductivity sensor is based on applying thin layers on a substrate (**Figure 1-1b**). This type uses thin conductive electrodes applied to the substrate, often in an interdigital structure. An active layer is applied to the electrodes. A heating layer on the other side of the substrate forms the heating element. The advantages of this type are smaller dimensions and higher accuracy due to the interdigital structure. The disadvantage is the need to heat the entire sensor, including the substrate, and the possibility of detecting gas from only one side of the sensor [1, 15, 23, 24].

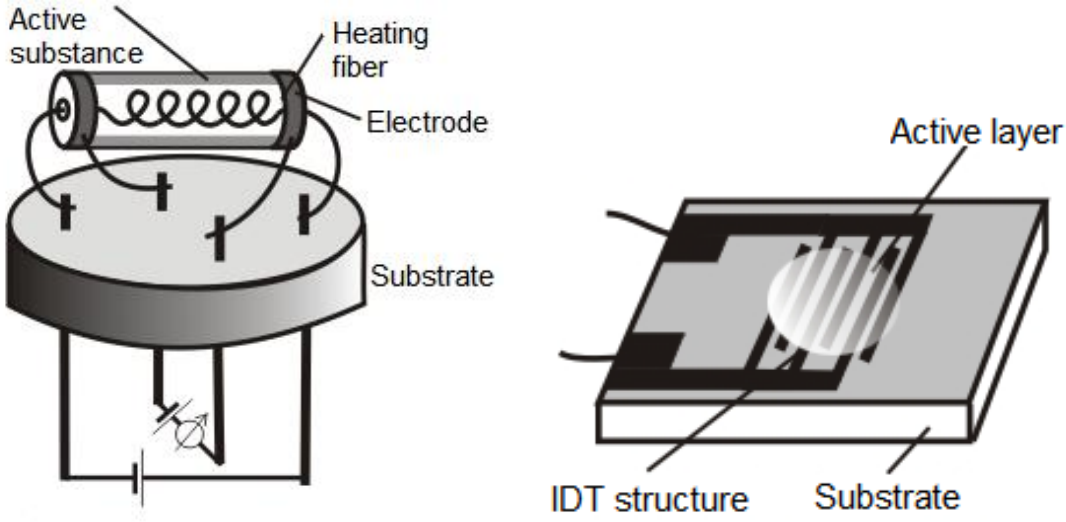

Figure 1-1 Principle schemes of conductivity sensors **a)** tubular, **b)** with IDT structure [1]

1.1.2 Optical infrared gas sensors

Infrared (IR) gas sensors use absorption spectrophotometry in the infrared region of the spectrum. This detection method can determine the composition of a gas mixture or detect a specific type of gas. These gases are often formed by a more complex or asymmetric molecule, which changes the molecule's energy state. IR sensors are unsuitable for detecting gases with a monoatomic or symmetric diatomic molecule that does not absorb radiation in the infrared. The essential components of the IR gas sensor are schematically shown in **Figure 1-2**.

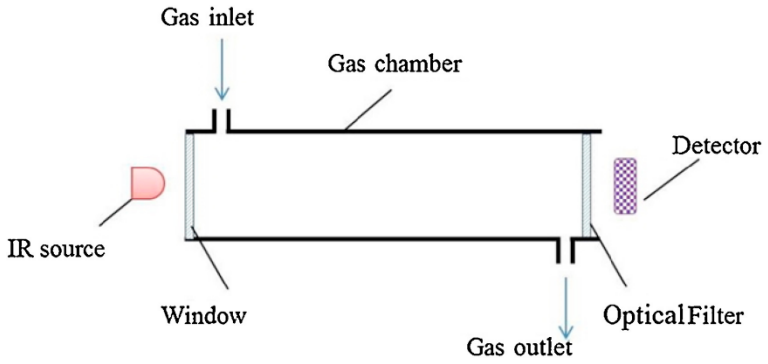

Figure 1-2 Principle scheme of infrared gas sensors [25]

The sensor consists of a test gas chamber through which the test gas or mixture passes. The infrared light source generates infrared radiation. IR passes through the window into the chamber. Some sensors require intermittent radiation, which can be created by periodically

turning the source on and off or inserting an aperture that reflects or absorbs the beam. A metal heating coil with a temperature of around 700 °C (based on Planck's distribution law), a heated MEMS silicon wafer, or a standard light bulb with a suitable filter can be used as an IR source. A filter is placed in front of the radiation detector, which filters out unwanted wavelengths and transmits only the wavelength radiation that absorbs the selected gas. The radiation detector measures the radiation intensity that the gas does not absorb. The most common type is a pyroelectric crystal. This element heats up due to the incident radiation and creates a charge on the crystal's sides. This arrangement corresponds to the Non-Dispersive Infrared sensor, i.e., an arrangement without beam dispersion, where the rays of the spectrum do not decompose, but part of the spectrum is absorbed. This principle's advantage is the possibility of measuring the active material without contact with the gas, accuracy, high selectivity using suitable filters, and a wide range of concentrations from 1 ppm to almost 100 % gas concentration [1, 25, 26].

1.1.3 Mass sensitive gas sensors

Mass sensitive gas sensors use weight gain due to gas interaction, which results in changes in other physical quantities. Quartz Crystal Microbalances (QCM) in **Figure 1-3** is the most used type, using the resonant measurement principle. An active layer, sensitive to a given gas, is applied to the piezo crystal surface. Due to surface reactions, molecules stay on the active layer and change mass, reflected in a resonant frequency change. The sensor usually consists of a quartz substrate with gold electrodes and an active layer. The resonant frequency is between 1 and 10 MHz [1]. Another type of mass sensor is the Surface Acoustic Wave sensor, which uses a surface acoustic wave. The principle is to create a Rayleigh acoustic wave on the substrate propagating through the sensitive part. The sensitive part absorbs gas molecules, which changes the acoustic wave's frequency, amplitude, and phase. The sensors include an acoustic wave transmitter, a wave propagation path, and a receiver. The operating frequency range is from 1 MHz to 1 GHz [1].

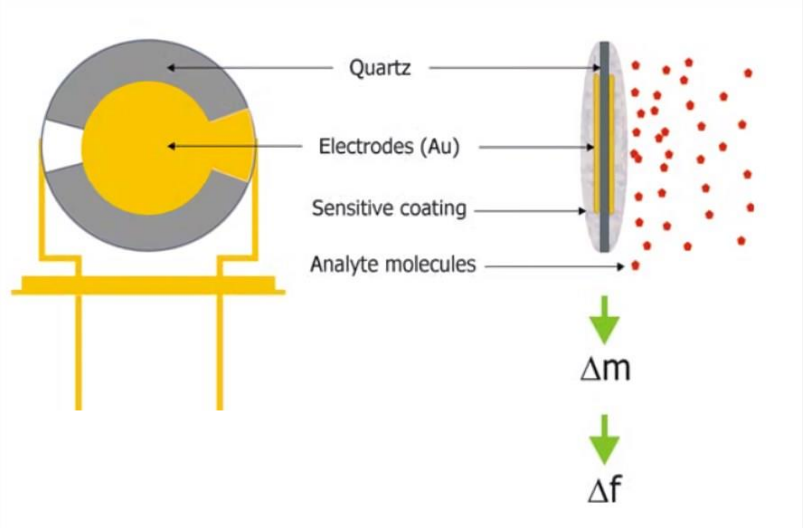

Figure 1-3 Principle scheme of QCM sensor [1]

1.2 Objectives of thesis

The primary objective of this work is to generate novel scientific knowledge in the interaction between sensitive materials (e.g., diamonds and 2D layers) with various gas molecules and VOCs. The author will become familiar with the basic principles and materials used in gas sensor applications to achieve this objective.

Conductivity sensors were selected as the primary focus, utilizing the active layer's conductivity change upon contact with gas molecules. NCD was chosen as the sensitive sensor layer for the primary material of the research. While previous studies have examined individual NCD with various terminations, this work aims to enhance its response by combining it with other materials into a hybrid structure or heterostructure. The study also examines changes in sensor characteristics at different temperatures and in response to different gases.

By addressing these objectives, this research aims to contribute to the advancement of gas-sensing technology through the development of novel materials and structures with enhanced performance characteristics.

This work is a commented collection of the author's publications with a linked text.

The main objectives of the thesis can be summarized as follows:

- Verify the functionality of H-NCD and 2D materials for gas sensing applications and measure their characteristics for comparison with new materials
- Research of suitable materials for combination with H-NCD to enhance the gas sensing response
- Research of materials preparation methods and their compatibility for the preparation of high-quality hybrid structures and heterostructures
- Verify the quality of active layers and refine the procedure and composition of materials to overcome any identified limitations
- Create a gas interaction model to understand new mechanisms in the hybrid-structure or heterostructure
- Verify gas sensitivity improvement for fabricated sensors with heterostructure containing diamond and 2D layer

2. State of The Art

Conductivity gas sensors are the most promising type of gas sensors. Developing new materials or material combinations for the sensing layer and the possibility of miniaturization and reduced power consumption makes them highly effective. For this reason, the following section focuses on conductivity gas sensors with solid-state materials, especially semiconductors.

2.1 Conductivity gas sensors

Sensor parameters are dependent on the properties of materials. The most used materials in an electronic device are Si and GaAs due to cost-effectiveness and easy ingot preparation. However, they are not suitable for gas-sensing applications. Conductivity gas sensors, also known as chemoresistive or solid-state semiconductor gas sensors, are typically based on 3D (MO_X or WBG semiconductors), 2D (TMD or graphene), or 1D (CNT or MO_X nanotubes) materials. Many factors influence the sensitivity and other parameters. Some factors are reflected in production, such as materials surface, additives, or natural properties of materials (substrate or active layer). The second category of factors is environmental influences, particularly temperature and humidity [2, 24].

The conductivity gas sensors use chemisorption, as illustrated in **Figure 2-1**, for n-type semiconductors [1, 3]. **Figure 2-1** shows the energy band for oxidizing and reducing gasses. In the case of an oxidation process with oxidation gas (NO_2), the energy barrier is increased for n-type, so the conductivity is reduced. Chemisorption of oxygen causes the transfer of electrons from the semiconductor to the gas, reduces the n-type semiconductor's conductivity, and respectively increases the p-type semiconductor's conductivity. In the case of a reduction process with reducing gas (NH_3), the energy barrier is decreasing for the n-type. It reacts with chemisorbed oxygen from the atmosphere to form new gaseous products. The reaction products are charge neutral. The excess electrons are transferred from the chemisorbed oxygen to the semiconductor, increasing the conductivity for the n-type or decreasing for the p-type. The gas detection is impossible in the case of redox-indifferent gases because no electron transfer occurs during the reaction. A heating element is used to facilitate the course of the chemical reactions and overcome the activation energy to overcome the energy barrier[1].

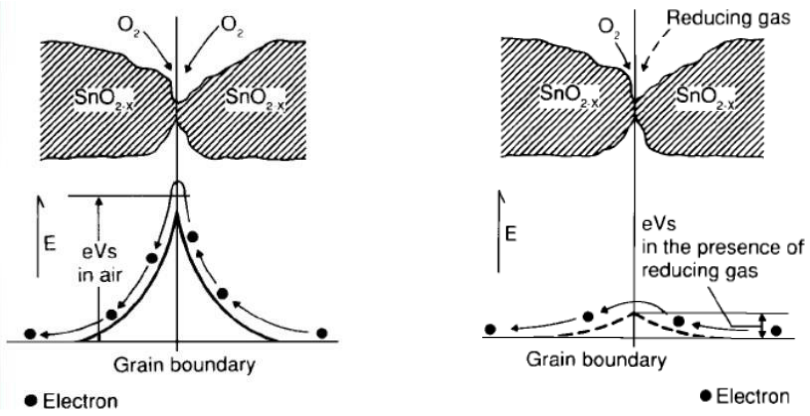

Figure 2-1 Energy band of n-type semiconductor during oxidation and reduction process [1]

The main limitation of current conductivity gas sensors is the necessary heating to a high temperature (300 °C for SnO_2 [21]). Heating consumes a large amount of energy, and the dimension cannot be reduced too much because sensor packaging is needed to protect other components [1]. The sensing properties and parameters depend on the type of thin layer.

2.1.1 3D nanocrystalline sensing layer

The first type is the 3D active material, typically prepared in crystalline form. The tiny grains (crystals) form the layer where the grain's size modifies the active layer's properties and responses [27–30]. The layer quality can be observed using a Scanning Electron Microscope (SEM). **Figure 2-2** demonstrates the SEM of a commercial TGS 826 sensor with a SnO_2 active layer. The electrical properties of this material can be confidently modified through various means, such as adjusting doping or layer thickness or controlling the average grain size [16, 31].

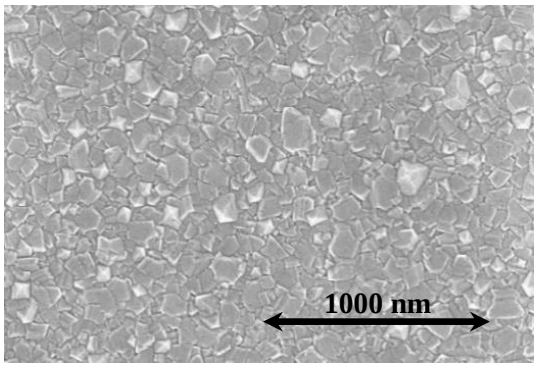

Figure 2-2 SEM image of TGS sensor with SnO_2 active layer [1]

Gas sensing is enabled by the main physical principle of tunneling through the potential wall between the grains, as illustrated in **Figure 2-3**. This quantum mechanical phenomenon demonstrates wave / particle duality, allowing charge carriers to pass through a potential wall. In classical mechanics, carriers are particles confined by the potential walls [2]. In quantum mechanics, the electron can also be described as a wave with a wavefunction. The wave function (equation 2-1) does not terminate abruptly on a wall with finite potential height. However, it declines exponentially, where the electron with wave function Ψ_A tunnel through the potential wall with width W and potential V_0. Tunneling losses reduce the resulting wave function Ψ_B. The probability of electron tunneling P_T through the final height and width barrier is none-zero [2, 28].

The nanocrystalline layer can be easily analyzed using a primary electrical circuit consisting of fundamental electrical components. **Figure 2-4** shows a series-parallel combination of a capacitor and a resistor used to analyze the layer. The figure displays three grains on a gold electrode. In this circuit, R_g represents the resistance of the grains due to the drift and diffusion of charged particles within the grains. R_{gs} is the resistance between the surfaces of the grains, while R_{ge} is the resistance between the grain and the electrode. The capacitance between grains due to the potential wall and the redistribution of water molecules on the surface is represented by C_{gs}. In contrast, C_{ge} represents the capacitance between the grain and electrode. The thin layer and gold electrode transition region are modeled by R_{ge} and C_{ge}, respectively. R_{gs} and C_{gs} are used to

model the transition region between the grains, which is crucial for gas sensing. In the presence of oxidation gas and n-type semiconductors, R_{gs} and C_{gs} increase, leading to a reduction in conductivity. Reducing gas increases conductivity as R_{gs} and C_{gs} decrease [4, 15, 32].

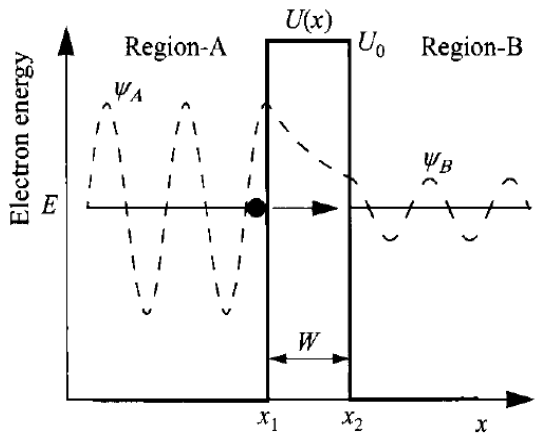

$$P_T = |\Psi_B|^2/|\Psi_A|^2 \qquad (2\text{-}1)$$

Figure 2-3 Tunnelling effect through a potential rectangular wall [2]

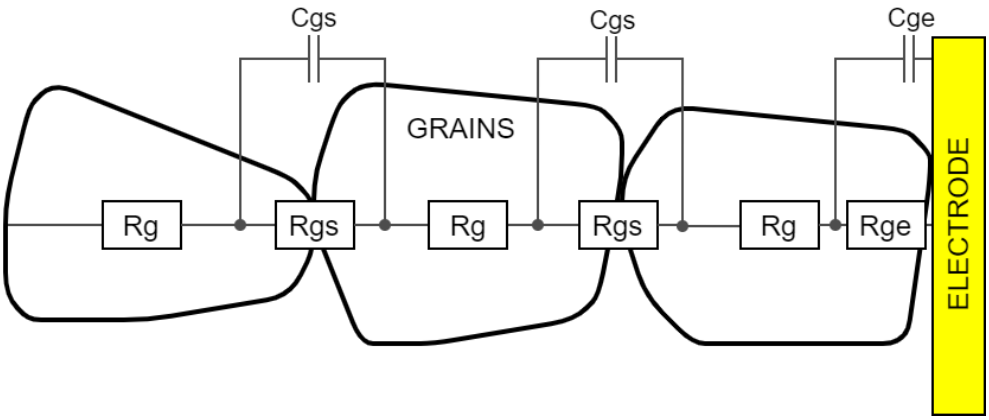

Figure 2-4 Electrical model representation of a nanocrystalline layer [4]

2.1.2 2D sensing monolayer

The second type of material is a 2D monolayer. These materials, unlike 3D, enable charge carriers to move in only two directions while being tightly confined in the third. The confinement results in quantized energy levels for motion in the third direction, which leads to the appearance of a 2D sheet embedded in a 3D world [33, 34]. Gas sensing and electrical properties significantly influence the behavior of charge carriers' gas. The type of charge carrier in charge carriers' gas is determined by the type of material used. Notably, the use of specific materials can result in the formation of a 2D electron gas (2DEG) or 2D hole gas (2DHG) [29, 35–39].

The thickness of a 2D material is typically only a few atoms. Ideally, the thickness is only 1 atom layer. The structure with only 1 atom thickness of carbon is graphene (the schematic drawing in **Figure 2-5**). Graphene is ideally composed of carbon atoms arranged in a honeycomb structure, a hexagonal lattice extending in a single sheet of atoms [36, 40].

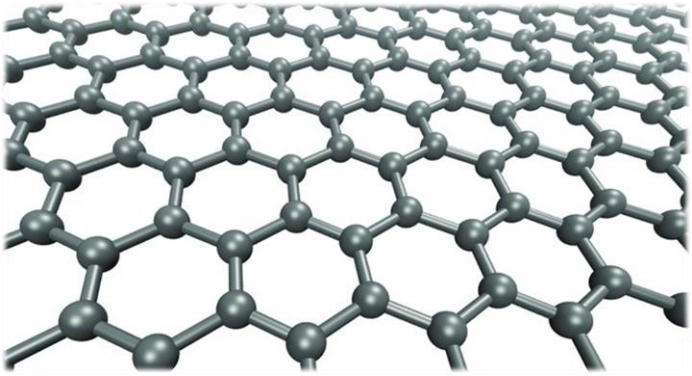

Figure 2-5 The schematic drawing of the crystal structure of graphene (gray–carbon) [40]

TMD materials, such as MoS_2 or $PtSe_2$, are another 2D material used as active material in gas sensors. TMDs are 2D semiconductors in MX_2 form, where M is a metal atom, and X is a chalcogen. Typically, Molybdenum or Tungsten is used as a metal, sandwiched between two layers of Sulfur or Selenium as the chalcogen. The layers are formed by a homogeneous material with three atom layers, ensuring consistent and accurate results (the schematic drawing in **Figure 2-6**) [29, 35].

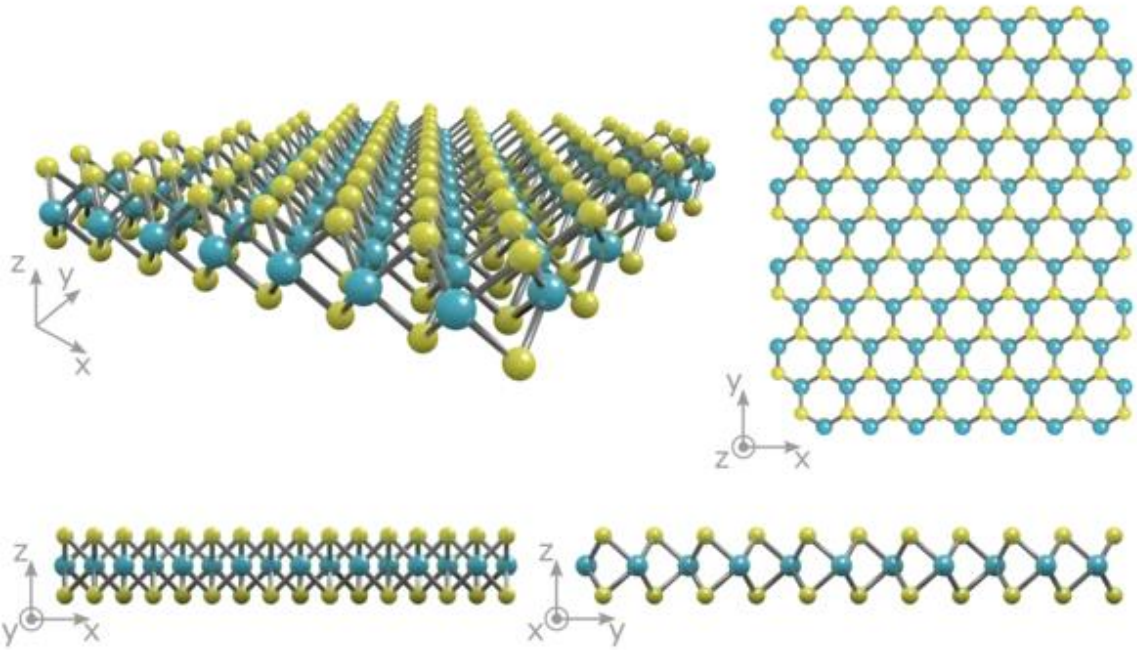

Figure 2-6 The schematic drawing of the crystal structure of MoS_2 (TMD) (blue–molybdenum, yellow–sulfur) [35]

A simple electrical circuit with essential components can be used to analyze the thin layer. It should be noted that the model of the thin layer is more complex than that of the nanocrystalline layer. **Figure 2-7** illustrates a model consisting of a parallel combination of layer capacitance (C_l) and a serial combination of layer resistance (R_l), which represents the charge transfer resistance and impedance between the electrode and layer (Z_{el}). Z_{el} is a parallel combination of the resistance between the electrode and layer (R_{el}) and the capacitance between

the electrode and layer (C_{el}). [4, 35]. Researchers can develop more effective and efficient conductivity gas sensors for various applications by understanding these sensing layers and their underlying principles.

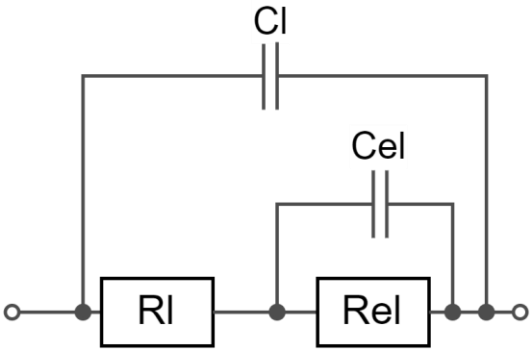

Figure 2-7 Electrical model representation of TMD monolayer [4]

2.1.3 1D nanowire

The third type is a 1D structure, also called nanotubes. These materials are prepared in wire or tube form. The charge carriers are tightly confined in two dimensions and can only move in one direction, making carriers appear as the wire embedded in a 3D world. This structure exhibits a high surface-to-volume ratio, significantly enhancing the material's and gas's interaction and improving gas responses [40, 41].

The typical 1D nanowire gas sensor material is carbon nanotubes (CNT) in **Figure 2-8 a)**. The wall thickness of CNT is only one atom, and the carbon atoms are arranged on a cylindrical surface with a length more significant than the diameter [40, 42]. However, other materials can also be used for gas sensing. The SnO_2 nanotube, the most used material as a 3D sensing layer, is in **Figure 2-8 b)**. The nanotube comprises SnO_2 molecules stacked together by Van der Waals forces. A heterostructure combining SnO_2 nanowires and MoS_2 flakes is also shown on the right [29].

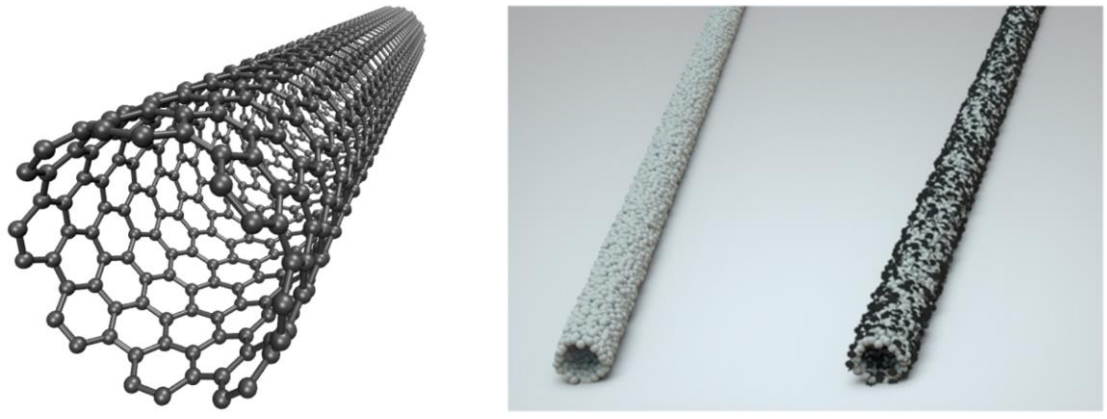

(a) (b)

Figure 2-8 The schematic drawing of the crystal structure of (a) CNT (gray–carbon) [40] and (b) MoS_2 / SnO_2 nanotubes (light grey– SnO_2, black – MoS_2) [29]

A straightforward electric circuit can be used to analyze the layer of a nanowire. The model (**Figure 2-9**) consists of a serial combination of the layer resistance R_l, representing the layer resistance, and the impedance between the electrode and layer Z_{el}, which is a parallel combination of the resistance between the electrode and layer R_{el}, and the capacitance between the electrode and layer C_{el} [4].

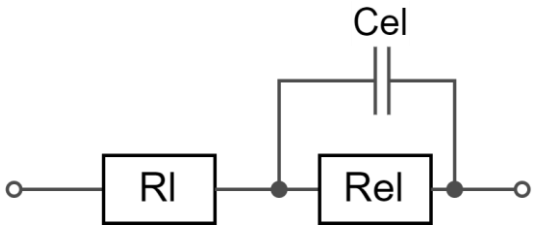

Figure 2-9 Electrical model representation of nanotube [4]

2.2 New approach and materials for conductivity gas sensors

Conductivity gas sensors are typically based on MO_X (e.g., SnO_2 or ZnO), WBG semiconductors (e.g., diamond), or 2D (e.g., TMDs or GO) active layers [2, 24]. The following subchapters present a list of materials for conductivity sensors with IDT structure. These novel materials improve gas responses and selectivity or reduce the operating temperature, thereby decreasing overall sensor consumption.

2.2.1 Carbon-based materials

Carbon is an element of great importance for all life on Earth and is considered one of the most significant elements in the periodic table. It is widely available in the Earth's lithosphere, ranking 17th in abundance, and is also present in the human body as the 2nd most abundant element. Carbon compounds play a crucial role in the world's energy industry. Fossil fuels, including natural gas and coal, are predominantly used for electricity generation and heating, while petroleum products fuel internal combustion engines, facilitating road and rail transport. Carbon-based chemical industry products, such as plastics, fibers, paints, and pharmaceuticals, are widely used daily [43, 44].

The diverse structure of carbon allows for a wide range of scientific and technological applications. The unique conformation of carbon molecules, type of the hybridization, determines its suitability for specific applications. For instance, graphene is suitable for superconductivity at room temperature, diamond is suitable for high thermal conductivity and biocompatibility, and CNT is suitable for molecular charge transport.

A neutral carbon atom has six electrons: two tightly bound near the nucleus (1s) and four valence electrons (two in the 2s subshell and two in the 2p subshell) [43, 45]. Carbon can bond in three different ways (single, double, and triple bonding) with many different elements. As a result, carbon has many different allotropic forms with entirely different properties [45]. Despite sharing the same building block, the carbon atom, their crystal structures differ. The sp hybridization

(linear) involves the hybridization of one s-orbital with one of the p-orbitals to form two sp-hybridized orbitals. The carbon atom binds to the new orbitals through diagonal symmetry, oriented at 180° angles. In the case of sp^2 hybridization (trigonal planar), one s-orbital combines with two p-orbitals to create three hybridized orbitals with trigonal symmetry and a characteristic angle of 120° between them. In the case of sp^3 hybridization, each carbon atom is arranged tetrahedrally. Four tetrahedra combine to form each tetrahedron, creating a strongly bonded, fully covalent crystal structure with a face-centered arrangement [17, 45].

Graphene and graphene oxides

Graphene is a carbon allotrope composed of a single layer of carbon atoms with sp^2 hybridization arranged in a hexagonal lattice nanostructure. It is valued for its exceptionally high tensile strength, high electrical conductivity, transparency, and being the thinnest two-dimensional material in the world. However, when it comes to use in conductivity sensors, its high conductivity may not be ideal. Therefore, some researchers have turned to GO, an oxidized form of graphene, as a potential alternative. Graphene oxide is a monoatomic material that is formed by the oxidation of graphite. It is highly dispersed in water and other solvents, making it easy to process. The oxygen present in its lattice results in very high resistivity, which can be reduced by modification. Graphene oxide can be reducible to reduced graphene oxide (rGO) through chemical, thermal, or electrochemical methods. As a result, rGO is commonly utilized in sensor applications due to its ability to maintain the properties of graphene while exhibiting higher resistance in the ground state [46–53].

There are various methods available for the development of GO. The first method is chemical vapor deposition (CVD), which requires high temperatures and relatively long deposition times, making it costly. Moreover, it is limited to substrates that can withstand high temperatures, challenging deposition on some materials. The second method is solution-based, such as modified Hummers [54]. This method consisted of several stages. The first stage of the synthesis was the initial intercalation of powder graphite by grinding with sodium chloride. Then, the mixture was washed several times with deionized water to remove sodium chloride [55], filtered on Teflon filters with a pore size of 0.45 µm, dried at room temperature and transferred to the reaction vessel. In the next step, concentrated sulfuric acid was added to the graphite and stirred using a magnetic stirrer. In the next step, the mixture was heated and stirred. During this time, an increase in the viscosity of the mixture and a change in its color from dark green to brownish were observed. The last step was the addition of deionized water and heating the mixture. The reaction was terminated by adding deionized water and hydrogen peroxide. The resulting mixture was filtered on Teflon filters with a pore size of 0.45 µm and washed several times with hydrochloric acid to remove unreacted Mn^{2+} ions [55, 56]. The rGO can be fabricated using ascorbic acid. The aqueous suspension of GO was mixed with an aqueous solution of ascorbic acid. The reaction mixtures were then placed in an ultrasonic bath and heated. During the reaction, the mixture changed from dark brown to black. After 60 min, an excess of 30 % hydrogen peroxide solution was added. The addition of hydrogen peroxide was intended to oxidize the unreacted reducing agent. The reaction product was filtered under vacuum through filters with a pore size of 0.45 µm [49]. The SH-GO is also produced from GO by functionalizing it with thiol groups. The first step was to prepare the GO mixture with toluene and phosphorus

sulfide. The mixture was refluxed for 7 days. The finished product was filtered on Teflon filters with a pore size of 0.45 μm, washed with toluene until the yellow color of the filtrate disappeared, and then with deionized water [57].

Diamond

Research has been conducted recently on diamonds and their various structures and uses. Diamond is the most exciting material from the group of WBG due to its ability to respond to oxidizing and reducing gases, light illumination, temperature variation, and other surrounding effects [58]. It comprises carbon with sp^3 hybridization in the diamond crystal structure [2]. Although it was previously classified as an insulator due to its wide bandgap (5.5 eV) [2], the diamond's unique properties make it a valuable material. It is necessary to modify the intrinsic diamond to prepare a quality semiconductor, for example, by doping it with foreign atoms or suitable termination. Natural diamonds have a lot of foreign atoms (impurities), such as metals, nitrogen, and others. However, finding the correct doping atoms can be challenging due to the small lattice constant of only 3.57 Å ($357 \cdot 10^{-12}$ m) [58]. Boron is the most used material, creating a p-type semiconductor, while phosphorus is used for n-type [28, 31]. Hydrogen terminated surface of the diamond reveals unique properties in induced subsurface p-type conductivity, also known as 2DHG [16, 17, 27, 59, 60]. Such a 2DHG top-layer is sensitive to exposed gas or organic molecules [16, 31, 61, 62].

There are various methods available for growing synthetic diamonds (not natural). The oldest method is the high-pressure / high-temperature (HPHT) process. However, it is worth noting that this method can produce both diamond particles and thin layers and flakes of diamonds due to uncontrollable conditions [32, 33]. Another method that can be used is CVD. Currently, the most used method is low-pressure plasma-enhanced CVD (PECVD). This method involves ionizing a mixture of gases using microwave radiation to ignite low-pressure plasma. The correct procedure produces a diamond phase near the surface of the substrate, which binds to the substrate with the nucleation center and eventually grows into a continuous diamond layer [13, 34]. Hydrogen terminated diamond layers are sensitive to various physical and material variables, including gases. As with most conductivity sensors, the parameters of the active layer can be adjusted by factors during fabrication, such as the preparation technology, layer thickness, type, or dopant [17, 63].

2.2.2 TMD materials

TMD monolayers are atomically thin semiconductors of the MX_2 type. These 2D materials comprise a layer of transition metal M (Mo or W) and two layers of chalcogen X (S, Se, or Te). TMD bulk crystals are formed by monolayers bonded to each other by van der Waals attraction, like graphite. Furthermore, it should be noted that TMD has properties that differ significantly from graphene. With their 2D nature and high spin-orbit coupling, TMD layers have been identified as promising materials for spintronic applications. Additionally, certain TMD monolayers have a direct band gap, making them potentially suitable for electronics as transistors and optics as emitters and detectors. One representative of TMD is MoS_2.

MoS_2 comprises a single layer of molybdenum and two layers of sulfur, with a total thickness of only 6.5 Å ($65 \cdot 10^{-11}$ m). The MoS_2 layer typically acts as an n-type semiconductor, with defects in the MoS_2 grains layer (grain edges or sulfur vacancies) serving as active sites for gas molecules [64]. It can be modified or doped with other materials, such as ZnO quantum dots or Ag-doped, to improve its sensing performance [36, 65, 66]. Gas sensing properties depend on the charge transfer between gas molecules and defects present in the layer [29, 35, 67].

Similar to previous materials, several methods for growing a MoS_2 layer exist. The oldest method is preparation from the liquid phase. A suspension is created by dissolving appropriate materials in deionized water and stirring. The particles are then mixed ultrasonically. Finally, the suspension is heated at 200°C. After cooling the autoclave to room temperature, separate the black precipitates [35]. The second method to synthesize TMD is CVD. It is one of the most used methods for synthesizing different TMDs due to its high adaptability. The process involves placing transition metal oxide (molybdenum oxide, etc.) and individual chalcogen (sulfur, etc.) precursors in a furnace with the substrate and heating them to high temperatures with inert gas. A special case of CVD synthesis is the carbide-free one-zone sulfurization method. In this method, a thin molybdenum layer is sputtered on the sample and then annealed in sulfur vapor at higher temperatures (500 - 800 °C) in nitrous ambient at standard pressure. In the first step, a thin Mo layer was deposited using DC magnetron sputtering in an Ar atmosphere at room temperature. Next, the predeposited Mo layers were sulfurized in a CVD chamber. The Mo layer was annealed in sulfur vapors at a high temperature of 800 °C in an N_2 atmosphere at ambient pressure. The substrate was placed together with the sulfur powder in the center of the furnace so that the temperature of the substrate and the powder were the same during the growth, unlike the standard CVD method, which uses a two-zone furnace with different temperatures for the sulfur powder and the Mo substrate [68–73].

2.2.3 Heterostructures and composites

Heterostructures are an exciting prospect for gas sensing applications, as they combine the sensing mechanisms of two materials, resulting in enhanced sensor responses and selectivity. Based on two components, the active layer can increase the sensitivity to gases than the materials themselves due to the synergic effect between both materials. In most cases, details about the synergistic effect are still unknown because of the complicated effects between the two materials [29, 74]. Current research explores the potential benefits of combining multiple materials and technology steps to enhance sensor response and lower operating temperature [12, 13, 30, 32, 35, 65, 75–96]. These studies investigate combining different materials to improve the responses to various gases and vapors. Heterostructures are primarily utilized to enable operation at room temperature, enhance response and reproducibility, and facilitate miniaturization. It is important to note that certain material combinations may not be suitable for gas response, as some heterostructures and composites may not respond to gases or could potentially impair the response. The example of heterostructure is shown in **Figure 2-10**.

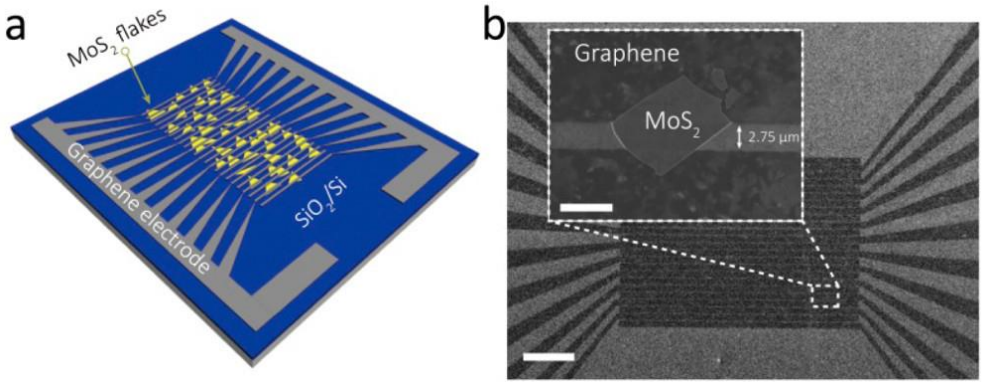

Figure 2-10 Graphene / MoS_2 heterostructure: (a) schematic drawing and (b) SEM images [75]

Furthermore, the production of the heterostructure may present certain challenges during manufacturing. Two materials can form a high-quality (hetero-) junction if their lattice constants are similar. Alternatively, a high-quality junction can still be grown even if the lattice constants differ significantly, if the epitaxial layer thickness is small enough. It is important to note that the size of the lattice constant mismatch is directly related to the maximum allowable height of the epitaxial layer. For instance, **Figure 2-11** illustrates an example of a junction between two different materials. Picture a) displays isolation materials with different lattice constants a_e and a_s prior to the junction. Picture b) displays the junction with a dislocation due to the material with lattice constant a_e being too high. Picture c) displays strained epitaxial material, which changes its lattice constant from a_e to a_s because of its small thickness. This phenomenon utilizes strained silicon technology, which alters the electron mobility and resistivity of the material [2, 28].

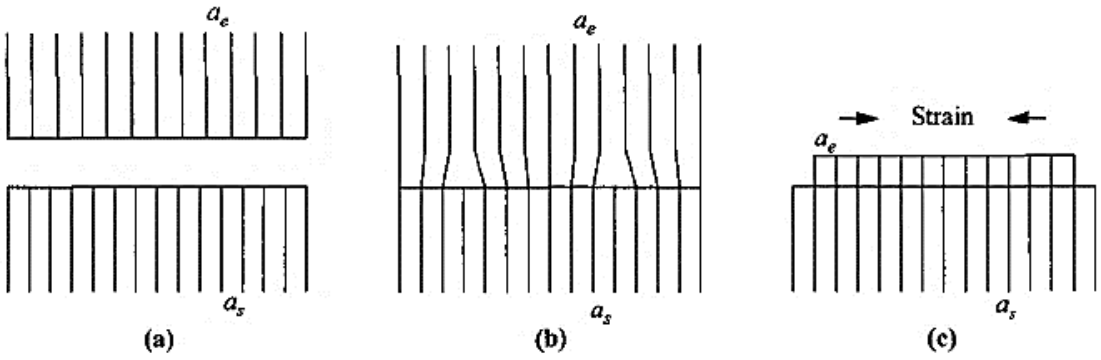

Figure 2-11 Junction of two materials with slightly inconsistent lattice constants [2]

2.3 Comparison of gas sensors

Research on air quality and gas sensors has been ongoing for a considerable period. In recent decades, there has been a notable rise in the need for air quality monitoring and pollutant detection, which has increased interest in this field of research. **Table 2-1** below presents a comparison of several sensors that have been laboratory fabricated and operate at room temperature. The table also includes two commercial sensors: the TGS826, which utilizes standard SnO_2 material working at around 300 °C, and the PY2055 IR sensor, which employs IR absorption by a particular gas.

Different concentrations of ethanol vapors C_2H_5OH, ammonia NH_3, and nitrogen dioxide NO_2 were utilized to measure the sensors at room temperature, except the commercial TGS826, employed for comparison with the commercial sensors. It is worth noting that the PY2055 sensor operates at room temperature, but it necessitates an IR source of the appropriate wavelength. According to the table, the V_2O_5 material exhibits the highest response to ethanol at 60 % [97], while the PANI / CNT heterostructure demonstrates the best response to ammonia at 452 % [88]. Additionally, the oxidized SWCNT achieves the best response to nitrogen dioxide at 32 % [98]. It should be noted that sensors with low response at room temperature can improve their response when the temperature is raised or when other catalysts, such as UV radiation [59], are used. However, these catalysts typically increase power consumption, enlarge the system, and prevent miniaturization. Therefore, it is recommended that research efforts be concentrated on developing composite materials that exhibit adequate response at room temperature without additional catalysts.

Table 2-1 Comparison of responses of various sensors for gas sensing at room temperature

Reagent	Reagent concentration	Material system	Response (%)	Lit.
Ethanol vapor	700 ppm	MoS_2	27.3	[99]
	100 ppm	g-C_3N_4 / Au	27.3	[12]
		g-CN	6	[13]
		g-CN / Ag	16	[13]
		V_2O_5	60	[97]
		TiO_2 / Au	16	[100]
		ZIF-8 / CNT	2	[91]
		GO	20	[55]
		AA-PRGO	35	[55]
		SH-PRGO	35	[55]
	50 ppm	TiO_2 / Au	4	[100]
	5 ppm	CNT	1.2	[101]
		CNT / TiO_2	3.6	[101]
		rGO after low energy ion beam reduction (10^{15} ions / cm^2)	1.2	[56]
NH_3	100 ppm	V_2O_5	45	[97]
		ZIF-8 / CNT	20	[91]
		PANI	13.8	[102]
		S and N co-doped quantum dots / PANI	39.4	[102]
		rGO / PANI	10	[46]
		Figaro TGS 826 (SnO_2) commercial sensor	16.9	[103]
	70 ppm	PANI / CNT	452	[88]
	50 ppm	Oxidized SWCNT	5	[98]
NO_2	100 ppm	H-diamond	5	[17]
		MoS_2 / H-NCD	15.7	[104]
		Figaro TGS 826 (SnO_2 at 300 °C) commercial sensor	47.8	[103]
		Pyreos PY2055 (IR Sensor) commercial sensor	46	[103]
	50 ppm	Oxidized SWCNT	32	[98]
	5 ppm	rGO after low energy ion beam reduction (10^{15} ions / cm^2)	2.2	[56]

3. Experimental part

The section presents the author's experimental work, including publications, conference papers, and related proceedings. The research involved fabricating various conductivity sensors with active layers and designing a new computer-controlled apparatus for sensor measurements.

3.1 Experimental apparatus for gas sensor measurement

The electrical parameters of the gas sensors are measured with a computer-controlled apparatus. It includes mass flow controllers (MFCs), bubblers, T-connectors, manual valves, a 4-input selection valve, test chambers, a source measure unit (SMU), temperature regulation, and data acquisition through a PC using a LabVIEW programming environment. **Figure 3-1** illustrates the 3D model of the gas mixture preparation, and **Figure 3-2** shows a photograph.

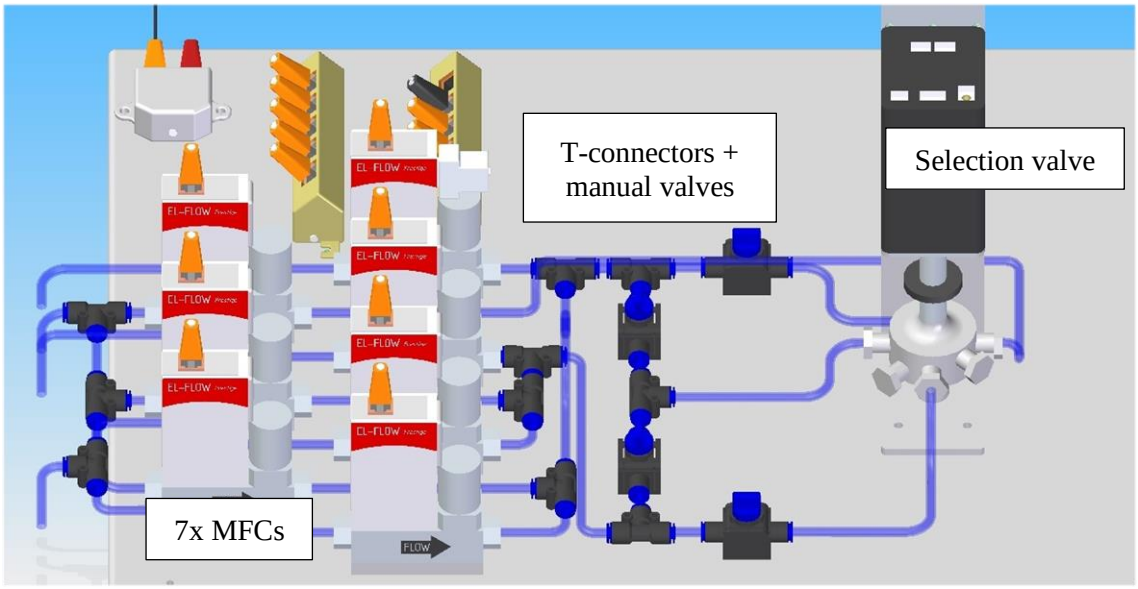

Figure 3-1 3D design of an experimental apparatus for gas sensor measurement

The apparatus part for preparing gas mixtures consists of seven MFCs, two bubblers, seven mixture T-connectors, four manual valves, and a 4-input selection valve. The Bronkhorst FG-201CV MFCs operate on the principle of using gas flow to cool the heating element [105]. The MFCs communicate and receive electrical power through the FLOWBUS, based on the RS-485 bus. The MFCs are followed by a T-connector mixer system that uses turbulent mixing of gases. Bubblers are used to humidify the air and alter the humidity of the testing mixture. One bubbler evaporates ethanol or other chemicals and creates a compound with chemical vapors at a specific concentration. Synthetic air is used to flush the chamber. The Valco EUTA 4VLSC4MWE2 valve, which has four inlets and two outlets (for selecting inlets and exhaust), is used to select the test mixture [106]. This valve can maintain constant flow rates for all gases.

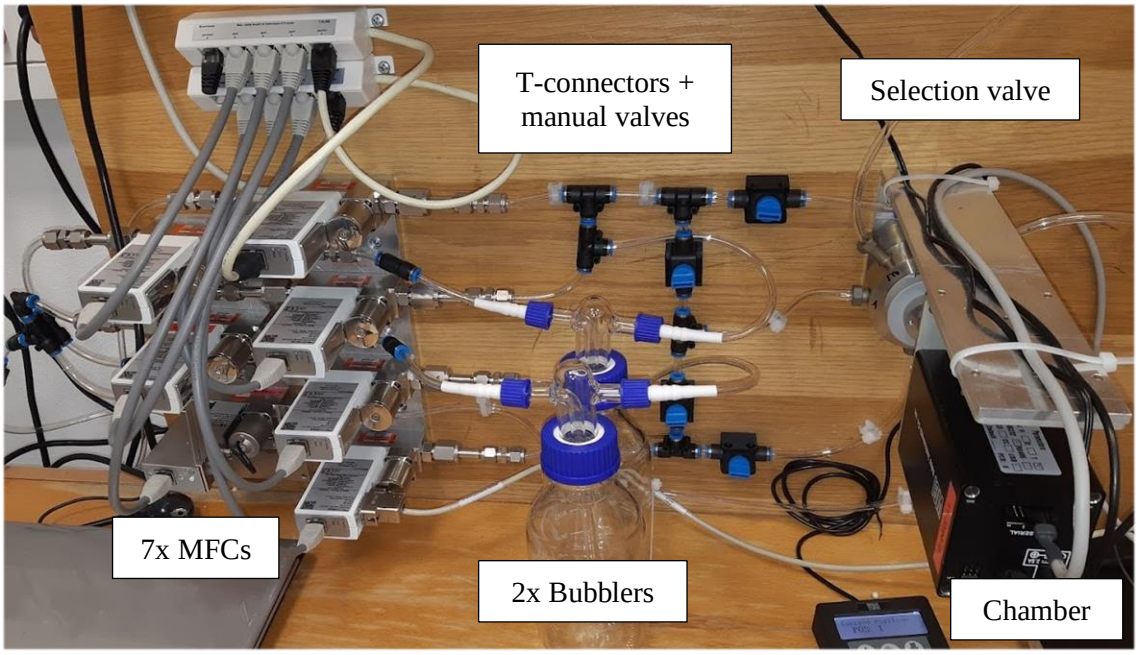

Figure 3-2 Photograph of an experimental apparatus for gas sensor measurement

The measured part of the apparatus involves the IDT-compatible measurement chamber, SMU Keithley 2401, and temperature regulation. Two different chambers were designed and fabricated for this purpose. The first chamber is designed specifically for IDT sensors with a substrate dimension of 6×10 mm and has a small volume (approximately 0.2 cm^3). The 3D model of this chamber is shown in **Figure 3-3**, and the photograph is shown in **Figure 3-4**. The measuring chamber comprises a base, a rear part with flexible measuring contacts, and a front part with the gas chamber. The front part of the sensor includes a small measuring chamber with a volume of approximately 0.2 cm^3, which covers only the active part of the sensor. The chamber also includes a temperature control assembly with a heating element and a Pt1000 temperature sensor. The chamber parts are fixed using neodymium magnets and cut-outs, allowing easy assembly during sensor replacement.

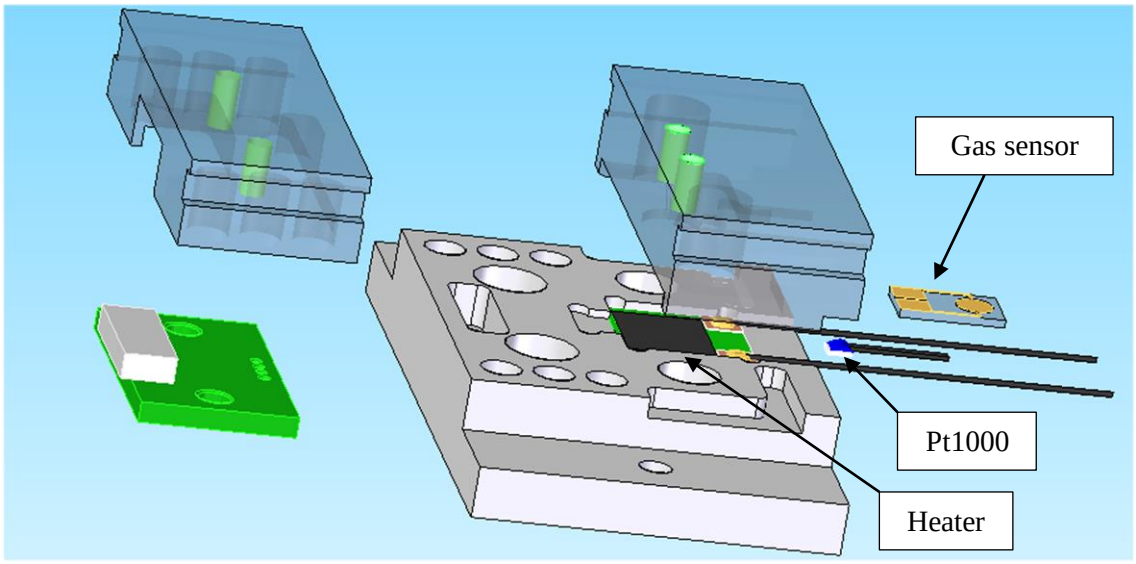

Figure 3-3 3D design of testing chamber for IDT 6×10 mm sensors

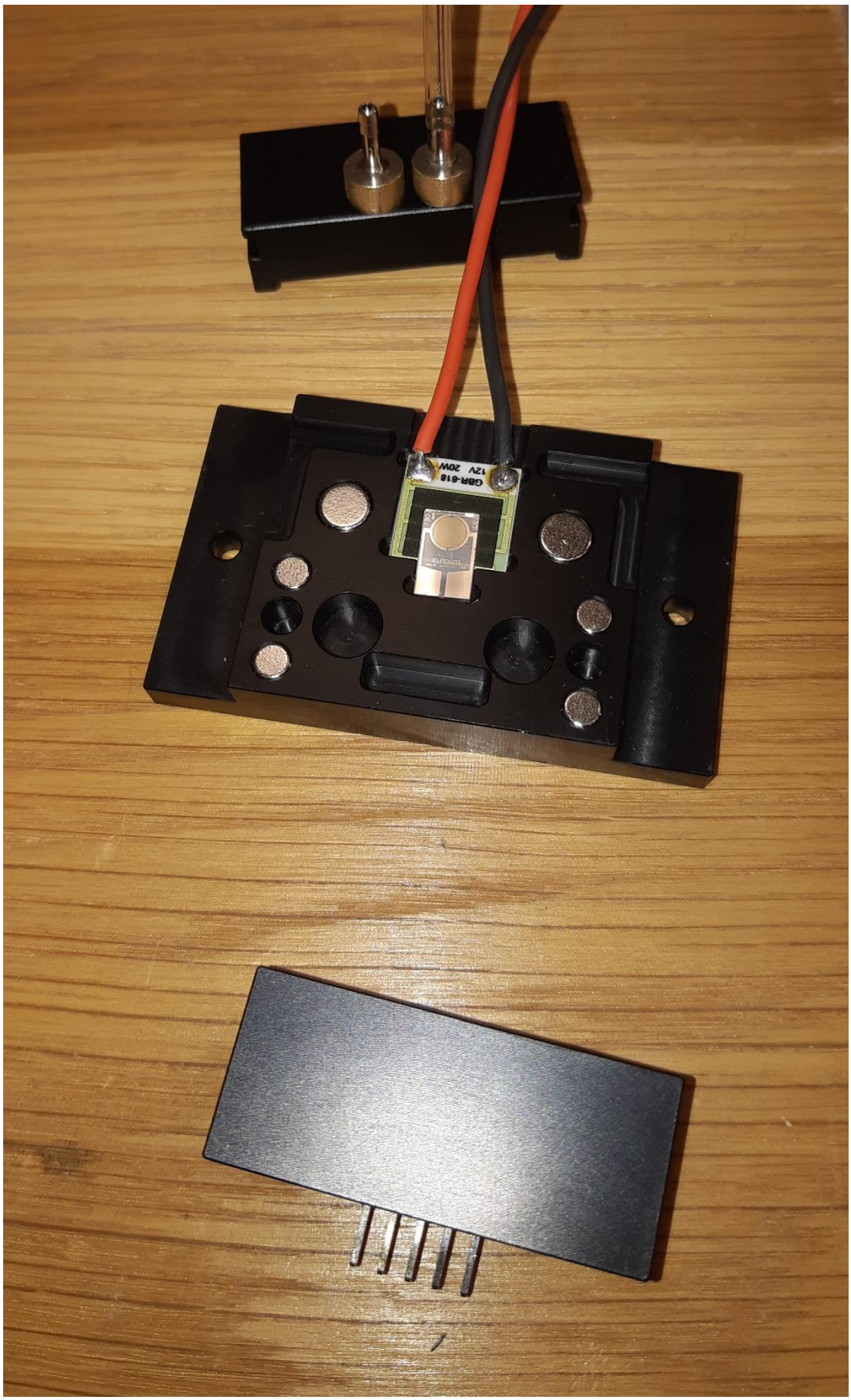

Figure 3-4 Photograph of a testing chamber for IDT 6×10 mm sensors

The second chamber type is a universal chamber with two 22 cm^3 cells and a partition between them (see **Figure 3-5**). Its larger size enables the installation and measurement of larger commercial sensors and necessary components, such as the radiation source for the IR sensor.

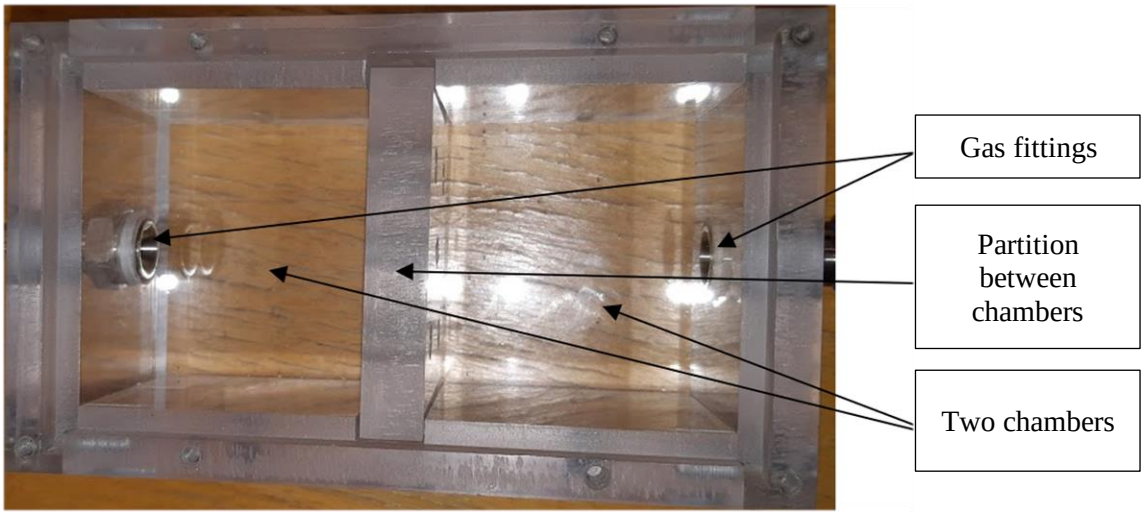

Figure 3-5 Photograph of a testing chamber for larger sensors

The SMU Keithley 2401 is utilized to measure the sensor's electrical resistance. It enables both two-wire (Ohm) and four-wire (Kelvin) DC resistance measurements and allows for selecting the energy source, current or voltage, and its value. The temperature regulation system comprises a heater element and a Pt1000 temperature sensor. The temperature can be adjusted from room temperature to 125 °C in the testing chamber.

3.2 Measurement and results

The gas responses of the sensors were measured at voltage 0.1 V and for two different temperatures, high temperature (125 °C) and room temperature (approximately 22 °C), for three testing gases: ethanol vapor, NH_3, and NO_2, each concentrated at 100 ppm. The gas-sensitive layer responses by a change in resistance measured at 0.1 V from steady state R_0 to actual resistance R_G in the presence of the tested gas. The resistance changes ΔR in the presence of active gas were calculated using equation (3-1).

$$\Delta_R = \left(\frac{R_G}{R_0} - 1\right) \cdot 100 = \left(\frac{R_G - R_0}{R_0}\right) \cdot 100\ (\%) \qquad (3\text{-}1)$$

The acquired data are categorized into two groups based on working temperatures: higher working temperature (around 125 °C) and room temperature (around 22 °C). Compared to individual materials, their combination in heterostructure significantly enhanced the gas responses. The responses are summarized and compared in **Table 3-1** for 125 °C and **Table 3-2** for 22 °C.

3.2.1 Measurement at 125 °C

At 125 °C, the temperature acts as a catalyst in the chemical reaction between gases / vapors and active materials. This catalyst improves the responses to gases, enhances sorption and chemical reactions between gases and active materials, and accelerates desorption, resulting in a faster sensor reset to steady-state resistance. The high temperature enhanced the response of almost all sensors. On the other hand, achieving higher temperatures requires a heating element, which increases the power consumption of sensor devices, making battery operation impractical or challenging for wearable electronics.

The best response to gases exhibited SH-GO / H-NCD and Au NPs / H-NCD heterostructures. The Au NPs / H-NCD sensor exposed to 100 ppm ethanol achieved the most significant response of 587 %. The second-best ethanol sensor is a heterostructure of SH-GO / H-NCD with a response of 554 %. All sensors demonstrate exceptional selectivity for oxidizing and reducing gases, displaying an inverse resistance change for oxidizing / reducing gas type, i.e., the sensors responded with the opposite sign of the change in resistance. The individual materials revealed low responses.

Table 3-1 Responses of sensors at 125 °C / 0.1 V exposed to 100 ppm ethanol vapor, 100 ppm NH_3 and 100 ppm NO_2. The table highlights the best and the second-best values in dark green and light green.

125 °C	Individual			H-NCD		
	100 ppm Ethanol	100 ppm NH_3	100 ppm NO_2	100 ppm Ethanol	100 ppm NH_3	100 ppm NO_2
Individual	No response			98	39	−13
MoS_2	Unmeasured					
rGO	148	−11	17	254	72	−39
SH-GO	46	8	−5	554	76	−47
Au NPs	No response			587	48	−47

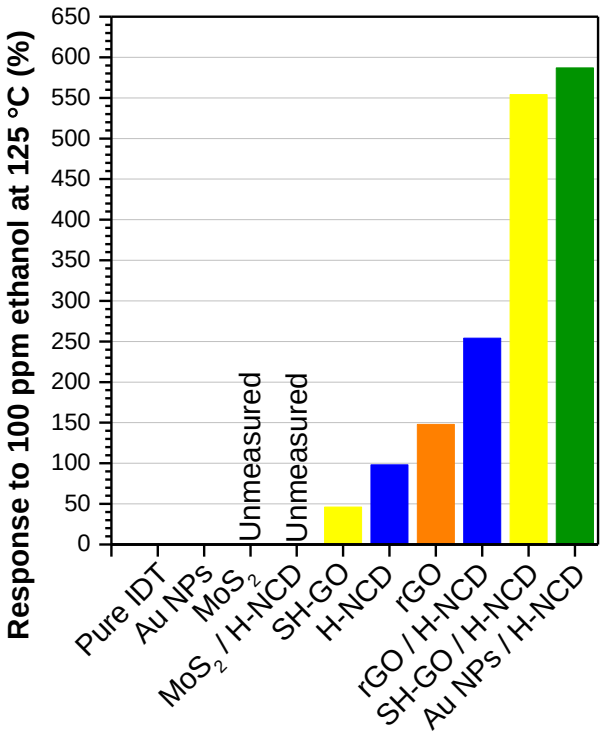

Graph 3-1 Responses of measured sensors to 100 ppm ethanol C_2H_5OH at 125 °C

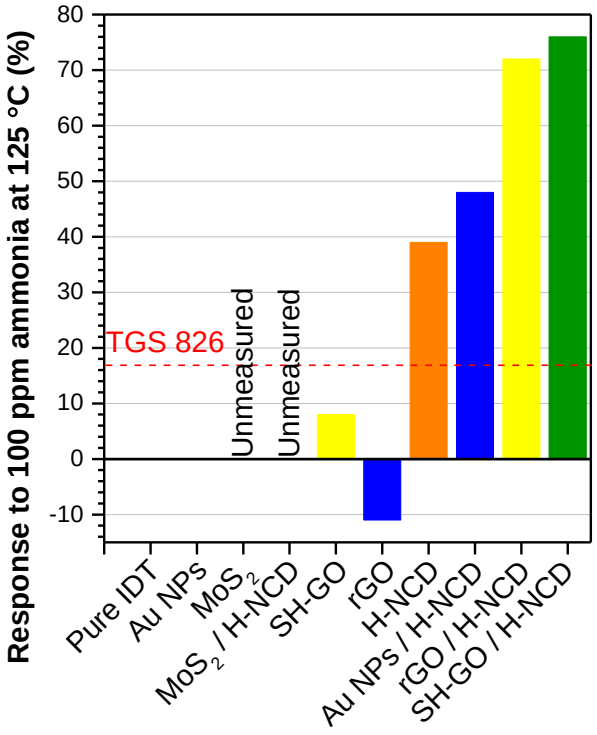

Graph 3-2 Responses of measured sensors to 100 ppm ammonia NH_3 at 125 °C

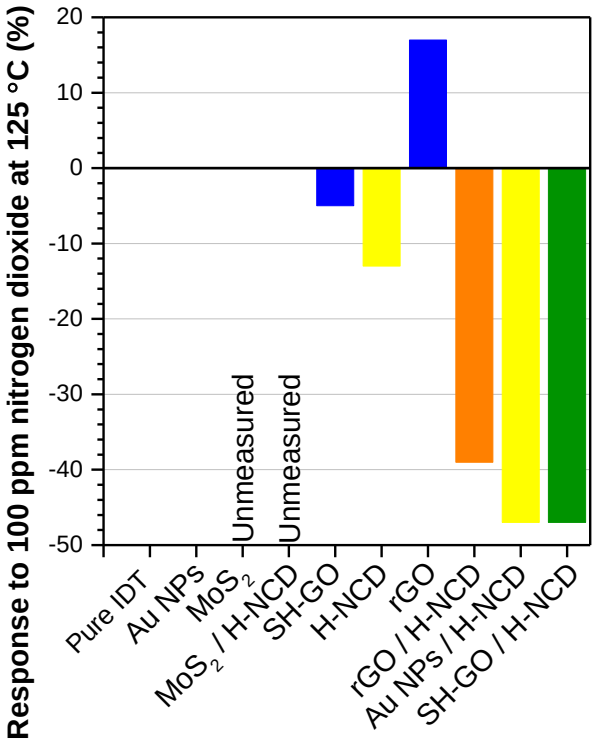

Graph 3-3 Responses of measured sensors to 100 ppm nitrogen dioxide NO_2 at 125 °C

3.2.2 Measurement at 22°C (room temperature)

Operating at room temperature allows for a more straightforward sensor design and lower power consumption. However, lower operating temperatures increase response and reset times. At 22 °C, the SH-GO / H-NCD heterostructure exhibited the best response to gases. This sensor achieved a 634 % response when exposed to 100 ppm ethanol. The second-best sensor was a MoS_2 / H-NCD heterostructure, although it lost the selectivity recognition for the oxidizing and reducing gases. The individual materials revealed low responses at room temperature.

Table 3-2 Responses of sensors at 22 °C / 0.1 V exposed to 100 ppm ethanol vapor, 100 ppm NH_3 and 100 ppm NO_2. The table highlights the best and the second-best values in dark green and light green.

RT (22 °C)	Individual			H-NCD		
	100 ppm Ethanol	100 ppm NH_3	100 ppm NO_2	100 ppm Ethanol	100 ppm NH_3	100 ppm NO_2
Individual	No response			3	0.5	−0.7
MoS_2	35	−0.7	1.8	248	17.8	15.7
rGO	130	−2	1.8	195	7.1	−2.2
SH-GO	16	0.6	−0.2	634	41	−19
Au NPs	No response			164	4.8	−4.7

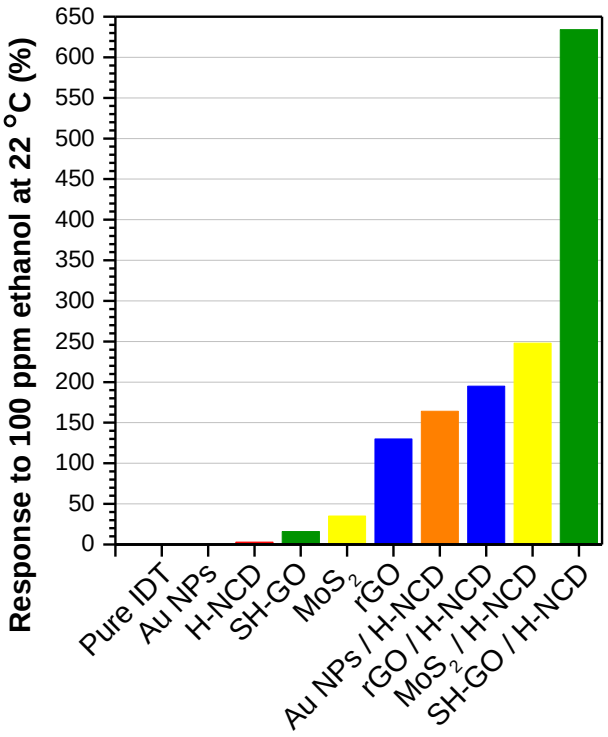

Graph 3-4 Responses of measured sensors to 100 ppm ethanol C_2H_5OH at 22 °C (room temperature)

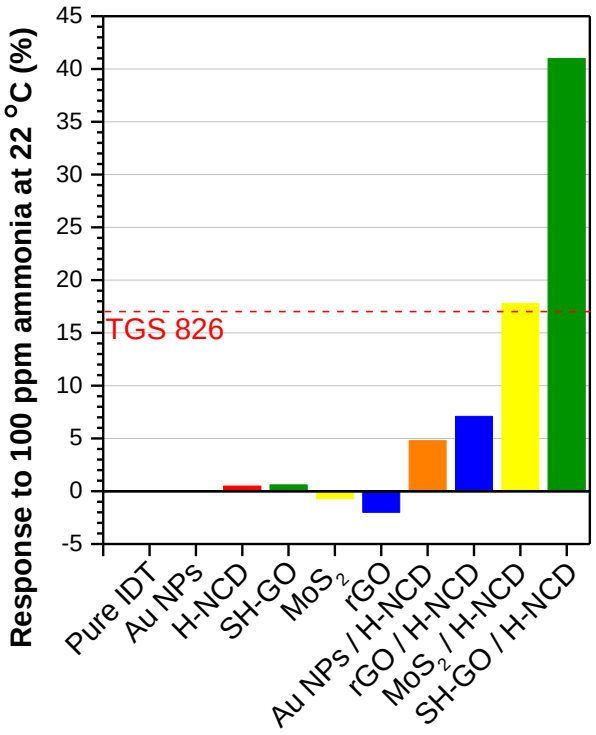

Graph 3-5 Responses of measured sensors to 100 ppm ammonia NH_3 at 22 °C (room temperature)

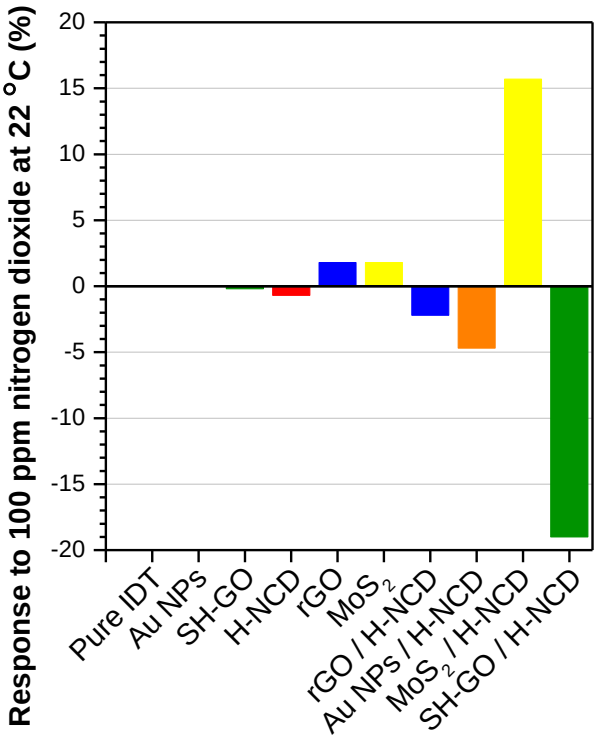

Graph 3-6 Responses of measured sensors to 100 ppm nitrogen dioxide NO_2 at 22 °C (room temperature)

3.3 Gas interaction models

3.3.1 SnO_2

The change in conductivity in SnO_2 is caused by chemisorption, reflecting the binding (sorption) of oxygen molecules on its solid surface by chemical bonding with electron transfer. **Figure 3-6** depicts a schematic view of the time-sequenced set of interactions. The transfer of electrons between substances is called the oxidation-reduction process [1, 15, 24, 107].

In the case of the oxidizing gas, NO_2 (**Figure 3-6 left**), free electrons are removed; thus, the conductivity of the n-type semiconductor is reduced. In **Figure 3-6a)**, NO_2 gas molecules are adsorbed on the surface of the SnO_2 bulk; the gas attacks the available Sn sites and removes electrons from the conduction band, forming NO_2^-, which increases the barrier between particles and reduces conductivity. Subsequently, in **Figure 3-6b)**, molecules of NO_2^- desorb as NO, leaving binding oxygen ions behind [24, 32]. After exposure to a non-oxidizing gas (in **Figure 3-6c)**), chemisorbed oxygen molecules with negative charges on the surface are released as O_2 with a neutral charge, and electrons are returned to SnO_2 [32], which returns the conductivity to its previous value.

Exposing the SnO_2 surface to the reducing gas NH_3 (**Figure 3-6 right**) transfers free electrons into the material and increases the conductivity of the n-type semiconductor. In **Figure 3-6d)**, molecules are adsorbed, react with binding oxygen ions, and create charge-neutral NO and

H_2O molecules. The excess electrons from the oxygen ions are transferred into semiconductors, increasing conductivity and reducing the barrier between particles [32]. After exposure to a non-reducing gas (in **Figure 3-6f)**), the conductivity returns to the previous value due to the sorption of two oxygen ions from the neutral O_2 and the removal of free electrons [32].

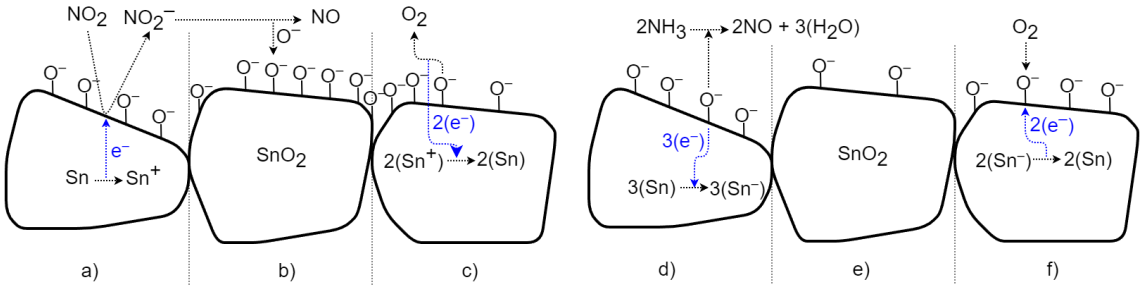

Figure 3-6 Schematic time process of gas interaction between the SnO_2 material and oxidizing and reducing gases

3.3.2 H-NCD

H-terminated NCD reveals a similar detection principle to the surface of SnO_2 but with the opposite effect on its surface conductivity. Contrary to the electron transfer mechanism for SnO_2, the H-NCD mechanism involves chemical reactions forming counter ions on its surface via an electron transfer model [17, 62, 108–110]. A widely established H-terminated diamond surface doping mechanism was used to explain the sensing mechanism. A thin layer of adsorbed water from the air is formed on the diamond surface [23, 111, 112]. The water molecule dissociates into the ions H_3O^+ and OH^-. The H_3O^+ ions attract electrons from the diamond sub-surface, forming the p-type surface conductivity on the H-terminated NCD (**Figure 3-7a, d)**).

If oxidizing gas molecules (NO_2) are present (**Figure 3-7b)**), the concentration of H_3O^+ ions rises due to a set of chemical reactions of the oxidizing gas with the adsorbed water monolayer. This causes a superiority of H_3O^+ molecules and creates a charge imbalance. Electrons are transferred from the diamond's top surface to the direction of positive ions. Next, the resultant holes increase the 2DHG conductivity [16, 23, 111]. After exposure to a non-oxidizing (air) gas (**Figure 3-7c)**), the number of H_3O^+ ions decreases, and again H_3O^+ equilibrates with OH^-. The electrons return to the diamond, and conductivity reduces to its original value [23].

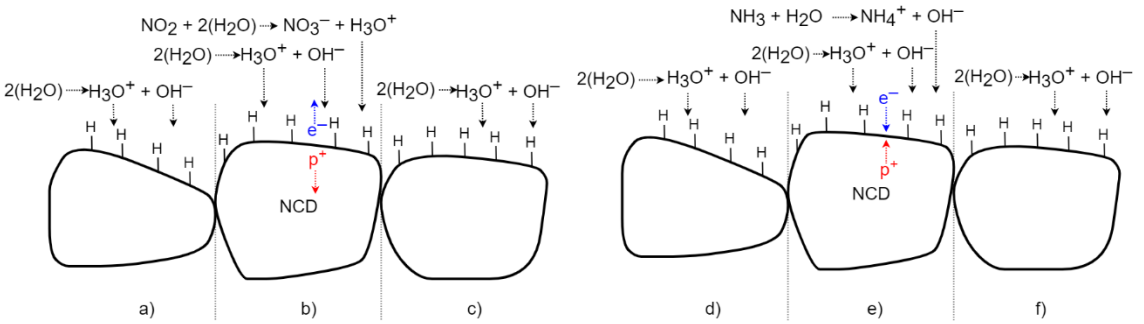

Figure 3-7 Schematic time process of gas interaction between the H-terminated NCD and oxidizing and reducing gases

In the case of a reducing gas, such as NH_3 (**Figure 3-7e)**), the concentration of OH^- ions increases due to the set of chemical reactions of the reducing gas with the adsorbed water monolayer. Due to the higher number of NH_4^+ ions, the concentration of the ions decreases, and electrons are shifted to the diamond and partially neutralize the 2DHG, reducing the diamond's surface conductivity [23, 113]. After exposure to a non-reducing (air) gas **Figure 3-7f)**, the number of OH^- ions decreases, and OH^- equilibrates with H_3O^+ again. The electrons return from the diamond, and the conductivity increases to the original value.

3.3.3 MoS_2

MoS_2 typically behaves as an n-type semiconductor [36]. MoS_2 uses the sorption of oxygen molecules on its solid surface through chemical bonding with electron transfer. Defects in MoS_2, such as flake edges and sulfur vacancies, serve as active sites for the investigated gas molecules. The gas sensing properties depend on the charge transfer between the gas molecules and defects in MoS_2. **Figure 3-8** illustrates the gas sensing mechanism based on previously published works [36, 77, 79, 89, 90, 92, 114]. The O_2 molecules from the air chemisorbs to the surface of the MoS_2 and form a native oxide, which acts as electron trap centers, extracting electrons from MoS_2 and generating O_2^-. This process leads to a decrease in the concentration of free electrons and a subsequent decrease in conductivity. It is important to note that the chemisorbed oxygen establishes the baseline resistance of the sensing layer. NO_2 gas causes the formation of NO_2^- ions, which increases the resistivity of the layer. When synthetic air is introduced, the NO_2^- ions react with chemisorbed O_2^- to form NO_2 and O_2. The two remaining electrons from the chemical reaction are released back into the conduction band of MoS_2 or form new O_2^- ions with O_2. Similarly, NH_3 gas reacts with chemisorbed O_2^- ions and produces H_2O and N_2. The reaction releases the remaining electron into MoS_2, reducing the sensing layer's resistivity [29, 114]. Upon recovery, when the reducing gas is replaced with synthetic air, O_2 chemisorbs onto the surface of MoS_2 from the atmosphere [29, 79, 89, 90, 104, 115].

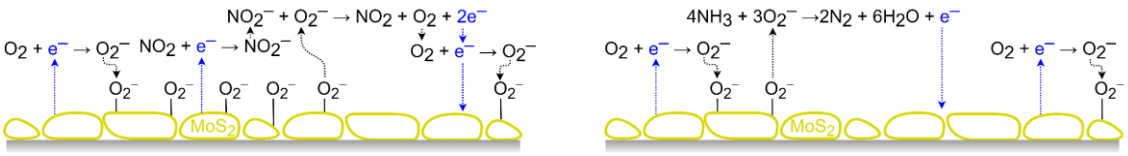

Figure 3-8 Schematic illustration of the gas sensing mechanism between a layer of MoS_2 nanoflakes and (left) oxidizing and (right) reducing gases

3.3.4 GOs

Graphene oxides are generally considered a p-type semiconductor without a bandgap, particularly in its single-layer form [55]. GO comprises an interlinked network of aromatic rings, with each ring containing π electrons in constant motion, creating a quasi-hole / electron vortex in the material. The aromatic structure of graphene is the primary factor behind its conductivity, serving as the underlying force for all graphene-based materials in terms of their conductive properties. During synthesizing graphene through chemical reactions, it is typical for the resulting product to have a damaged structure. Conversely, graphene oxide contains a variety of functional groups, including sp^3 and sp^2 carbon, hydroxyl, carbonyl, or carboxyl, which can interfere with

the flow of electricity. As a result, this interference can lead to an electrical insulator behavior [49, 55]. The material displays a favorable affinity for gases and vapors, albeit with weak conductivity.

It has been observed that rGO, a partially reduced form of graphene oxide with a higher C / O ratio and an improved conductivity pathway, exhibits a more pronounced core sensing effect related to the aromatic structure. This results in a higher sensing response, increased sensitivity to concentration, and improved response / recovery [56]. However, rGO may exhibit weaker selectivity towards different analytes. The SH-GO sample contains SH groups and is considered a versatile material similar to GO with OH groups but with a reconstructed sp^2 carbon backbone. SH-GO has been found to exhibit excellent conductivity and a significantly higher affinity for gold electrodes than rGO. The electron cloud formed by the aromatic rings in the graphene structure can be influenced by external factors, resulting in electron enrichment or depletion and subsequently leading to the formation of 2DHG. This electron exchange depends on the compound's impact on the aromatic ring. Ethanol vapor or reducing gas, NH_3, can share electrons with the electron cloud and reduce the number of holes. In contrast, it can be observed that the oxidizing gas NO_2 withdraws electrons in **Figure 3-9**. It is important to note that the main phenomenon is the physical sorption of NO_2 molecules onto the graphene structure. The primary objective of functionalizing graphene-based materials is to improve selectivity and affinity for specific analytes [55].

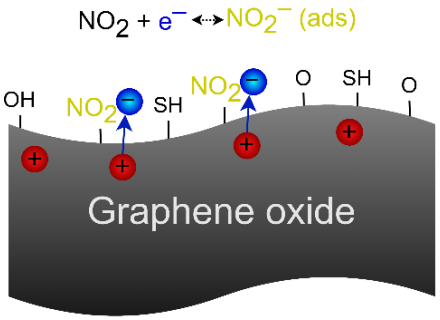

Figure 3-9 Schematic illustration of the gas sensing mechanism between a GO and NO_2

3.3.5 H-NCD with Au NPs

The detection mechanism of H-NCD with Au NPs is based on a gas interaction model like the one mentioned above. The presence of Au NPs creates local electrically conductive islands (regions), significantly reducing the steady-state resistance, which allows a more significant number of free charge carriers to tunnel through the Au NPs instead of the barriers, resulting in a more efficient detection process, as illustrated in **Figure 3-10a)**. The equivalent circuit diagram (**Figure 3-10b)**) demonstrates that the Au NPs are represented by a resistor connected in parallel to the barrier resistor, resulting in a lower final resistance value than the H-NCD layer alone. The Au NPs / H-NCD hybrid structure effectively utilizes conductive Au NPs to reduce the steady-state resistance value while maintaining the functionality of the H-NCD gas sensing layer.

Combining these two parameters results in a higher final percentage value for primary resistance. Although the presence of Au NPs reduces the total response of the diamond surface

due to partial overcoating of the H-NCD functional layer, a higher concentration of Au NPs leads to increased power consumption for sensor measurement, as a higher current is required for the same measurement voltage. Additionally, determining the ideal size of Au NPs is important. The nanoparticles should be small enough to avoid covering a large active layer area but large enough to create a shortcut between the two NCD grains.

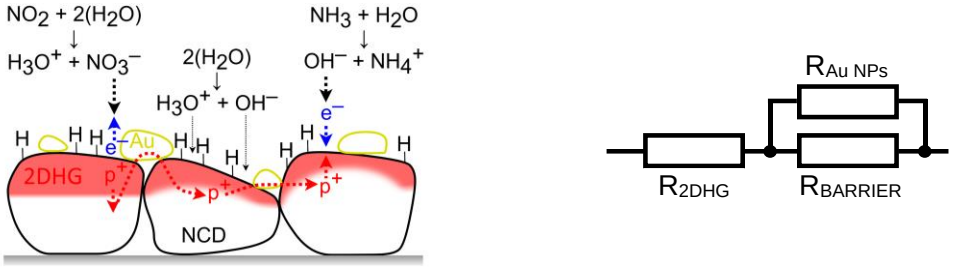

a) b)

Figure 3-10 a) gas interaction model and b) substitute circuit diagram of the H-NCD layer with Au NPs

3.3.6 MoS_2 / H-NCD heterostructure

The MoS_2 / H-NCD / SiO_2 / Si heterostructure exhibits dual conductivity, compromising p-type H-NCD [16] and n-type MoS_2 [114]. This distinctive material platform enables differentiation between reactions attributed to the various conductivity types in reducing and oxidizing gases [74]. Gas interaction is influenced by several factors, such as charge injection into / out of the depletion region, surface short-cuts from diamond or MoS_2 layers, modulation of the p-type diamond subsurface conductivity by MoS_2 (the gating-like effect), and the gradual degradation of the p-type diamond subsurface conductivity due to the deposition of MoS_2. Although the primary origin is still under investigation, the simplified model should be based on coupling two conduction paths via H-NCD or MoS_2 layers. The change in resistance of the MoS_2 / H-NCD layer is caused by chemical reactions forming counter ions on H-NCD and chemisorption of oxygen molecules on the solid surface of MoS_2 through chemical bonding with electron transfer. Notably, the gas-sensing properties depend highly on the charge carrier concentrations for both materials. **Figure 3-11** illustrates the gas sensing mechanism for two parallel-coupled layers. In the presence of oxidizing gas molecules (**Figure 3-11**), the number of charge carriers increases for H-NCD and decreases for MoS_2, resulting in charge carrier transport primarily occurring through the diamond rather than the MoS_2 layer. It is important to note that the charge carrier transport mainly prevails through the diamond layer rather than the MoS_2 layer. In contrast, this charge carrier transport is scattered at the diamond grain boundaries. Conversely, as shown in **Figure 3-11b**, the reducing gas decreases the number of charge carriers for H-NCD and increases it for MoS_2. These findings demonstrate the superior conductivity of MoS_2 over H-NCD in the presence of reducing gas. This leads to a decrease in the resistance of MoS_2 nanoflakes, enabling more charge carriers to flow through them with lower resistance than through the potential barriers between individual diamond grains. However, the total area coverage of H-NCD blocks the final charge transport. NH_3 has a higher total resistance than NO_2 due to the low surface coverage of MoS_2 nanoflakes and the significant impact of H-NCD on gas reduction. The MoS_2 / H-NCD heterostructure exhibits increased resistance in the presence of both reducing and oxidizing gases. This resistance change is characterized by two mutually

constrained components: 1) the horizontal component representing the current through the H-NCD and 2) the vertical component representing the current through the MoS_2 / H-NCD. The schematic illustration of this phenomenon is shown in **Figure 3-12**. The current, flowing through the p-n junction, tunnels through the space charge region (SCR). When gas is applied, the width of the SCR (w_{SCR}) increases, which in turn increases the resistance.

Equation (3-2) calculates the w_{SCR} from the concentrations of free charge carriers injected into the semiconductors by the gases. As described in the previous models, the concentration of free charge carriers in H-NCD (N_A) increases with oxidizing gas (NO_2) and decreases with reducing gas (NH_3). Conversely, for n-type MoS_2, the concentration (N_D) decreases with NO_2 and increases with NH_3. Next, these calculations also indicate that the SCR width increases for both types of gas, leading to a decrease in the number of charge carriers tunneling through the SCR and an increase in total resistance. Equation (3-3) calculates the current flowing through the H-NCD, measured by the interdigital electrodes, while the additional resistance accounts for the distance between adjacent fingers. The presence of oxidizing or reducing gas varies the dimensions of the 2DHG, causing an increase in the width of the SCR and a decrease in the cross-sectional area S. Consequently, the total length l increases, leading to an increase in the total resistance.

$$w_{SCR} = x_N + x_P = \sqrt{\frac{2\varepsilon_S V_D}{e}\left(\frac{N_A + N_D}{N_A N_D}\right)} \qquad (m) \tag{3-2}$$

$$Resistance\ R = \rho \cdot \frac{l}{S} \qquad (\Omega) \tag{3-3}$$

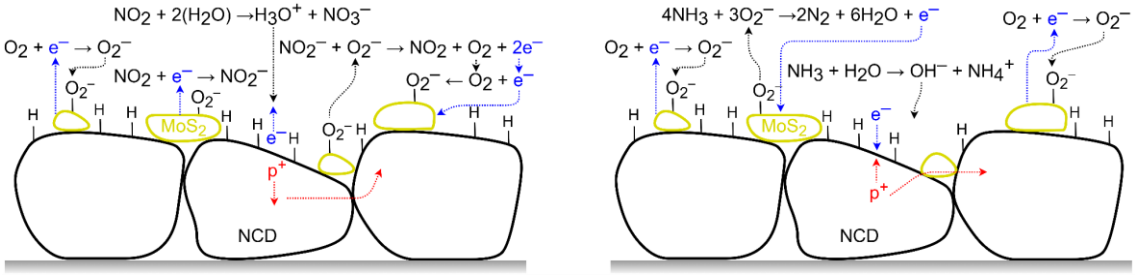

Figure 3-11 Schematic illustration of the gas sensing mechanism and charge transport for two parallel connected layers represented by MoS_2 nanoflakes and H-NCD exposed to the (left) oxidizing and (right) reducing gas

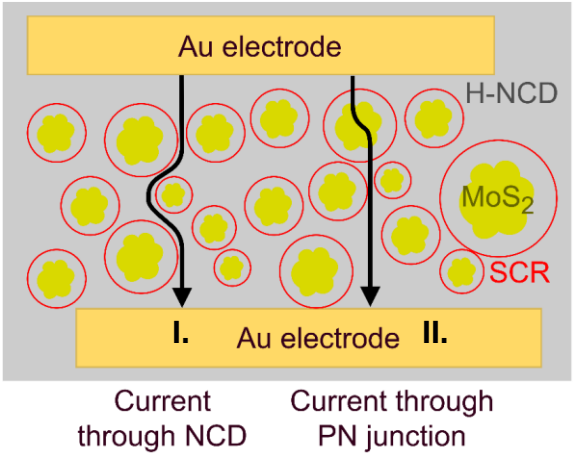

Figure 3-12 Schematic illustration of two ways (I. and II.) for the current flow between IDT electrodes, I. - horizontal flow through H-NCD, and II. – combined horizontal / vertical flow, horizontal through H-NCD and MoS_2 and vertical through MoS_2 / H-NCD heterostructure

3.3.7 SH-GO / H-NCD heterostructures

The SH-GO / H-NCD heterostructures utilize the gas interaction models, resulting in an enhanced gas response. Both materials exhibit p-type conductivity (2DHG), providing a unique material platform where similar conductivity types react analogously to reducing and oxidizing gases despite their different functional mechanisms. The gases are adsorbed into the water adlayer of the diamond-based gas sensor and then undergo electrolytic dissociation [16]. The SH-GO functionality depends on charge transfer between the oxide surface and analyte gas [47, 48, 55, 116].

Several factors may influence gas interaction, such as the surface injection of charge carriers, surface short-circuits between H-NCD and SH-GO, and modulation of diamond subsurface conductivity (transistor-like effect). The highly sensitive transition between materials is likely the primary reason for the high response to gases and vapors.

Near H-NCD, water molecules dissociate into OH^- and H_3O^+ ions due to electron transfer from the diamond. This phenomenon leads to the formation of a 2DHG subsurface layer in the diamond, which exhibits high resistivity. On the other hand, the SH-GO layer demonstrates p-type conductivity [117], characterized by a high concentration of holes and low resistance. When these two materials are combined, a thin film of OH^- and H_3O^+ ions remains between the layers. According to research, the combination of materials appears to achieve the optimal steady-state resistance value [3], superior to H-NCD's high resistance and SH-GO's low resistance. Furthermore, this combination produces the most sensitive part of the sensors, specifically the transition region between layers [47]. This region is susceptible and exhibits non-linear characteristics in response to the presence of the analyte and changes in free charge carriers' concentration in both layers. As illustrated in **Figure 3-13**, this structure appears to operate similarly to a transistor. The presence of gases can alter the number of holes and conductivity, which in turn can affect the potential and displacement of H_3O^+ and OH^-, and imbalance near the H-NCD can affect the concentration of holes in 2DHG. This mechanism is comparable to that of a metal-insulator-semiconductor field-effect transistor (MISFET), where

the conductivity of a two-dimensional hole gas (2DHG) is modulated by the potential or concentration of free charge carriers in the semi-hydrogenated graphene oxide (SH-GO) layer.

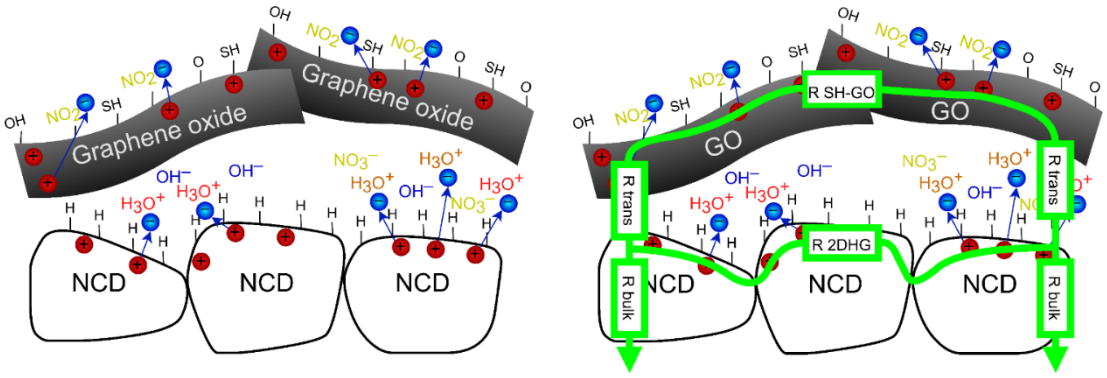

Figure 3-13 Gas interactions between the oxidizing gas (NO_2) and SH-GO / H-NCD heterostructure

4. Author's publication

4.1 Hydrogen-Terminated Diamond Surface as a Gas Sensor: A Comparative Study of its Sensitivities

Authors: Michal Kočí, Alexander Kromka, Adam Bouřa, Ondrej Szabó, Miroslav Husák

Journal: Sensors (IF 3.85)

DOI: 10.3390/s21165390

4.1.1 Abstract

A nanocrystalline diamond (NCD) layer is used as an active (sensing) part of a conductivity gas sensor. The properties of the sensor with an NCD with H-termination (response and time characteristic of resistance change) are measured by the same equipment with a similar setup and compared with commercial sensors, a conductivity sensor with a metal oxide (MO_X) active material (resistance change), and an infrared pyroelectric sensor (output voltage change) in this study. The deposited layer structure is characterized and analyzed by Scanning Electron Microscopy (SEM) and Raman spectroscopy. Electrical properties (resistance change for conductivity sensors and output voltage change for the IR pyroelectric sensor) are examined for two types of gases, oxidizing (NO_2) and reducing (NH_3). The parameters of the tested sensors are compared and critically evaluated. Subsequently, differences in the gas sensing principles of these conductivity sensors, namely H-terminated NCD and SnO_2, are described.

4.1.2 Summary

An NCD layer with H-termination was used as the active layer of the conductivity sensors. The crystallographic morphology of the prepared sensors with H-terminated NCD thin layers was confirmed by SEM and Raman spectroscopy. The SEM showed a continuous diamond layer on the electrode and glass, and the Raman spectra exhibit a sharp diamond peak for both parts. Fabricated H-terminated NCD sensors revealed sensor characteristics comparable to two commercial sensors in a similar testing setup after they were exposed to the reducing and oxidizing gases. The fabricated sensors have smaller dimensions and require a shorter amount of time for the first measurement, and thus they require less energy than the commercial TGS 826. Still, the TGS 826 sensor had a faster response to ammonia, due to a larger active surface area and a geometrical arrangement that allowed the gas access from all sides [22]. The infrared PY2055 sensor exhibits the highest selectivity, but it requires an IR source, which increases the consumption of electrical energy and demands on the size of the sensor system. It reacts only to nitrogen dioxide (selective gas), as declared in the manufacturer's datasheet [26]; this was confirmed by measurements. The lower value of the time response is due to the higher volume of the test chamber. Overall, it is possible to conclude that hydrogen-terminated diamond expands the family of wide-bandgap semiconductors, where gas detection is possible even at temperatures

of 100 °C. Moreover, its surface sensitivity can be enhanced not only by geometrical design (IDT distance) or surface morphology (nanorods) but also by using diamond-based composites, metal oxides, or transition metal dichalcogenide monolayers operated at low temperatures, with a reliable, reproducible response tuned to specific gas sensing applications.

4.1.3 Author's contribution

In this research, I was responsible for designing and implementing the measuring apparatus, testing the fabricated sensors with an H-NCD active layer, evaluating the measured data, comparing them with commercial gas sensors, and summarizing the interaction model between the gas and the H-NCD active layer, or SnO_2 (used as a commercial sensor), and writing and revising the paper. Furthermore, I contributed to the production of the H-NCD active layer. The co-authors collaborated on various aspects of the research, including in the preparation of the H-NCD active layer (Szabó), the design of the test apparatus (Bouřa) and the discussion of the measured results and the summarization of the gas interaction model (Kromka and Husák).

4.1.4 Paper's contributions

This research paper compares a new type of sensor, which uses H-NCD as the active layer, with commercially available sensors. The main objective of this paper is to demonstrate the superiority of the diamond-based gas sensor over other types of sensors, particularly metal oxides that use a similar detection principle. The article describes and compares three types of sensors: the commercial conductivity TGS 826, the infrared PY 2055, and the laboratory IDT with the H-NCD layer. This paper compares sensor properties, including the electrical response and power consumption, and finally presents the H-NCD gas interaction model. Additionally, it provides a detailed description of the experimental setup, including test chambers specifically designed for a particular application.

4.2 Enhanced gas sensing capabilities of diamond layers using Au nanoparticles

Authors: Michal Kočí, Ondrej Szabó, Gabriel Vanko, Miroslav Husák, Alexander Kromka

Journal: Diamond and Related Materials (IF 4.1)

DOI: 10.1016/j.diamond.2023.110218

4.2.1 Abstract

The nanocrystalline diamond (NCD) film reveals a unique combination of physical, chemical, and optoelectronic properties, which makes it a promising material for various sensing applications. To improve a gas sensor's response, selectivity, or reproducibility, its surface is often modified with specific terminations, functional groups or (bio)molecules, thin films, etc. In this work, the NCD surface modification was achieved by a) layer morphology variation using two different types of chemical vapor deposition (CVD) systems, b) top surface termination (H-NCD and O-NCD), and c) Au nanoparticles (Au NPs). The properties of each structure are measured, compared and subsequently evaluated. The electrical properties (resistance changes) are measured for two types of active gas (oxidizing gas NO_2 and reducing gas NH_3) in a temperature range from 22 °C to 125 °C. Neutral synthetic air (80 % nitrous and 20 % oxygen) was applied for flushing and resetting the sensors. Thin film fabrication, analysis (scanning electron microscopy), and measurement of electrical properties are described. Surface morphology greatly influences gas response because a large active surface area (higher roughness or 3D-like surface) enhances interaction with gas molecules. While the termination of the NCD with hydrogen is essential for the functionality of the gas sensor, the Au nanoparticles further enhanced the dynamic response of the sensor and magnitude.

4.2.2 Summary

The four active layers were designed, prepared and measured at three different temperatures for two active gases. The H-NCD active layers were prepared by two different systems (linear and focused plasma systems). A linear plasma system prepared H-NCD, O-NCD, and H-NCD / Au NPs hybrid structures. The measurements revealed that the hybrid structure exhibits preferable responses to exposed gas compared with H-NCD without Au NPs at all measured temperatures. The O-NCD had an almost unmeasurable response to both gases due to the absence of subsurface conductivity and is not appropriate for gas sensing applications. The H-NCD prepared in a focused plasma system can be grown quickly due to a high growth rate at a higher temperature. It was highly conductive, but the planar-like surface morphology revealed a smaller active area and thus a smaller reaction to gases. The H-NCD prepared in a linear plasma system produced bottom-up porous-like 3D diamond layers [118], which had sufficient gas responses. The response of 3D H-NCD was about 40 % for both gases at 125 °C but less than 1 % for lower temperatures. The Au NPs enhanced the responses at all temperatures by decreasing the steady-state resistance value. The response was about 50 % at 125 °C and about 5 % at 22 °C (room temperature). This hybrid structure allows a reduction in the working temperature and thus

power consumption for heating. Although the current for measuring the structure will increase, but it is negligible compared to the heating power. Our findings represent a promising alternative solution to the new class of gas sensors due to miniaturization and low power consumption compared to commercial MO_X gas sensors. Overall, one can conclude that the hybrid Au-NCD structure enhances the gas responses at high and room temperatures. However, the optimum concentration of Au NPs for these conditions must be found.

4.2.3 Author's contribution

In this research, I was responsible for testing the produced sensors with an NCD active layer with different modifications (O-terminated, H-terminated or with Au NPs), evaluating the measured data, comparing them with other gas sensors and summarizing the interaction model between the gas and H-NCD, and writing and revising the paper. I also participated in the preparation of active layers. Co-authors collaborated on various aspects of the project. The co-authors participated in preparing the H-NCD active layer (Szabó), discussing the measured results, and summarizing the gas interaction model (Vanko, Kromka and Husák).

4.2.4 Paper's contributions

This paper compares the responses of different modifications to H-NCD, including the decoration of H-NCD with Au NPs, which significantly reduced steady-state resistance. The article thoroughly investigates and describes four types of gas sensors based on a diamond active layer. The active layers were prepared using two different systems. The best sample was identified as H-NCD decorated with Au NPs, which greatly enhance gas sensing capabilities. A new measurement chamber was designed and fabricated for gas sensor testing, including its electrical properties and responses to different types of gases (reducing and oxidizing) and different temperatures. The article compares gas sensors prepared by different systems with different parameters. Furthermore, the article discusses the decoration of H-NCD with gold nanoparticles to increase gas responses significantly.

4.3 Improved Gas Sensing Capabilities of MoS2/Diamond Heterostructures at Room Temperature

Authors: Michal Kočí, Tibor Izsák, Gabriel Vanko, Michaela Sojková, Jana Hrdá, Ondrej Szabó, Miroslav Husák, Karol Végsö, Marian Varga, Alexander Kromka

Journal: ACS Applied Materials & Interfaces (IF 10.38)

DOI: 10.1021/acsami.3c04438

4.3.1 Abstract

Molybdenum disulfide (MoS_2) and nanocrystalline diamond (NCD) have attracted considerable attention due to their unique electronic structure and extraordinary physical and chemical properties in many applications, including sensor devices in gas sensing applications. Combining MoS_2 and H-terminated NCD (H-NCD) in a heterostructure design can improve the sensing performance due to their mutual advantages. In this study, the synthesis of MoS_2 and H-NCD thin films using appropriate physical / chemical deposition methods and their analysis in terms of gas sensing properties in their individual and combined forms are demonstrated. The sensitivity and time domain characteristics of the sensors were investigated for three gases: oxidizing NO_2, reducing NH_3 and neutral synthetic air. It was observed that the MoS_2 / H-NCD heterostructure-based gas sensor exhibits improved sensitivity to oxidizing NO_2 (0.157 %·ppm^{-1}) and reducing NH_3 (0.188 %·ppm^{-1}) gases compared to individual active materials (individual MoS_2 achieves responses of 0.018 %·ppm^{-1} for NO_2 and −0.0072 %·ppm^{-1} for NH_3, respectively almost no response for individual H-NCD at room temperature). Different gas interaction model pathways were developed to describe the current flow mechanism through the sensing area with / without heterostructure. The gas interaction model independently considers the influence of each material (chemisorption for MoS_2 and surface doping mechanism for H-NCD) as well as the current flow mechanism through the formed p-n heterojunction.

4.3.2 Summary

MoS_2 / Si, MoS_2 / SiO_2 / Si, H-NCD / SiO_2 / Si and MoS_2 / H-NCD / SiO_2 / Si structures were used to fabricate conductivity gas sensors and tested at room temperature (22 °C). The active layers of MoS_2 and H-NCD were analyzed by SEM, Raman spectroscopy, contact angle and GIWAXS measurements in their individual and combined forms. In terms of gas sensing properties, MoS_2 and H-NCD showed poor responses at room temperature. However, by combining them into a MoS_2 / H-NCD heterostructure, the gas sensing parameters were significantly improved. The formed heterostructure, consisting of the p-type subsurface conductive H-NCD layer and the n-type conductive MoS_2 nanoflakes, resulted in a synergistic effect that enhanced the gas response. While well-established interactions of gas molecules were experimentally validated for the particular form of MoS_2 and H-NCD layers, the MoS_2 / H-NCD heterostructure did not reveal such a specific behavior. The presented model pointed out the influence of the p-n junction, especially the geometrical variation of the space charge region, after its exposure to the tested gases. Unfortunately, this heterostructure abolishes the selectivity,

i.e., increased resistance was observed for oxidizing and reducing gases with different responses. However, the combination of a MoS_2 / H-NCD heterostructure with a single MoS_2 layer within one sensor chip seems to be a promising solution to overcome this limitation. This sensor can select the gas type on the MoS_2 according to a mark of resistance change and the gas concentration by the size resistance change of the MoS_2 / H-NCD. In conclusion, this article introduces a new class of conductivity gas sensors that can provide miniaturization and reduction of power consumption compared to commercial sensors. The presented TMD / diamond heterostructures could be very suitable for portable devices or energy-harvesting applications.

4.3.3 Author's contribution

In this research, I was responsible for testing the produced sensors combining MoS_2 and H-NCD materials, evaluating the measured data, comparing them with other gas sensors and designing a model of the interaction between the gas and the active layer, especially for a new heterostructure combining p-type and n-type semiconductor, which use the space charge region to improve gas response, and writing and revising the paper. Co-authors collaborated on various aspects of the project. The co-authors prepared a new heterostructure for gas sensors (Izsák, Sojková, Hrdá, Szabó and Végsö) and discussed the measured results and summarized the gas interaction model (Izsák, Vanko, Husák, Varga and Kromka).

4.3.4 Paper's contributions

This research paper investigates and describes an innovative heterostructure for gas sensors that combines H-NCD and MoS_2 to enhance gas sensing abilities. The heterostructure is compared with individual H-NCD and MoS_2 layers. The electrical properties of these different materials, including their responses to different concentrations of reducing and oxidizing gases and time characteristics, are then tested using specialized equipment designed for testing gas sensors. The text confidently describes the synthesis processes for each active layer, characterizes the layers, and presents an experimental setup with testing chambers. Additionally, it compares electrical responses and gas interaction models. The model emphasizes the significant impact of the p-n junction, specifically highlighting changes in the geometry of the space charge region when exposed to tested gases. Finally, the results are critically evaluated.

4.4 Gas sensors based on diamond heterostructures for air quality monitoring

Authors: Michal Kočí, Ondrej Szabó, Tibor Izsák, Michaela Sojková, Marcin Godzierz, Paweł Wróbel, Miroslav Husák, Alexander Kromka

Journal: Conference Proceedings - NANOCON 2023

DOI: 10.37904/nanocon.2023.4785

4.4.1 Abstract

Currently, great emphasis is placed on air quality and the presence of pollutants, whether on toxic substances (NH_3 or CO), substances that reduce the quality of life (CO_2) or chemical vapors from industries (acetone or ethanol). Attention is therefore focused on new gas-sensing materials enabling detection even at low (up to room) temperatures with sufficient response and short reaction time.

Here, we investigate the suitability of hydrogen-terminated nanocrystalline diamond (H-NCD) films and their heterostructures with molybdenum disulfide (MoS_2), graphene oxide (GO), reduced GO (rGO), thiol functionalized GO (SH-GO), or gold nanoparticles (Au NPs) for gas sensing applications. Electrical properties are measured for oxidizing gas NO_2, reducing gas NH_3, and chemical vapor of ethanol (C_2H_5OH), and at temperatures varied from room temperature to 125 °C. All tested gases were used with a concentration of up to 100 ppm. Synthetic air is used as the flushing gas. The measured parameters of the tested sensors are compared, both with each other and with commercial sensors, and subsequently evaluated. In contrast to the individual forms of employed materials with limited response to the exposed gases, the H-NCD heterostructures revealed better sensing properties. In particular, the Au NPs / H-NCD heterostructures revealed a higher response at 125 °C in contrast to H-NCD, MoS_2 / H-NCD had quite good response even at room temperature and GO / H-NCD revealed high sensitivity to chemical vapor, which further improved for the SH-GO / H-NCD.

4.4.2 Summary

The newly introduced heterostructures H-NCD and the second material (MoS_2, GO, rGO, SH-GO or Au NPs) were designed, fabricated, and tested. The measurements revealed that most heterostructures exhibit preferable responses to exposed gas compared with individual materials at high and room temperatures. Even, the responses of some heterostructures are comparable with commercial gas sensors at 22 °C.

At a high temperature of 125 °C, all heterostructures and individual materials respond very well. At these conditions, the best responses exhibited SH-GO / H-NCD and Au NPs / H-NCD heterostructures with responses over 47 % for all tested gases, which are well comparable with commercial sensors. The power consumption for our heater should be still optimized, but it is much lower than the power needed for commercial sensors. For room temperature applications, individual materials and some heterostructures have very low, almost

immeasurable, responses. The best combination of materials with good responses is SH-GO / H-NCD and MoS_2 / H-NCD. These sensors have a response of over 15 % for all tested gases. These high responses are attributed to the optimum steady-state resistance, further enhanced by the synergistic effect at the interface of active materials.

In conclusion, our findings represent a promising alternative solution as the new class of gas sensors suitable for portable or energy-harvesting applications due to miniaturization and low power consumption. For now, however, the reproducibility of sensor production technology needs to be scaled up and optimized to meet industrial uses.

4.4.3 Author's contribution

The research effectively summarizes and compares fabricated sensors based on H-NCD, MoS_2, GO, rGO, SH-GO, Au NPs, and their heterostructures. I was responsible for evaluating and comparing the measured data and proposing further improvements. The co-authors provided valuable input during the discussion and contributed to developing the subsequent research and improving gas sensors.

4.4.4 Paper's contributions

This article presents a comparison of conductive gas sensors based on various materials, including H-NCD, MoS_2, GOs, and heterostructures such as MoS_2 / H-NCD, GO / H-NCD, rGO / H-NCD, SH-GO / H-NCD, and Au NPs / H-NCDs. This comparison discusses the differences in gas sensor responses at different temperatures. The sensors were tested at both room temperature (22°C) and elevated temperature (125°C). The results show that the fabricated heterostructures perform better than the individual materials. These findings were used to compare responses at different temperatures and identify the most appropriate replacement for commercial conductivity sensors that operate at high temperatures.

4.5 Highly sensitive gas and ethanol vapor sensors based on carbon heterostructures for room temperature detection

Authors: Michal Kočí, Pawel S. Wrobel, Marcin Godzierz, Ondrej Szabó, Slavka Pusz, Štěpán Potocký, Miroslav Husák, Alexander Kromka

Prepared and submitted article

4.5.1 Abstract

Graphene oxides (GOs) and hydrogen-terminated nanocrystalline diamond (H-NCD) have attracted considerable attention due to their unique electronic structure and extraordinary physical and chemical properties in many applications, including gas sensing. At present, much attention is paid to air quality and the presence of pollutants due to toxicity (NH_3, NO_2 or CO), harm to the quality of life (CO_2) or volatile organic compounds (VOC) from industry (acetone or ethanol). Attention is therefore focused on new gas-sensing materials that can detect at low temperatures (down to room temperature) with sufficient sensitivity and short response times. The heterostructure combining GOs and H-NCD improves the sensing performance. In this study, the synthesis of GOs (graphene oxide (GO), reduced graphene oxide (rGO) and thiol-functionalized graphene oxide (SH-GO)) and H-NCD thin films using appropriate physical/chemical deposition methods and their analysis in terms of gas sensing properties in their individual and combined forms are demonstrated. Responses to the presence of gases are measured for NO_2, NH_3, and ethanol vapor at room temperature around 22 °C. All tested gases were used at concentrations up to 100 ppm. Synthetic air is used as a carrier and purge gas. It was observed that the SH-GO / H-NCD achieves the best response for ethanol vapor, more than 630 %, in contrast to individual forms of materials that showed limited response to exposed gases. SH-GO / H-NCD heterostructures exhibited excellent sensing properties. The gas interaction model considers the effect of each material independently and identifies the probable primary mechanism within the heterostructure.

4.5.2 Summary

Conductive gas sensors based on carbon structures were fabricated and successfully tested against oxidizing and reducing gases (NO_2 and NH_3, resp.) and ethanol vapor in the 10 to 100 ppm range at room temperature (21.5 ± 0.5 °C). High selectivity was achieved by proper selection of the active/sensing layer. Particularly, GO, rGO, SH-GO and their heterostructures with H-NCD were studied. Regarding gas sensing properties, H-NCD and GOs showed poor to satisfactory responses at room temperature. However, combining them into a heterostructure significantly improved the gas sensing parameters, especially for SH-GO and H-NCD heterostructure. The active layers were also analyzed by SEM and Raman spectroscopy to verify the morphology and chemical structure of individual materials and their heterostructures. Regarding gas sensing properties, GO, rGO and SH-GO responded well to ethanol vapor. The formation of heterostructure with H-NCD improved mild responses to NH_3 and NO_2.

The best results/sensitivity was achieved for the combination of SH-GO and H-NCD. Such a heterostructure enhanced the response 40 times for ethanol vapor, 82 times for NH_3 and 27 times for NO_2 compared to individual materials. Finally, this article presents an innovative model explaining the detection mechanism for the SH-GO / H-NCD heterostructure. The formed heterostructure comprising p-type materials created a synergistic effect that enhanced the sensor response. The most important part of the heterostructure is the transition interlayer between the materials, which most affects the presence of the gas. This part is very sensitive with nonlinear characteristics to the gas's presence and the change in free change carriers' concentration in both layers. The results are promising for detecting various gases, including those used (NO_2, NH_3 and C_2H_5OH). In conclusion, the main advantages of this new structure are its small dimensions, the diameter of the active part of only 3.5 mm, functionality at room temperature, excellent response to ethanol vapor, and excellent responses to tested and industrially essential gases. The mentioned characteristics of the sensor can be advantageously used in low-power, portable and/or sensor-node applications.

4.5.3 Author’s contribution

In this research, I was responsible for the preparation of heterostructures combining GOs and H-NCD materials using the drop-casting method, testing the manufactured sensors, evaluating the measured data, comparing them with other gas sensors, and designing an innovative model of the interaction between the gas and the active layer, especially for the new heterostructure combining two semiconductors exhibiting p-type conductivity, and writing and revising the paper. The co-authors prepared the GOs material (Wrobel), the H-NCD material (Szabó) and discussed the measured results and the gas interaction model (Godzierz, Pusz, Potocký, Husák and Kromka).

4.5.4 Paper’s contributions

This paper describes and investigates a new type of heterostructure that combines two carbon-based materials, H-NCDs and GOs, to improve responses to gases, particularly to the chemical vapor, ethanol. The electrical properties of these materials, such as their responses to various concentrations of reducing and oxidizing gases and time characteristics, are subsequently evaluated using the optimized gas sensor testing setup. The article compares the designed and manufactured heterostructures and other laboratory-prepared sensors, as well as individual materials. It provides detailed information on the preparation procedures of individual materials and heterostructures, focusing on the gas interaction between these materials and gases. The model highlights the significant impact of the transition region between the two materials, which results in the modulation of the p-type conductivity. Finally, the results are critically evaluated.

5. Conclusion

The increasing demand for gas sensors and air quality monitoring necessitates the development of novel sensor types and active layer materials. This requirement has led to rapid improvements in fabrication technology and procedures, with new methods and machinery being developed for industrial and scientific applications.

This thesis investigated gas sensors and materials suitable for conductivity type. The text discusses the gas sensors, focusing on carbon-based materials, including diamond and graphene oxide, and TMD materials, such as MoS_2. Diamond layers are often used in biosensors due to their biocompatibility and non-reactivity with most materials. Recent advancements in diamond CVD synthesis and exploration of potential applications have been noted. This thesis utilized three different gas-sensitive materials to fabricate heterostructures, improving gas sensing parameters. The findings were summarized, published in impacted journals, and presented at international conferences.

The thesis explored six types of gas sensors:

a. Individual material forms
   (a) Diamond-based gas sensor utilizing an H-NCD layer with an IDT structure
   (b) TMD-based gas sensor utilizing MoS_2 with an IDT structure
   (c) Graphene oxide (GO)-based sensors utilizing various modifications
b. Novel heterostructures
   (a) Hybrid structure utilizing diamond with gold nanoparticles
   (b) MoS_2/H-NCD heterostructure
   (c) GO/H-NCD heterostructures (rGO/H-NCD and SH-GO/H-NCD)

The first fabricated and characterized sensor was the diamond-based gas sensor utilizing an H-terminated NCD layer with an IDT structure for gas sensing. This sensor demonstrated the ability to detect and differentiate between oxidizing and reducing gases. The primary challenge in parameter measurement was the variability in sensor responses due to slight differences in thin film nucleation, deposition, and film character. A series of sensors were fabricated and classified into categories based on measured data to address this issue. The higher power consumption of the heater, necessitated by the sensor's inability to operate at low temperatures, remains a subject for further research and development. A simplified model based on the measured results was proposed, and the findings were published in Sensors, 2021.

The second type was a TMD-based gas sensor employing MoS_2 with IDT structure as its active material. The MoS_2 layers were prepared in a two-step process. Firstly, a thin layer of Mo was deposited at room temperature using DC magnetron sputtering. Next, the pre-deposited Mo layers were sulfurized in a custom-designed CVD chamber. The Mo layer was annealed in sulfur vapors at a high temperature in an N_2 atmosphere at ambient pressure. In this method, the substrate and sulfur powder were placed together in the center of the furnace to ensure equal temperature during growth. This approach differs from the standard CVD method, which typically uses a two-zone furnace with different temperatures for the sulfur powder and Mo substrate. The sensor exhibited reactions that were opposite to oxidizing and reducing gases compared to H-NCD, which is attributed to the different semiconductor types (p-type 2DHG of

NCD and n-type of MoS_2). While the sensor revealed full functionality even at room temperature, the sensor response was low. The results have been published in the journal ACS Applied Materials and Interfaces, 2023.

The third type of sensor utilized GO with various modifications to enhance gas responses. GO was prepared using a modified Hummers method from graphite powder. The GO reduction resulting in rGO was carried out using ascorbic acid. SH-GO was synthesized through a multi-step process involving phosphorus sulfide treatments. All graphene-based layers (GO, rGO, and SH-GO) demonstrated favorable responses to ethanol vapors, exhibiting p-type semiconductor behavior like H-NCD. These sensors can be operated at room temperature, albeit with potentially lower response rates. The results have been submitted to the journal.

The fourth type was a modified diamond sensor with Au NPs. Au NPs were prepared by evaporating a thin layer of Au on H-NCD, followed by annealing in hydrogen microwave plasma. This treatment resulted in the formation of nanoparticles (droplets) with diameters ranging from 5 to 40 nm on the diamond surface. Au NPs were chosen for their chemical stability and minimal impact on the H-NCD active layer. The Au NPs enhanced the responses at all temperatures by decreasing the steady-state resistance. This hybrid heterostructure potentially decreases the working temperature and reduces power consumption for heating. While measurement current may increase, it is negligible compared to the heating power. The results have been published in the journal Diamond and Related Materials, 2023.

The fifth type combines TMD and H-NCD materials into MoS_2 / H-NCD heterostructure. This combination significantly improved the gas sensing parameters. The p-type subsurface conductive H-NCD layer and the n-type conductive MoS_2 nanoflakes resulted in a synergistic effect that enhanced the gas response. However, the heterostructure abolishes the selectivity to the reducing and oxidizing gas, i.e., increasing resistance for both gases with different response magnitudes. However, it is worth noting that the combination of two different sensors has been found to overcome this limitation. The MoS_2 / H-NCD heterostructure detects the concentration by the resistance change, while the second sensor (MoS_2 or H-NCD) identified the gas type based on a resistance change marker. The sensor fabrication process involves preparing MoS_2 on an H-NCD substrate. The reproducibility of the fabrication technology is sufficient, as demonstrated by two sensors with similar responses. These results were published in the journal ACS Applied Materials and Interfaces in 2023.

The last sixth type combines different GOs with H-NCD materials represented by the rGO / H-NCD and SH-GO / H-NCD heterostructures. These heterostructures significantly improved the gas sensing parameters, especially for the SH-GO / H-NCD heterostructure. This heterostructure enhanced the response 40 times for ethanol vapor, 82 times for NH_3, and 27 times for NO_2. The p-type materials created a synergistic effect that enhanced the gas response. The interface of these materials is crucial, affecting the analyte presence and free charge carrier concentration in both layers. The results have been submitted to the journal.

In conclusion, this thesis contributes to the advancement of gas-sensing technology by exploring novel materials and heterostructures. The findings provide valuable insights for developing more efficient and sensitive gas sensors with potential environmental monitoring, industrial safety, and healthcare applications. Future work should focus on addressing challenges

such as reproducibility and power consumption while exploring the miniaturization potential of wide bandgap semiconductors and 2D material-based gas sensors.

5.1 My scientific contribution

My scientific contribution to the presented research activities is the implementation and characterization of new and unique materials and heterostructures in the field of diamond-based gas sensors. I have focused my research on developing heterostructure gas sensors based on utilizing synergistic effects to increase response and reduce operating temperature. This was achieved by applying the well-known electrical and electromechanical gas sensing principles, enhanced by the extraordinary properties of thin films. Well-established film preparation synthesizes were employer to create new heterostructures that revealed improved room-temperature gas sensing properties and reduced power consumption.

The first three types of sensors, namely H-NCDs, TMDs, and GOs, are well-understood materials commonly used in various electronic applications, including sensors for environmental variables such as humidity and light. Based on the gas-sensing measurements, I concluded that these individual materials are unsuitable for gas sensors operating at room temperature. At elevated temperatures, they achieved sufficient responses to the testing gases. In this thesis, I employed them to verify the functionality, gas response, fabrication process tuning and to measure responses to compare new heterostructures. I also used them to design, implement, and parameterize the apparatus for testing responses to various gases and chemical vapors.

Based on my knowledge and experience gained from individual materials (H-NCD, MoS_2, rGO and GO-SH), with support from colleagues, I have designed and realized several innovative heterostructures combining two different materials to improve the responses, particularly at room temperature. Namely, these include Au NPs / H-NCD, MoS_2 / H-NCD, rGO / H-NCD and SH-GO / H-NCD. All studies have proven that the fabricated heterostructures perform better-sensing properties than the individual materials. These findings indicate future ways to replace commercial conductivity sensors operating at high temperatures.

In my thesis and already published research articles, I have focused on a detailed description of the preparation of the material structures, their characterization by various methods (SEM, Raman, etc.), and mainly on the gas-sensing measurements used for the description and understanding of the interaction models between gases and active layers. This comprehensive approach is found as crucial for further development and improvement of these structures for gas sensing applications. In presenting the interaction models, I have tried not only to describe everything in the text, but also to illustrate the possible paths graphically and, where appropriate, with the mathematical equations and calculations.

5.2 Prospects and future work

During my Ph.D. work, several promising research directions were identified:

- A new electrode structure utilizes 3 electrodes: two for IDT and one as a Gate electrode. The gate electrode under the IDT and active layer modifies and/or tunes the response to different gases. This solution may restore selectivity without increasing power consumption because only an electrical charge is needed, not an electrical current.

- A new sensor platform consisting of two or more heterostructures or hybrid-structures integrated and miniaturized at one substrate. This sensor platform would exhibit different responses to the same gases, enabling or offering accurate gas type identification, concentration determination, or the gas mixture's entire composition using a suitable evaluation algorithm.

- Implement a hybrid sensor combining different detection methods, such as a conductivity sensor with an IDT structure and a mass QCM sensor, into one sensor device. This approach would allow simultaneous evaluation of the conductivity and mass properties of a gas or gas mixture. Careful design is necessary to ensure the sensor types do not interfere with each other and potentially enhance each other's properties.

6. References

[1] K. Štulík, J. Barek, J. Janata, V. Král, M. Kronďák, and M. Šťastný, *SENZORY: General Aspects of Chemical Sensing*. VŠCHT Praha, 2007.

[2] Sze, S. M. and Ng, K. K., *Physics of semiconductor devices*, 3rd ed. Hoboken: Wiley, 2007.

[3] Fraden, J., *Handbook of modern sensors: Physics, designs, and applications*, 3rd ed. New York: Springer, 2004.

[4] Bonavita, A., Caddemi, A., Donato, N., Accordino, P., Galvagno, S., Neri, G., and IEEE, "Electrical characterization and modeling of thin-film humidity sensors," in pp. 673–676.

[5] Seekaew, Y., Phokharatkul, D., Wisitsoraat, A., and Wongchoosuk, C., "Highly sensitive and selective room-temperature NO 2 gas sensor based on bilayer transferred chemical vapor deposited graphene," *Applied Surface Science*, vol. 404, pp. 357–363, 2017, doi: 10.1016/j.apsusc.2017.01.286.

[6] Valentini, L., Armentano, I., Kenny, J. M., Cantalini, C., Lozzi, L., and Santucci, S., "Sensors for sub-ppm NO2 gas detection based on carbon nanotube thin films," *Appl. Phys. Lett.*, vol. 82, no. 6, pp. 961–963, 2003, doi: 10.1063/1.1545166.

[7] Dhall, S., Mehta, B. R., Tyagi, A. K., and Sood, K., "A review on environmental gas sensors: Materials and technologies," *Sensors International*, vol. 2, p. 100116, 2021, doi: 10.1016/j.sintl.2021.100116.

[8] E. M. Campo, E. A. Dobisz, and L. A. Eldada, Eds., *Nanoengineering: Fabrication, Properties, Optics, and Devices XIV*: SPIE, Aug. 2017 - Aug. 2017.

[9] Gao, J., Wu, H., Zhou, J., Yao, L., Zhang, G., Xu, S., Xie, Y., Li, L., and Shi, K., "Mesoporous In 2 O 3 nanocrystals: synthesis, characterization and NO x gas sensor at room temperature," *New J. Chem.*, vol. 40, no. 2, pp. 1306–1311, 2016, doi: 10.1039/C5NJ02214B.

[10] Rai, S. K., Yang, F., Kao, K. W., Agarwal, A., Gwo, S. J., and Yeh, J. A., "Pentacene Coated Atop of Ultrathin InN Gas Sensor Device for the Selective Sensing of Ammonia Gas for Liver Malfunction Application," *ECS JOURNAL OF SOLID STATE SCIENCE AND TECHNOLOGY*, vol. 7, no. 7, Q3208-Q3214, 2018, doi: 10.1149/2.0301807jss.

[11] Raju, P. and Li, Q., "Review—Semiconductor Materials and Devices for Gas Sensors," *J. Electrochem. Soc.*, vol. 169, no. 5, p. 57518, 2022, doi: 10.1149/1945-7111/ac6e0a.

[12] Nasri, A., Jaleh, B., Daneshnazar, M., and Varma, R. S., "Sensing Properties of g-C3N4/Au Nanocomposite for Organic Vapor Detection," *Biosensors*, vol. 13, no. 3, 2023, doi: 10.3390/bios13030315.

[13] Nihal, Sharma, R., Kaur, N., Sharma, M., Choudhary, B. C., and Goswamy, J. K., "Improved room temperature ethanol vapors sensing using silver nanoparticles decorated graphitic carbon nitride (Ag-gCN) nanocomposite," *Materials Letters*, vol. 342, p. 134343, 2023, doi: 10.1016/j.matlet.2023.134343.

[14] European Road Safety Observatory (ERSO), "Monitoring Road Safety in the EU: towards a comprehensive set of Safety Performance Indicators: 2018," 2018. Accessed: Sep. 20 2023. [Online]. Available: https://road-safety.transport.ec.europa.eu/system/files/2021-07/ersosynthesis2018-performanceindicators.pdf

[15] Wang, C., Yin, L., Zhang, L., Xiang, D., and Gao, R., "Metal Oxide Gas Sensors: Sensitivity and Influencing Factors," *Sensors*, vol. 10, pp. 2088–2106, 2010, doi: 10.3390/s100302088.

[16] Helwig, A., Mueller, G., Garrido, J. A., and Eickhoff, M., "Gas sensing properties of hydrogen-terminated diamond," *SENSORS AND ACTUATORS B-CHEMICAL*, vol. 133, no. 1, pp. 156–165, 2008, doi: 10.1016/j.snb.2008.02.007.

[17] Gurbuz, Y., Kang, W. P., Davidson, J. L., Kinser, D. L., and Kerns, D. V., "Diamond microelectronic gas sensors," *SENSORS AND ACTUATORS B-CHEMICAL*, vol. 33, 1-3, pp. 100–104, 1996.

[18] Abedi, S. P., Rahmani, M. B., and Rezaii, F., "α-Fe 2 O 3 thin films deposited by a facile spray pyrolysis technique for enhanced ethanol sensing," *Phys. Scr.*, vol. 98, no. 5, p. 55901, 2023, doi: 10.1088/1402-4896/acc6a0.

[19] Ananthi, S., Kavitha, M., Balamurugan, A., Ranjith Kumar, E., Magesh, G., Abd El-Rehim, A. F., Srinivas, C., Anilkumar, P., Suryakanth, J., and Sharmila Rahale, C., "Synthesis, analysis and characterization of camellia sinensis mediated synthesis of NiO nanoparticles for ethanol gas sensor applications," *Sensors and Actuators B: Chemical*, vol. 387, p. 133742, 2023, doi: 10.1016/j.snb.2023.133742.

[20] Gouveia, J. D., Novell-Leruth, G., Viñes, F., Illas, F., and Gomes, J. R., "The Ti2CO2 MXene as a nucleobase 2D sensor: A first-principles study," *Applied Surface Science*, vol. 544, p. 148946, 2021, doi: 10.1016/j.apsusc.2021.148946.

[21] FIGARO USA, INC., *TGS 826 - for the Detection of Ammonia: Product information.* [Online]. Available: https://www.figarosensor.com/product/docs/TGS%20826%20%2805_04%29.pdf (accessed: Dec. 22 2020).

[22] FIGARO USA, INC., *FIGARO GAS SENSORS: 1-Series and 8-Series: Product catalogue.* [Online]. Available: https://www.figarosensor.com/product/docs/figaro_tgs_serien.pdf (accessed: Feb. 1 2020).

[23] Davydova, M., Kulha, P., Laposa, A., Hruska, K., Demo, P., and Kromka, A., "Gas sensing properties of nanocrystalline diamond at room temperature," *BEILSTEIN JOURNAL OF NANOTECHNOLOGY*, vol. 5, pp. 2339–2345, 2014, doi: 10.3762/bjnano.5.243.

[24] Sharma, A., Tomar, M., and Gupta, V., "SnO2 thin film sensor with enhanced response for NO2 gas at lower temperatures," *SENSORS AND ACTUATORS B-CHEMICAL*, vol. 156, no. 2, pp. 743–752, 2011, doi: 10.1016/j.snb.2011.02.033.

[25] Dinh, T.-V., Choi, I.-Y., Son, Y.-S., and Kim, J.-C., "A review on non-dispersive infrared gas sensors: Improvement of sensor detection limit and interference correction," *SENSORS AND ACTUATORS B-CHEMICAL*, vol. 231, pp. 529–538, 2016, doi: 10.1016/j.snb.2016.03.040.

[26] Pyreos Limited, *Thin Film Pyroelectric Dual Channel Sensor: Product information.* [Online]. Available: https://pyreos.com/wp-content/uploads/2020/11/Pyreos-Analog-TO-Two-Channels.pdf (accessed: Dec. 22 2020).

[27] Sato, H. and Kasu, M., "Electronic properties of H-terminated diamond during NO2 and O-3 adsorption and desorption," *DIAMOND AND RELATED MATERIALS*, vol. 24, pp. 99–103, 2012, doi: 10.1016/j.diamond.2011.12.004.

[28] Adachi, S., *Properties of group-IV, III-V and II-VI semiconductors*. Hoboken: Wiley, 2005.

[29] Liu, A., Lv, S., Jiang, L., Liu, F., Zhao, L., Wang, J., Hu, X., Yang, Z., He, J., Wang, C., Yan, X., Sun, P., Shimanoe, K., and Lu, G., "The gas sensor utilizing polyaniline/ MoS2 nanosheets/ SnO2 nanotubes for the room temperature detection of ammonia," *SENSORS AND ACTUATORS B-CHEMICAL*, vol. 332, 2021, doi: 10.1016/j.snb.2021.129444.

[30] Tan, Y. and Zhang, J., "Highly sensitive ethanol gas sensors based on Co-doped SnO2 nanobelts and pure SnO2 nanobelts," *Physica E: Low-dimensional Systems and Nanostructures*, vol. 147, p. 115604, 2023, doi: 10.1016/j.physe.2022.115604.

[31] Joshi, R. K., Weber, J. E., Hu, Q., Johnson, B., Zimmer, J. W., and Kumar, A., "Carbon monoxide sensing at room temperature via electron donation in boron doped diamond films," *SENSORS AND ACTUATORS B-CHEMICAL*, vol. 145, no. 1, pp. 527–532, 2010, doi: 10.1016/j.snb.2009.12.070.

[32] Wang, Y., Zhao, Z., Sun, Y., Li, P., Ji, J., Chen, Y., Zhang, W., and Hu, J., "Fabrication and gas sensing properties of Au-loaded SnO2 composite nanoparticles for highly sensitive hydrogen detection," *SENSORS AND ACTUATORS B-CHEMICAL*, vol. 240, pp. 664–673, 2017, doi: 10.1016/j.snb.2016.09.024.

[33] Kannan, P. K., Late, D. J., Morgan, H., and Rout, C. S., "Recent developments in 2D layered inorganic nanomaterials for sensing," *Nanoscale*, vol. 7, no. 32, pp. 13293–13312, 2015, doi: 10.1039/c5nr03633j.

[34] Kim, S., Konar, A., Hwang, W.-S., Lee, J. H., Lee, J., Yang, J., Jung, C., Kim, H., Yoo, J.-B., Choi, J.-Y., Jin, Y. W., Lee, S. Y., Jena, D., Choi, W., and Kim, K., "High-mobility and low-power thin-film transistors based on multilayer MoS2 crystals," *Nature communications*, vol. 3, p. 1011, 2012, doi: 10.1038/ncomms2018.

[35] Yu, X., Chen, X., Ding, X., Yu, X., Zhao, X., and Chen, X., "Facile fabrication of flower-like MoS2/nanodiamond nanocomposite toward high-performance humidity detection," *SENSORS AND ACTUATORS B-CHEMICAL*, vol. 317, 2020, doi: 10.1016/j.snb.2020.128168.

[36] Akbari, E., Jahanbin, K., Afroozeh, A., Yupapin, P., and Buntat, Z., "Brief review of monolayer molybdenum disulfide application in gas sensor," *PHYSICA B-CONDENSED MATTER*, vol. 545, pp. 510–518, 2018, doi: 10.1016/j.physb.2018.06.033.

[37] Yu, X., Li, Y., Cheng, J., Liu, Z., Li, Q., Li, W., Yang, X., and Xiao, B., "Monolayer Ti_2CO_2: A Promising Candidate for NH_3 Sensor or Capturer with High Sensitivity and Selectivity," *ACS applied materials & interfaces*, vol. 7, no. 24, pp. 13707–13713, 2015, doi: 10.1021/acsami.5b03737.

[38] Hantanasirisakul, K. and Gogotsi, Y., "Electronic and Optical Properties of 2D Transition Metal Carbides and Nitrides (MXenes)," *ADVANCED MATERIALS*, vol. 30, no. 52, 2018, doi: 10.1002/adma.201804779.

[39] Shaik, M., Rao, V. K., Gupta, M., Murthy, K. S. R. C., and Jain, R., "Chemiresistive gas sensor for the sensitive detection of nitrogen dioxide based on nitrogen doped graphene nanosheets," *RSC Adv.*, vol. 6, no. 2, pp. 1527–1534, 2016, doi: 10.1039/C5RA21184K.

[40] Armano, A. and Agnello, S., "Two-Dimensional Carbon: A Review of Synthesis Methods, and Electronic, Optical, and Vibrational Properties of Single-Layer Graphene," *C-JOURNAL OF CARBON RESEARCH*, vol. 5, no. 4, 2019, doi: 10.3390/c5040067.

[41] Peng, X., Chu, J., Wang, L., Duan, S., and Feng, P., "Boron-doped diamond nanowires for CO gas sensing application," *Sensors and Actuators B: Chemical*, vol. 241, pp. 383–389, 2017, doi: 10.1016/j.snb.2016.10.009.

[42] Naje, A. N., Ibraheem, R. R., and Ibrahim, F. T., "Parametric Analysis of NO2 Gas Sensor Based on Carbon Nanotubes," *Photonic Sens*, vol. 6, no. 2, pp. 153–157, 2016, doi: 10.1007/s13320-016-0304-1.

[43] Morgan, J. W. and Anders, E., "Chemical Composition of Earth, Venus, and Mercury," *Proceedings of the National Academy of Sciences of the United States of America*, vol. 77, no. 12, pp. 6973–6977, 1980.

[44] Dariyal, P., Sharma, S., Chauhan, G. S., Singh, B. P., and Dhakate, S. R., "Recent trends in gas sensing via carbon nanomaterials: outlook and challenges," *Nanoscale advances*, vol. 3, no. 23, pp. 6514–6544, 2021, doi: 10.1039/D1NA00707F.

[45] M. Jawaid, Ed., *Functionalized graphene nanocomposites and their derivatives: Synthesis, processing and applications*. Amsterdam Netherlands: Elsevier, 2019.

[46] Ding, L., Qin, Z., Dou, Z., Shen, Y., Cai, Y., Zhang, Y., and Zhou, Y., "Morphology-promoted synergistic effects on the sensing properties of polyaniline ultrathin layers on reduced graphene oxide sheets for ammonia and formaldehyde detection," *J Mater Sci*, vol. 53, no. 10, pp. 7595–7608, 2018, doi: 10.1007/s10853-018-2109-7.

[47] Drewniak, S., Drewniak, Ł., and Pustelny, T., "Mechanisms of NO2 Detection in Hybrid Structures Containing Reduced Graphene Oxide: A Review," *Sensors (Basel, Switzerland)*, vol. 22, no. 14, 2022, doi: 10.3390/s22145316.

[48] Pham, C. V., Eck, M., and Krueger, M., "Thiol functionalized reduced graphene oxide as a base material for novel graphene-nanoparticle hybrid composites," *Chemical Engineering Journal*, vol. 231, pp. 146–154, 2013, doi: 10.1016/j.cej.2013.07.007.

[49] Zhu, X., Liu, Q., Zhu, X., Li, C., Xu, M., and Liang, Y., "Reduction of Graphene Oxide Via Ascorbic Acid and Its Application for Simultaneous Detection of Dopamine And Ascorbic Acid," *International Journal of Electrochemical Science*, vol. 7, no. 6, pp. 5172–5184, 2012, doi: 10.1016/S1452-3981(23)19612-X.

[50] Schedin, F., Geim, A. K., Morozov, S. V., Hill, E. W., Blake, P., Katsnelson, M. I., and Novoselov, K. S., "Detection of individual gas molecules adsorbed on graphene," *Nature materials*, vol. 6, no. 9, pp. 652–655, 2007, doi: 10.1038/nmat1967.

[51] Yavari, F. and Koratkar, N., "Graphene-Based Chemical Sensors," *The journal of physical chemistry letters*, vol. 3, no. 13, pp. 1746–1753, 2012, doi: 10.1021/jz300358t.

[52] Zhang, S., Pang, J., Li, Y., Ibarlucea, B., Liu, Y., Wang, T., Liu, X., Peng, S., Gemming, T., Cheng, Q., Liu, H., Yang, J., Cuniberti, G., Zhou, W., and Rümmeli, M. H., "An effective formaldehyde gas sensor based on oxygen-rich three-dimensional graphene," *Nanotechnology*, vol. 33, no. 18, 2022, doi: 10.1088/1361-6528/ac4eb4.

[53] Liu, F., Xiao, M., Ning, Y., Zhou, S., He, J., Lin, Y., and Zhang, Z., "Toward practical gas sensing with rapid recovery semiconducting carbon nanotube film sensors," *Sci. China Inf. Sci.*, vol. 65, no. 6, 2022, doi: 10.1007/s11432-021-3286-3.

[54] Sun, X., Liu, Z., Welsher, K., Robinson, J. T., Goodwin, A., Zaric, S., and Dai, H., "Nano-Graphene Oxide for Cellular Imaging and Drug Delivery," *Nano research*, vol. 1, no. 3, pp. 203–212, 2008, doi: 10.1007/s12274-008-8021-8.

[55] Wrobel, P. S., Wlodarski, M. D., Jedrzejewska, A., Placek, K. M., Szukiewicz, R., Kotowicz, S., Tokarska, K., Quang, H. T., Mendes, R. G., Liu, Z., Trzebicka, B., Rummeli, M. H., and Bachmatiuk, A., "A comparative study on simple and practical chemical gas sensors from chemically modified graphene films," *Mater. Res. Express*, vol. 6, no. 1, p. 15607, 2019, doi: 10.1088/2053-1591/aae6be.

[56] Kumar, R., Avasthi, D. K., and Kaur, A., "Fabrication of chemiresistive gas sensors based on multistep reduced graphene oxide for low parts per million monitoring of sulfur dioxide

at room temperature," *Sensors and Actuators B: Chemical*, vol. 242, pp. 461–468, 2017, doi: 10.1016/j.snb.2016.11.018.

[57] Bachmatiuk, A., Mendes, R. G., Hirsch, C., Jähne, C., Lohe, M. R., Grothe, J., Kaskel, S., Fu, L., Klingeler, R., Eckert, J., Wick, P., and Rümmeli, M. H., "Few-layer graphene shells and nonmagnetic encapsulates: a versatile and nontoxic carbon nanomaterial," *ACS nano*, vol. 7, no. 12, pp. 10552–10562, 2013, doi: 10.1021/nn4051562.

[58] Liao, M., Shen, B., and Wang, Z., *Ultra-wide bandgap semiconductor materials*. Amsterdam: Elsevier, 2019.

[59] Laposa, A., Kroutil, J., Davydova, M., Taylor, A., Voves, J., and Husak, M., "Inkjet Seeded CVD-Grown Hydrogenated Diamond Gas Sensor Under UV-LED Illumination," *IEEE SENSORS JOURNAL*, vol. 20, no. 3, pp. 1158–1165, 2020, doi: 10.1109/JSEN.2019.2946947.

[60] Takagi, Y., Shiraishi, K., Kasu, M., and Sato, H., "Mechanism of hole doping into hydrogen terminated diamond by the adsorption of inorganic molecule," *SURFACE SCIENCE*, vol. 609, pp. 203–206, 2013, doi: 10.1016/j.susc.2012.12.015.

[61] Liskova, J., Babchenko, O., Varga, M., Kromka, A., Hadraba, D., Svindrych, Z., Burdikova, Z., and Bacakova, L., "Osteogenic cell differentiation on H-terminated and O-terminated nanocrystalline diamond films," *International journal of nanomedicine*, vol. 10, pp. 869–884, 2015, doi: 10.2147/IJN.S73628.

[62] Kromka, A., Davydova, M., Rezek, B., Vanecek, M., Stuchlik, M., Exnar, P., and Kalbac, M., "Gas sensing properties of nanocrystalline diamond films," *DIAMOND AND RELATED MATERIALS*, vol. 19, 2-3, pp. 196–200, 2010, doi: 10.1016/j.diamond.2009.10.006.

[63] Nahlik, J., Laposa, A., Voves, J., Kroutil, J., Drahokoupil, J., and Davydova, M., "A High Sensitivity UV Photodetector With Inkjet Printed ZnO/Nanodiamond Active Layers," *IEEE SENSORS JOURNAL*, vol. 19, no. 14, pp. 5587–5593, 2019, doi: 10.1109/JSEN.2019.2893572.

[64] Mak, K. F., Lee, C., Hone, J., Shan, J., and Heinz, T. F., "Atomically thin MoS_2: a new direct-gap semiconductor," *Physical review letters*, vol. 105, no. 13, p. 136805, 2010, doi: 10.1103/PhysRevLett.105.136805.

[65] Wang, F., Liu, H., Hu, K., Li, Y., Zeng, W., and Zeng, L., "Hierarchical composites of MoS2 nanoflower anchored on SnO2 nanofiber for methane sensing," *CERAMICS INTERNATIONAL*, vol. 45, no. 17, pp. 22981–22986, 2019, doi: 10.1016/j.ceramint.2019.07.342.

[66] Lee, E., Yoon, Y. S., and Kim, D.-J., "Two-Dimensional Transition Metal Dichalcogenides and Metal Oxide Hybrids for Gas Sensing," *ACS sensors*, vol. 3, no. 10, pp. 2045–2060, 2018, doi: 10.1021/acssensors.8b01077.

[67] Niu, Y., Wang, R., Jiao, W., Ding, G., Hao, L., Yang, F., and He, X., "MoS2 graphene fiber based gas sensing devices," *CARBON*, vol. 95, pp. 34–41, 2015, doi: 10.1016/j.carbon.2015.08.002.

[68] Sojkova, M., Siffalovic, P., Babchenko, O., Vanko, G., Dobrocka, E., Hagara, J., Mrkyvkova, N., Majkova, E., Izak, T., Kromka, A., and Hulman, M., "Carbide-free one-zone sulfurization method grows thin MoS2 layers on polycrystalline CVD diamond," *SCIENTIFIC REPORTS*, vol. 9, 2019, doi: 10.1038/s41598-018-38472-9.

[69] Sojkova, M., Hrda, J., Volkov, S., Vegso, K., Shaji, A., Vojtekova, T., Slusna, L. P., Gal, N., Dobrocka, E., Siffalovic, P., Roch, T., Gregor, M., and Hulman, M., "Growth of PtSe2 few-layer films on NbN superconducting substrate," *APPLIED PHYSICS LETTERS*, vol. 119, no. 1, 2021, doi: 10.1063/5.0053309.

[70] Shaji, A., Vegso, K., Sojkova, M., Hulman, M., Nadazdy, P., Hutar, P., Slusna, L. P., Hrda, J., Bodik, M., Hodas, M., Bernstorff, S., Jergel, M., Majkova, E., Schreiber, F., and Siffalovic, P., "Orientation of Few-Layer MoS2 Films: In-Situ X-ray Scattering Study During Sulfurization," *JOURNAL OF PHYSICAL CHEMISTRY C*, vol. 125, no. 17, pp. 9461–9468, 2021, doi: 10.1021/acs.jpcc.1c01716.

[71] Chromik, S., Rosová, A., Dobročka, E., Kobzev, A. P., Hulman, M., Sojkova, M., Hutár, P., and Machajdík, D., "MoS2 thin films prepared by sulfurization," in *Nanoengineering: Fabrication, Properties, Optics, and Devices XIV*, San Diego, United States, Aug. 2017 - Aug. 2017, p. 56. [Online]. Available: https://www.spiedigitallibrary.org/conference-proceedings-of-spie/10354/2273846/MoS2-thin-films-prepared-by-sulfurization/10.1117/12.2273846.full

[72] Chromik, Š., Sojková, M., Vretenár, V., Rosová, A., Dobročka, E., and Hulman, M., "Influence of GaN/AlGaN/GaN (0001) and Si (100) substrates on structural properties of extremely thin MoS 2 films grown by pulsed laser deposition," *Applied Surface Science*, vol. 395, pp. 232–236, 2017, doi: 10.1016/j.apsusc.2016.06.038.

[73] Sojkova, M., Vegso, K., Mrkyvkova, N., Hagara, J., Hutar, P., Rosova, A., Caplovicova, M., Ludacka, U., Skakalova, V., Majkova, E., Siffalovic, P., and Hulman, M., "Tuning the orientation of few-layer MoS2 films using one-zone sulfurization," *RSC Adv.*, vol. 9, no. 51, pp. 29645–29651, 2019, doi: 10.1039/c9ra06770a.

[74] Dolores Petit-Dominguez, M., Quintana, C., Vazquez, L., Del Pozo, M., Cuadrado, I., Maria Parra-Alfambra, A., and Casero, E., "Synergistic effect of MoS2 and diamond nanoparticles in electrochemical sensors: determination of the anticonvulsant drug valproic acid," *MICROCHIMICA ACTA*, vol. 185, no. 7, 2018, doi: 10.1007/s00604-018-2793-7.

[75] Cho, B., Yoon, J., Lim, S. K., Kim, A. R., Kim, D.-H., Park, S.-G., Kwon, J.-D., Lee, Y.-J., Lee, K.-H., Lee, B. H., Ko, H. C., and Hahm, M. G., "Chemical Sensing of 2D Graphene/MoS2 Heterostructure device," *ACS applied materials & interfaces*, vol. 7, no. 30, pp. 16775–16780, 2015, doi: 10.1021/acsami.5b04541.

[76] Qu, F., Liu, H., Guarecuco, R., Jiao, Y., and Yang, M., "Mesoporous InN/In2O3 heterojunction with improved sensitivity and selectivity for room temperature NO2 gas sensing," *Nanotechnology*, vol. 27, no. 38, p. 385501, 2016, doi: 10.1088/0957-4484/27/38/385501.

[77] Reddeppa, M., Park, B.-G., Murali, G., Choi, S. H., Chinh, N. D., Kim, D., Yang, W., and Kim, M.-D., "NOx gas sensors based on layer-transferred n-MoS2/p-GaN heterojunction at room temperature: Study of UV light illuminations and humidity," *SENSORS AND ACTUATORS B-CHEMICAL*, vol. 308, 2020, doi: 10.1016/j.snb.2020.127700.

[78] Saravanan, A., Huang, B.-R., Chu, J. P., Prasannan, A., and Tsai, H.-C., "Interface engineering of ultrananocrystalline diamond/MoS2-ZnO heterostructures and its highly enhanced hydrogen gas sensing properties," *Sensors and Actuators B: Chemical*, vol. 292, pp. 70–79, 2019, doi: 10.1016/j.snb.2019.04.108.

[79] Luo, H., Cao, Y., Zhou, J., Feng, J., Cao, J., and Guo, H., "Adsorption of NO2, NH3 on monolayer MoS2 doped with Al, Si, and P: A first-principles study," *CHEMICAL PHYSICS LETTERS*, vol. 643, pp. 27–33, 2016, doi: 10.1016/j.cplett.2015.10.077.

[80] Luo, Y. and Zhang, C., "Pt-activated TiO2-MoS2 nanocomposites for H2 detection at low temperature," *Journal of Alloys and Compounds*, vol. 747, pp. 550–557, 2018, doi: 10.1016/j.jallcom.2018.03.068.

[81] Lv, M.-S., Li, Y.-N., Chen, G.-L., Gao, R., Zhang, X.-F., Deng, Z.-P., Xu, Y.-M., Huo, L.-H., and Gao, S., "Biotemplate synthesis of NiO/ZnO tubes rich in oxygen vacancies for enhanced sensing detection of hydrazine at low temperature," *Sensors and Actuators B: Chemical*, vol. 385, p. 133684, 2023, doi: 10.1016/j.snb.2023.133684.

[82] Madvar, H. R., Kordrostami, Z., and Mirzaei, A., "Sensitivity Enhancement of Resistive Ethanol Gas Sensor by Optimized Sputtered-Assisted CuO Decoration of ZnO Nanorods," *Sensors (Basel, Switzerland)*, vol. 23, no. 1, 2022, doi: 10.3390/s23010365.

[83] Meng, F.-L., Li, H.-H., Kong, L.-T., Liu, J.-Y., Jin, Z., Li, W., Jia, Y., Liu, J.-H., and Huang, X.-J., "Parts per billion-level detection of benzene using SnO2/graphene nanocomposite composed of sub-6 nm SnO2 nanoparticles," *Analytica chimica acta*, vol. 736, pp. 100–107, 2012, doi: 10.1016/j.aca.2012.05.044.

[84] Morelli, L., Ricciardella, F., Koole, M., Persijn, S., and Vollebregt, S., "Functionalisation of Multi-Layer Graphene-Based Gas Sensor by Au Nanoparticles," in *4th International Conference nanoFIS 2020 - Functional Integrated nanoSystems*, p. 1.

[85] Nicley, S. S., Drijkoningen, S., Pobedinskas, P., Raymakers, J., Maes, W., and Haenen, K., "Growth of Boron-Doped Diamond Films on Gold-Coated Substrates with and without Gold Nanoparticle Formation," *Crystal Growth & Design*, vol. 19, no. 6, pp. 3567–3575, 2019, doi: 10.1021/acs.cgd.9b00488.

[86] Seekaew, Y., Wisitsoraat, A., and Wongchoosuk, C., "ZnO quantum dots decorated carbon nanotubes-based sensors for methanol detection at room temperature," *DIAMOND AND RELATED MATERIALS*, vol. 132, p. 109630, 2023, doi: 10.1016/j.diamond.2022.109630.

[87] Tung, T. T., Castro, M., Pillin, I., Kim, T. Y., Suh, K. S., and Feller, J.-F., "Graphene–Fe3O4/PIL–PEDOT for the design of sensitive and stable quantum chemo-resistive VOC sensors," *CARBON*, vol. 74, pp. 104–112, 2014, doi: 10.1016/j.carbon.2014.03.009.

[88] Wu, G., Du, H., Cha, Y. L., Lee, D., Kim, W., Feyzbar-Khalkhali-Nejad, F., Oh, T.-S., Zhang, X., and Kim, D.-J., "A wearable mask sensor based on polyaniline/CNT nanocomposites for monitoring ammonia gas and human breathing," *Sensors and Actuators B: Chemical*, vol. 375, p. 132858, 2023, doi: 10.1016/j.snb.2022.132858.

[89] Yan, H., Song, P., Zhang, S., Yang, Z., and Wang, Q., "Facile synthesis, characterization and gas sensing performance of ZnO nanoparticles-coated MoS2 nanosheets," *Journal of Alloys and Compounds*, vol. 662, pp. 118–125, 2016, doi: 10.1016/j.jallcom.2015.12.066.

[90] Yan, H., Song, P., Zhang, S., Zhang, J., Yang, Z., and Wang, Q., "A low temperature gas sensor based on Au-loaded MoS2 hierarchical nanostructures for detecting ammonia," *CERAMICS INTERNATIONAL*, vol. 42, no. 7, pp. 9327–9331, 2016, doi: 10.1016/j.ceramint.2016.02.160.

[91] Yan, W., Zhou, S., Ling, M., Peng, X., and Zhou, H., "NH3 Sensor Based on ZIF-8/CNT Operating at Room Temperature with Immunity to Humidity," *Inorganics*, vol. 10, no. 11, p. 193, 2022, doi: 10.3390/inorganics10110193.

[92] Zhou, Y., Liu, G., Zhu, X., and Guo, Y., "Ultrasensitive NO2 gas sensing based on rGO/MoS2 nanocomposite film at low temperature," *Sensors and Actuators B: Chemical*, vol. 251, pp. 280–290, 2017, doi: 10.1016/j.snb.2017.05.060.

[93] Barthwal, S., Singh, B., and Singh, N. B., "ZnO-SWCNT Nanocomposite as NO2 gas sensor," *Materials Today: Proceedings*, vol. 5, no. 7, pp. 15439–15444, 2018, doi: 10.1016/j.matpr.2018.05.030.

[94] Dilonardo, E., Penza, M., Alvisi, M., Di Franco, C., Rossi, R., Palmisano, F., Torsi, L., and Cioffi, N., "Electrophoretic deposition of Au NPs on MWCNT-based gas sensor for tailored gas detection with enhanced sensing properties," *Sensors and Actuators B: Chemical*, vol. 223, pp. 417–428, 2016, doi: 10.1016/j.snb.2015.09.112.

[95] Kareem, M. H., Hussein, H. T., and Abdul Hussein, A. M., "Study of the effect of CNTs, and (CNTs-ZnO) on the porous silicon as sensor for acetone gas detection," *Optik*, vol. 259, p. 168825, 2022, doi: 10.1016/j.ijleo.2022.168825.

[96] Kwon, Y. J., Mirzaei, A., Kang, S. Y., Choi, M. S., Bang, J. H., Kim, S. S., and Kim, H. W., "Synthesis, characterization and gas sensing properties of ZnO-decorated MWCNTs," *Applied Surface Science*, vol. 413, pp. 242–252, 2017, doi: 10.1016/j.apsusc.2017.03.290.

[97] George, A., Raj, A., and Yang, Q., "Structural characteristics and gas sensing response of V2O5 nanorod thinfilms deposited by hot filament CVD," *Sensors and Actuators B: Chemical*, vol. 378, p. 133078, 2023, doi: 10.1016/j.snb.2022.133078.

[98] Hur, J., Park, S., Kim, J. H., Cho, J. Y., Kwon, B., Lee, J. H., Bae, G. Y., Kim, H., Han, J. T., and Lee, W. H., "Ultrasensitive, Transparent, Flexible, and Ecofriendly NO 2 Gas Sensors Enabled by Oxidized Single-Walled Carbon Nanotube Bundles on Cellulose with Engineered Surface Roughness," *ACS Sustainable Chem. Eng.*, vol. 10, no. 10, pp. 3227–3235, 2022, doi: 10.1021/acssuschemeng.1c07559.

[99] Chakraborty, B., Gayakwad, A., Sahai, M., Manjuladevi, V., Gupta, R. K., and Bhattacharyya, P., "Correlation of Volumetric Vaporsorption and Vapor Sensing Phenomenon of Flower-Like MoS 2 -Based Sensor," *IEEE Sensors J.*, vol. 23, no. 6, pp. 5858–5865, 2023, doi: 10.1109/JSEN.2023.3242763.

[100] Shooshtari, M., Vollebregt, S., Vaseghi, Y., Rajati, M., and Pahlavan, S., "The sensitivity enhancement of TiO2-based VOCs sensor decorated by gold at room temperature," *Nanotechnology*, vol. 34, no. 25, 2023, doi: 10.1088/1361-6528/acc6d7.

[101] Shooshtari, M. and Salehi, A., "An electronic nose based on carbon nanotube -titanium dioxide hybrid nanostructures for detection and discrimination of volatile organic compounds," *Sensors and Actuators B: Chemical*, vol. 357, p. 131418, 2022, doi: 10.1016/j.snb.2022.131418.

[102] Gavgani, J. N., Hasani, A., Nouri, M., Mahyari, M., and Salehi, A., "Highly sensitive and flexible ammonia sensor based on S and N co-doped graphene quantum dots/polyaniline hybrid at room temperature," *Sensors and Actuators B: Chemical*, vol. 229, pp. 239–248, 2016, doi: 10.1016/j.snb.2016.01.086.

[103] Kočí, M., Kromka, A., Bouřa, A., Szabó, O., and Husák, M., "Hydrogen-Terminated Diamond Surface as a Gas Sensor: A Comparative Study of Its Sensitivities," *Sensors*, vol. 21, no. 16, 2021, doi: 10.3390/s21165390.

[104] Barzegar, M., Iraji zad, A., and Tiwari, A., "On the performance of vertical MoS2 nanoflakes as a gas sensor," *Vacuum*, vol. 167, pp. 90–97, 2019, doi: 10.1016/j.vacuum.2019.05.033.

[105] Bronkhorst, *FG-201CV: High Performance Mass Flow Controller for Gases.* [Online]. Available: https://www.bronkhorst.com/int/products/gas-flow/el-flow-prestige/fg-201cv/ (accessed: Jan. 17 2022).

[106] Valco, *Valco 1/4" Common Outlet Selectors: 4 position selectors.* [Online]. Available: https://www.vici.com/vval/sc_4.php (accessed: Jan. 17 2022).

[107] Wang, S.-C. and Shaikh, M. O., "A Room Temperature H_2 Sensor Fabricated Using High Performance Pt-Loaded SnO_2 Nanoparticles," *Sensors (Basel, Switzerland)*, vol. 15, no. 6, pp. 14286–14297, 2015, doi: 10.3390/s150614286.

[108] Crawford, K. G., Maini, I., Macdonald, D. A., and Moran, D. A., "Surface transfer doping of diamond: A review," *Progress in Surface Science*, vol. 96, no. 1, p. 100613, 2021, doi: 10.1016/j.progsurf.2021.100613.

[109] Hubík, P., Mareš, J. J., Kozak, H., Kromka, A., Rezek, B., Krištofik, J., and Kindl, D., "Transport properties of hydrogen-terminated nanocrystalline diamond films," *DIAMOND AND RELATED MATERIALS*, vol. 24, pp. 63–68, 2012, doi: 10.1016/j.diamond.2011.10.021.

[110] Kromka, A., Babchenko, O., Izak, T., Hruska, K., and Rezek, B., "Linear antenna microwave plasma CVD deposition of diamond films over large areas," *Vacuum*, vol. 86, no. 6, pp. 776–779, 2012, doi: 10.1016/j.vacuum.2011.07.008.

[111] Davydova, M., Stuchlik, M., Rezek, B., Larsson, K., and Kromka, A., "Sensing of phosgene by a porous-like nanocrystalline diamond layer with buried metallic electrodes," *SENSORS AND ACTUATORS B-CHEMICAL*, vol. 188, pp. 675–680, 2013, doi: 10.1016/j.snb.2013.07.079.

[112] Kawarada, H., "Diamond p-FETs using two-dimensional hole gas for high frequency and high voltage complementary circuits," *J. Phys. D: Appl. Phys.*, vol. 56, no. 5, p. 53001, 2023, doi: 10.1088/1361-6463/aca61c.

[113] Mueller, G., Krstev, I., Maier, K., Helwig, A., Stutzmann, M., and Garrido, J., "Resettable, low-temperature accumulation gas sensors based on hydrogenated diamond transducers," *EUROSENSORS 2015*, vol. 120, pp. 590–593, 2015, doi: 10.1016/j.proeng.2015.08.733.

[114] Neetika, Kumar, A., Chandra, R., and Malik, V. K., "MoS2 nanoworm thin films for NO2 gas sensing application," *THIN SOLID FILMS*, vol. 725, 2021, doi: 10.1016/j.tsf.2021.138625.

[115] Shokri, A. and Salami, N., "Gas sensor based on MoS2 monolayer," *Sensors and Actuators B: Chemical*, vol. 236, pp. 378–385, 2016, doi: 10.1016/j.snb.2016.06.033.

[116] Yan, X., Wu, Y., Li, R., Shi, C., Moro, R., Ma, Y., and Ma, L., "High-Performance UV-Assisted NO2 Sensor Based on Chemical Vapor Deposition Graphene at Room Temperature," *ACS omega*, vol. 4, no. 10, pp. 14179–14187, 2019, doi: 10.1021/acsomega.9b00935.

[117] Nurazzi, N. M., Abdullah, N., Demon, S. Z. N., Halim, N. A., Azmi, A. F. M., Knight, V. F., and Mohamad, I. S., "The frontiers of functionalized graphene-based nanocomposites

as chemical sensors," *Nanotechnology Reviews*, vol. 10, no. 1, pp. 330–369, 2021, doi: 10.1515/ntrev-2021-0030.

[118] Varga, M., Potocký, Š., Domonkos, M., Ižák, T., Babčenko, O., and Kromka, A., "Great Variety of Man-Made Porous Diamond Structures: Pulsed Microwave Cold Plasma System with a Linear Antenna Arrangement," *ACS omega*, vol. 4, no. 5, pp. 8441–8450, 2019, doi: 10.1021/acsomega.9b00323.

7. List of publications and internships

7.1 Publications with DOI

7.1.1 Lead author

	Title	Authors	Journal + Year	DOI
1.	Hydrogen-Terminated Diamond Surface as a Gas Sensor: A Comparative Study of its Sensitivities	**M. Kočí**, O. Szabó, G. Vanko, M. Husák, A. Kromka	Sensors, 2021	10.3390/ s21165390
2.	Enhanced gas sensing capabilities of diamond layers using Au nanoparticles	**M. Kočí**, O. Szabó, G. Vanko, M. Husák, A. Kromka	Diamond and Related Materials, 2023	10.1016/ j.diamond. 2023.110218
3.	Improved Gas Sensing Capabilities of MoS_2/Diamond Heterostructures at Room Temperature	**M. Kočí**, T. Izsák, G. Vanko, M. Sojková, J. Hrdá, O. Szabó, M. Husák, K. Végsö, M. Varga, A. Kromka	ACS Applied Materials and Interfaces, 2023	10.1021/ acsami. 3c04438
4.	Gas sensors based on diamond heterostructures for air quality monitoring	**M. Kočí**, O. Szabó, T. Izsák, M. Sojková, M. Godzierz, P. Wróbel, M. Husák, A. Kromka	Conference Proceedings - NANOCON 2023	10.37904/ nanocon. 2023.4785

7.2 Conferences

7.2.1 Lead author

	Title	Authors	Conferences Year	Award
1.	Development and measurement of gas sensors based on diamond and transition metal dichalcogenide materials	**M. Kočí**, T. Izsák, G. Vanko, M. Sojková, M. Husák, A. Kromka	ADEPT 2021	
2.	Development and measurement of gas sensors for room temperature applications	**M. Kočí**	POSTER 2022	1st place in Best Poster Competition
3.	$PtSe_2$ and MoS_2 active layers for gas sensing at room temperature	**M. Kočí**, T. Izsák, G. Vanko, M. Sojková, M. Husák, A. Kromka	ADEPT 2022	
4.	Enhancement of diamond gas sensor responses by gold nanoparticles	**M. Kočí**, O. Szabó, M. Husák, A. Kromka	NANOCON 2022	
5.	Room temperature ethanol detection using carbon materials	**M. Kočí**	POSTER 2023	1st place in Best Poster Competition
6.	Room temperature gas sensors based on the diamond molybdenum disulfide and diamond graphene oxide structure	**M. Kočí**, T. Izsák, P. Wróbel, M. Godzierz, O. Szabó, G. Vanko, M. Sojková, S. Pusz, Š. Potocký, M. Husák, A. Kromka	ADEPT 2023	Honorary award of the company KVANT
7.	Gas sensors based on diamond heterostructures for air quality monitoring	**M. Kočí**, O. Szabó, T. Izsák, M. Sojková, M. Godzierz, P. Wróbel, M. Husák, A. Kromka	NANOCON 2023	3rd place in Best Poster Contest
8.	Diamond and 2D material heterostructures as a novel platform for room temperature detection of gases	**M. Kočí**, O. Szabó, T. Izsák, M. Godzierz, P. Wróbel, G. Vanko, M. Sojková, A. Kromka, M. Husák	ADEPT 2024	Complimentary place in student oral presentation competition

7.2.2 Co-author

	Title	Authors	Conferences Year
1.	Highly Sensitive Ethanol Vapor Sensor based on Reduced Graphene Oxide	O. Szabó, **M. Kočí**, P. Wróbel, R. Jackivová, U. Szeluga, S. Pusz, A. Kromka, Š. Potocký	NANOCON 2022
2.	Chemical vapor deposition of diamond films on QCM substrates	A. Kromka, **M. Kočí**, O. Szabó, K. Aubrechtová Dragounová, G. Vanko, T. Izsák, M. Varga	ADEPT 2023
3.	Diamond-coated quartz crystal microbalance: fabrication, characterization and applications - detection of gas molecules and sars-cov-2 proteins	A. Kromka, M. Varga, **M. Kočí**, O. Szabó, T. Izsák, K. Aubrechtová Dragounová, M. Gál, M. Vojs, J. Korčeková, A. Poturnayová	ADEPT 2023
4.	Challenges and Applications of Diamond and Transition Metal Dichalcogenide Heterostructures	M. Varga, **M. Kočí**, M. Sojkova, S. Chromik, J. Hrda, J. Fait, Z. Remeš, K. Aubrechtova Dragounova, M. Hulman, A. Kromka	NANOCON 2023

7.3 Internships

7.3.1 Long-term internships

Institution / place	Duration	Year
PROFACTOR GmbH Steyr-Gleink, Rakousko	16 weeks	2024

7.3.2 Short-term internships

Institution / place	Duration	Year
Elektrotechnický ústav SAV Bratislava, Slovensko	1 week	2021
Centrum Materiałów Polimerowych i Węglowych, Polskej Akademii Nauk Zabrze, Polsko	1 week	2022
Institute of Minerals and Materials Technology, Council of Scientific and Industrial Research, Ministry of Science and Technology, Government of India Bhubaneswar, Indie	2 weeks	2022
Elektrotechnický ústav SAV Bratislava, Slovensko	1 week	2022
Centrum Materiałów Polimerowych i Węglowych, Polskej Akademii Nauk Zabrze, Polsko	1 week	2023
Institute of Minerals and Materials Technology, Council of Scientific and Industrial Research, Ministry of Science and Technology, Government of India Bhubaneswar, Indie	2 weeks	2023

Appendix

I. Hydrogen-Terminated Diamond Surface as a Gas Sensor: A Comparative Study of its Sensitivities II

II. Enhanced gas sensing capabilities of diamond layers using Au nanoparticles XVIII

III. Improved Gas Sensing Capabilities of MoS_2/Diamond Heterostructures at Room Temperature XXVIII

IV. Gas sensors based on diamond heterostructures for air quality monitoring XXXVIII

I. Hydrogen-Terminated Diamond Surface as a Gas Sensor: A Comparative Study of its Sensitivities

Authors: Michal Kočí, Alexander Kromka, Adam Bouřa, Ondrej Szabó, Miroslav Husák

sensors

MDPI

Article

Hydrogen-Terminated Diamond Surface as a Gas Sensor: A Comparative Study of Its Sensitivities

Michal Kočí [1,2,*], Alexander Kromka [1], Adam Bouřa [2], Ondrej Szabó [1] and Miroslav Husák [2]

[1] Department of Diamond and Associated Materials, Institute of Physics of the Czech Academy of Sciences, 162 00 Prague, Czech Republic; kromka@fzu.cz (A.K.); szabo@fzu.cz (O.S.)
[2] Department of Microelectronics, Faculty of Electrical Engineering, Czech Technical University in Prague, 166 27 Prague, Czech Republic; bouraa@fel.cvut.cz (A.B.); husak@fel.cvut.cz (M.H.)
* Correspondence: kocim@fzu.cz or kocimic1@fel.cvut.cz

Abstract: A nanocrystalline diamond (NCD) layer is used as an active (sensing) part of a conductivity gas sensor. The properties of the sensor with an NCD with H-termination (response and time characteristic of resistance change) are measured by the same equipment with a similar setup and compared with commercial sensors, a conductivity sensor with a metal oxide (MO_X) active material (resistance change), and an infrared pyroelectric sensor (output voltage change) in this study. The deposited layer structure is characterized and analyzed by Scanning Electron Microscopy (SEM) and Raman spectroscopy. Electrical properties (resistance change for conductivity sensors and output voltage change for the IR pyroelectric sensor) are examined for two types of gases, oxidizing (NO_2) and reducing (NH_3). The parameters of the tested sensors are compared and critically evaluated. Subsequently, differences in the gas sensing principles of these conductivity sensors, namely H-terminated NCD and SnO_2, are described.

Keywords: nanocrystalline diamond (NCD); metal oxide (MO_X); gas detectors

Citation: Kočí, M.; Kromka, A.; Bouřa, A.; Szabó, O.; Husák, M. Hydrogen-Terminated Diamond Surface as a Gas Sensor: A Comparative Study of Its Sensitivities. *Sensors* **2021**, *21*, 5390. https://doi.org/10.3390/s21165390

Academic Editors: Carlos R. Michel and Janusz Smulko

Received: 12 June 2021
Accepted: 5 August 2021
Published: 10 August 2021

1. Introduction

At present, great emphasis is placed on air quality and the detection of either toxic substances (NH_3, CO, etc.) or substances that reduce the quality of life (CO_2, etc.). Air quality is one of the significant properties to be monitored. The growing number of harmful substances released into the air, especially from industry, reduces the quality of life. Considering this, gas sensors, such as carbon monoxide, carbon dioxide, or nitrogen dioxide sensors, are almost essential for industry and everyday life. Over the last 20 years, the demand for quality and detection properties of sensors has increased significantly. For this reason, high demands are placed on the development of new types of sensors for the detection of various kinds of gases that achieve high accuracy, reproducibility, sensitivity, and stability. With the development of new materials and processing, smaller, more accurate, and cheaper sensors with a lower production cost can be developed. In order to increase a sensor's performance, it is necessary to use novel sensing materials, surface modification, or new fabrication processes. Currently, great attention is paid to wide-bandgap (WBG) semiconductors. To date, the most used material for gas monitoring is MO_X, especially SnO_2 [1]. MO_X is used due to its low price and flexible production. On the other hand, these sensors have a very high operating temperature, between 300 and 450 °C [1,2].

Diamond is the most interesting material from the group of WBGs due to its ability to respond to oxidating and reducing gases, light illumination, temperature variation, and other surrounding conditions [3]. Diamond is a material that consists of carbon in the diamond crystal structure [4]. Due to a wide bandgap (5.5 eV), diamond was previously classified as an insulator. To prepare a quality semiconductor, it is necessary to modify the intrinsic diamond, for example, by doping it with foreign atoms. Natural diamonds

have many foreign atoms (impurities) such as metals, nitrogen, etc. It is difficult to find the correct doping atoms because the diamond lattice constant is very small, only 3.57 Å (3.57×10^{-10} m) [3]. The most usual material is boron, which creates a p-type semiconductor [5,6]. There are several ways to prepare a synthetic diamond layer. The most used method is chemical vapor deposition (CVD) [6–8]. In most cases, hydrogen (>90%) and methane are present in a vacuum chamber, where they chemically react and form a thin layer of NCD on the substrate. The most used deposition technique is plasma-enhanced CVD (PECVD), or plasma-assisted CVD (PACVD), where plasma enhances the chemical reactions at lower temperatures. This method is not selective, and the layer grows on the whole substrate. The grown diamond is a hydrogen-terminated surface that reveals unique properties in induced subsurface p-type conductivity, also known as 2D hole gas (2DHG) [2,7–9]. Such a 2DHG top layer is sensitive to exposed gas or organic molecules [2,6]. The gas sensing properties of hydrogen-terminated diamond were explored thoroughly in previous works [2,6,7,9–12].

However, a comparison of a diamond-based gas sensor's performance with other gas sensor types is still missing. The responses of the sensors with an NCD active layer prepared by PECVD, which can be a suitable alternative for commercial MO_X gas sensors, were measured in this work and compared with two commercial sensors (the conductivity (MO_X) sensor TGS 826 and pyroelectric sensor PY2055). The conductivity sensor TGS 826 uses SnO_2 as an active material, which is currently the most widely used detection material due to its low cost, sufficient responsivity, and easy adjustment for a given gas. The infrared pyroelectric sensor Pyreos PY2055 uses absorption spectrophotometry in the infrared region of the spectrum, which is very selective and slightly temperature-dependent. All these sensors were tested in oxidizing and reducing gas mixtures at concentrations up to 100 ppm.

2. Experimental

2.1. Experimental Setup for Gas Sensor Testing

The electrical parameters of the gas sensors are measured with a computer-controlled system consisting of mass flow controllers (MFCs), bubblers, a 4-input selection valve, a test chamber, a source measure unit (SMU), and data acquisition through a PC using the LabVIEW program, as shown in Figures 1 and 2. Bronkhorst FG-201CV MFCs work on the principle of cooling the heating element using the gas flow. The FLOWBUS bus, which is based on the RS-485 bus, is used for communication with the control PC. At the same time, the bus provides electrical power to the flow meters. The MFCs are followed by a T-connector mixer system, which uses a turbulent mixing of gases and bubblers to control the humidity. The manual valves are used to reconfigure the system between two different mixtures and one mixture with two active gases. This system has the ability to supply two different mixtures via a Valco EUTA selection valve with 4 inputs and 2 outputs. For chamber flushing, synthetic air is used. An advantage of the system is its ability to create two different mixtures with different concentrations and humidity. The sensors with the H-terminated NCD layer are placed in the testing chamber (Figure 3). This chamber is designed for interdigital conductivity sensors. The testing chamber consists of a base, a rear part with flexible measuring contacts, a front part that allows the connection of a test mixture with a small test chamber with a volume of about 0.2 cm^3 above the sensitive part of the sensor, and a temperature control assembly consisting of a heating element and a Pt1000 temperature sensor. Each part of the chamber is entered and attached by neodymium magnets and cut-outs in individual parts. This method allows quick and easy assembly and disassembly in case of a sensor replacement. This chamber and the Tektronix PWS4602 SMU allow two- or four-wire DC resistance measurements. In our case, the four-wire DC method was used. The advantage of using this SMU is the ability to choose the energy source, either current or voltage, and its value. A heating element is used to regulate the temperature. It heats the entire chamber and the sensor to a maximum temperature of 125 °C. A Pt1000 thermometer measures the current temperature.

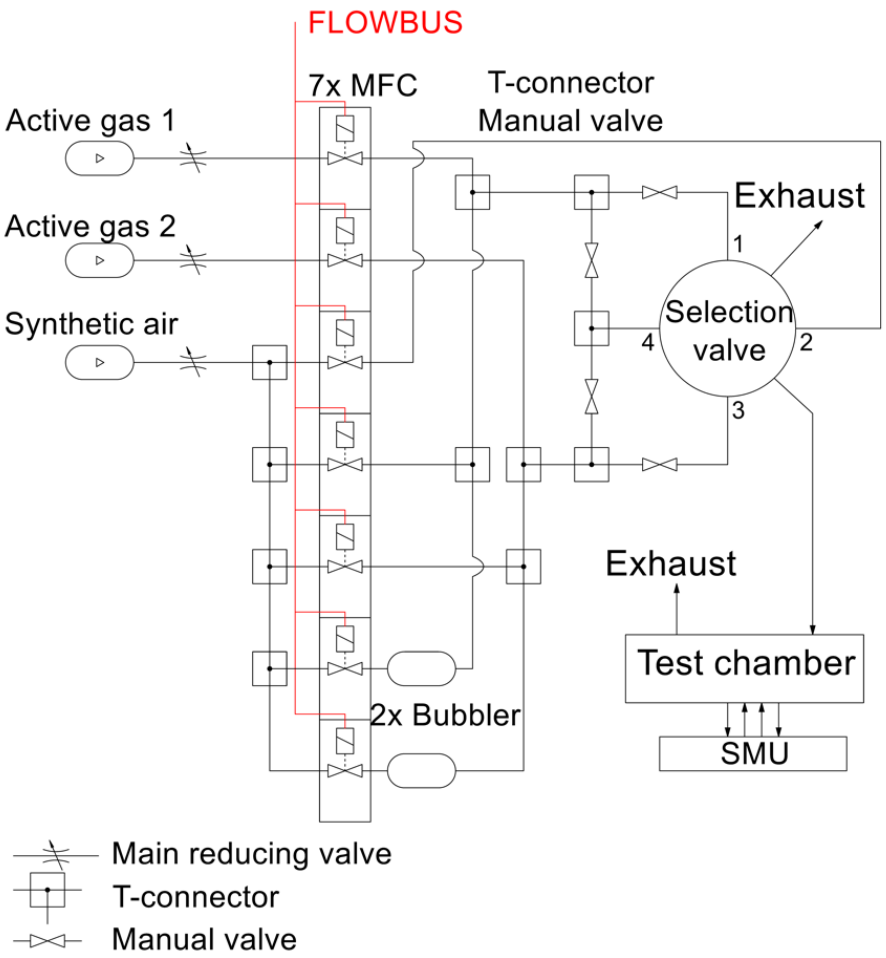

Figure 1. Schematic diagram of experimental setup for gas sensor testing.

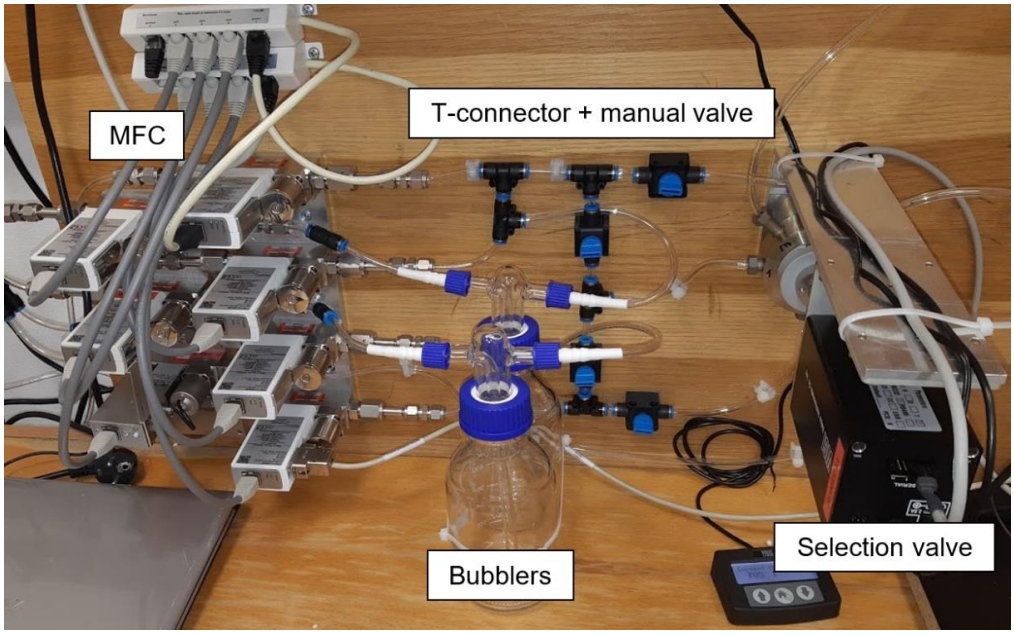

Figure 2. Photo of experimental setup for gas sensor testing.

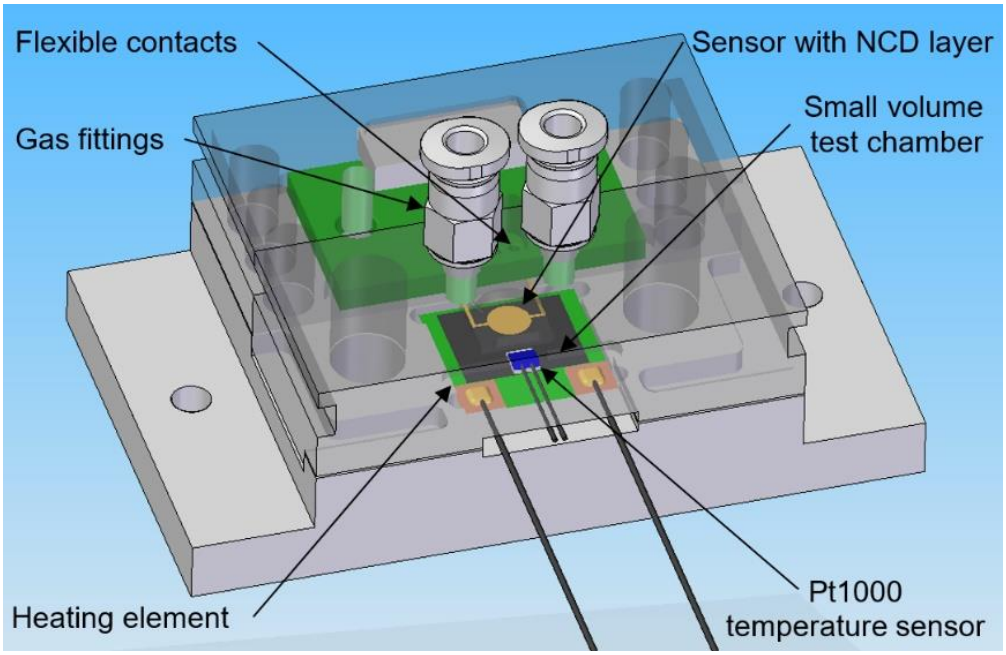

Figure 3. 3D design of testing chamber for NCD sensors with H-termination.

The commercial sensors are placed in a universal test chamber made out of polycarbonate Macrolon (Figure 4) with two identical and separated sections and with the partition between the sections. The volume of one cell is 22 cm^3. Its larger dimension aggravates the time characteristic, but it allows the installation and measurement of bigger commercial sensors, including the radiation source for the IR sensor PY2055.

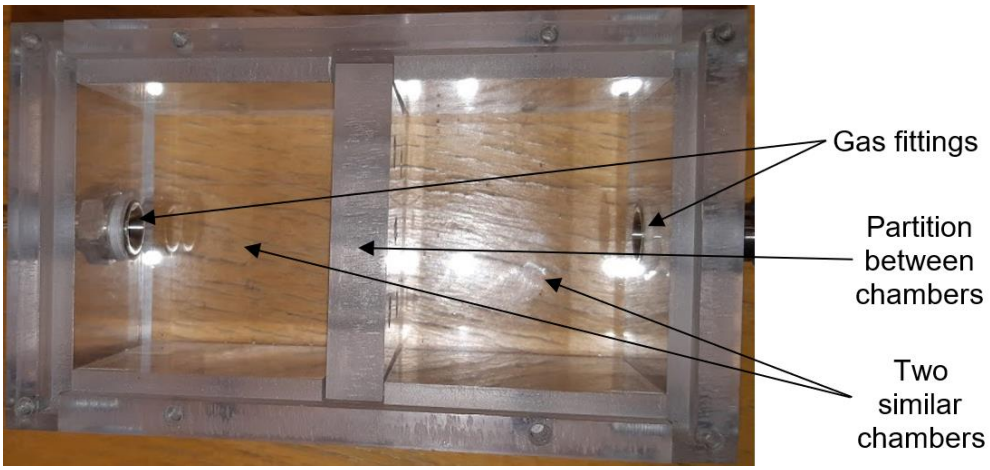

Figure 4. Photo of testing chamber for commercial sensors (top view).

2.2. Sensor Elements with H-Terminated NCD

The H-terminated NCD is grown using the microwave PECVD technique on the interdigital (IDT) structure ED-IDE1-Au with 90 pairs of 10/10/0.2 µm electrodes (10 µm width of the conductive gold-titanium electrodes, 10 µm gap between electrodes, and 200 nm thickness of electrodes) from Micrux Technologies. These IDT elements show good adhesion of gold electrodes to transparent glass substrates, which are thermally stable during the growth of the diamond layer at temperatures around 500 °C. Photographs and schematics of the diamond sensor are shown in Figure 5.

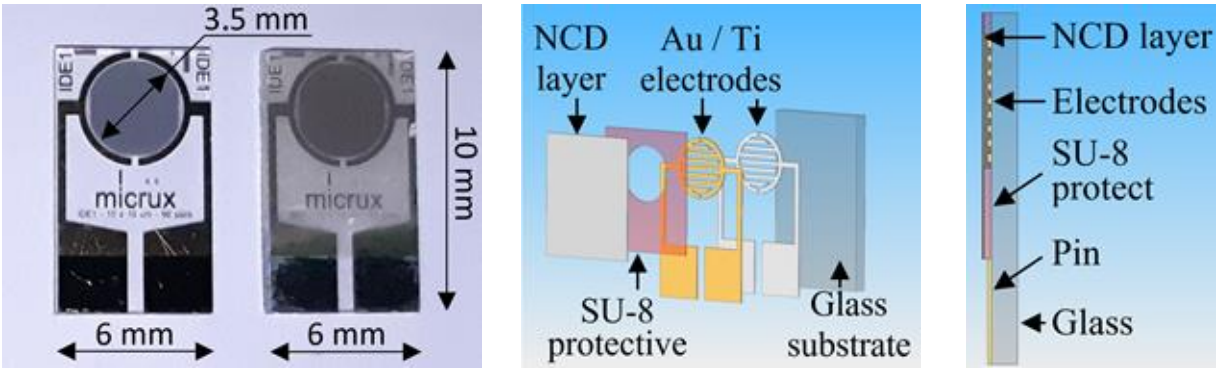

Figure 5. Photographs of (**a**) IDT structure on a glass substrate and (**b**) sensor with NCD active layer, (**c**) exploded schematic view, and (**d**) schematic cross-section.

The preparation of the H-terminated NCD layer includes three parts: the preparation of the adhesive NCD layer, preparation of the final NCD layer, and functionalization of the layer by termination. In the first part of the deposition, an adhesive layer is optimized to prevent peeling off due to the different thermal expansion coefficients of diamond and the substrate. The deposition system, where the adhesive diamond interlayer is first prepared, is represented by two linear microwave antennas, which induce minimal thermal stress due to low temperatures (<400°C). This adhesive diamond layer was prepared at a thickness of 110 nm at low temperatures and a low deposition rate (about 4.4 nm/h). The process parameters of the system with linear antennas are the following: the power of the microwave (MW) generators = 1.7 kW, working pressure = 0.15 mbar of the gas mixture (150 sccm (standard cubic centimeters per minute) H_2, 5 sccm CH_4, 20 sccm CO_2), deposition time = 25 h, and substrate temperature during deposition = 290 °C. In the second part, a final diamond layer is prepared in a focused plasma system. This system is characterized by a high diamond growth rate at higher temperatures (>500 °C). The diamond layer is prepared at a thickness of 150 nm (a deposition rate of about 50 nm/h). The process parameters of the focused plasma system are the following: the power of the MW generators = 1.5 kW, working pressure = 30 mbar of the gas mixture (300 sccm H_2 and 3 sccm CH_4), deposition time = 3 h, and maximal substrate temperature during deposition = 520 °C. After deposition, it is necessary to functionalize the diamond layer by termination. The NCD layers are plasma-activated in hydrogen microwave plasma immediately after the deposition in a focused plasma system for 20 min (the power of the MW generators = 1.5 kW, working pressure = 30 mbar at 500 °C). Both sensors were technologically processed at the same time.

The surface morphologies of the H-terminated NCD layer found using an SEM are shown in Figure 6. Figure 6b shows the surface of NCD on Au-Ti electrodes and glass (a gap between the electrodes). Figure 6a,c show enlarged surfaces of the sensor's active layer. The figure on the left is the NCD layer above the electrode, and the NCD layer above the glass (a gap between the electrodes) is on the right. On both substrate material parts (glass and electrode), continuous thin films, revealing nanosized crystal features, are grown. Raman spectra from both of these parts (Figure 7) exhibit a narrow peak at 1332 cm^{-1} attributed to diamond, and two broad bands labelled D and G at 1350 and 1595 cm^{-1} are recognizable as disordered sp^2 carbon phases and graphitic phases; a fingerprint of trans-polyacetylene segments located at the grain boundaries of the NCD films is visible at 1150 and 1500 cm^{-1} [13]. The quality of the hydrogen termination is indirectly verified by the measurement of the water contact angle. The H-terminated NCD is hydrophobic. A higher contact angle means more terminated hydrogen on the surface and thus a better response to the exposed gas. The minimal contact angle for good sensing properties is about 90° [8]. The fabricated layers revealed similar contact angles over 100° (104° for

sensor No. 1 and 101° for sensor No. 2). However, the contact angle does not reflect the electronic quality of the induced p-type channel; therefore, both H-terminated NCD layers were tested, too.

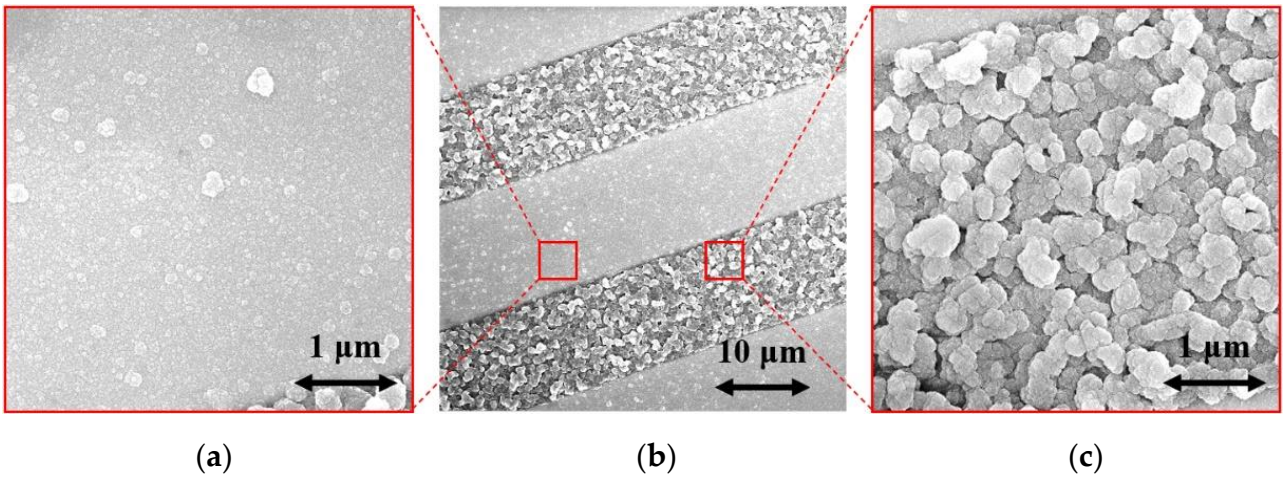

Figure 6. SEM images of (**a**) NCD on electrode, (**b**) NCD on IDT structure, and (**c**) NCD on glass.

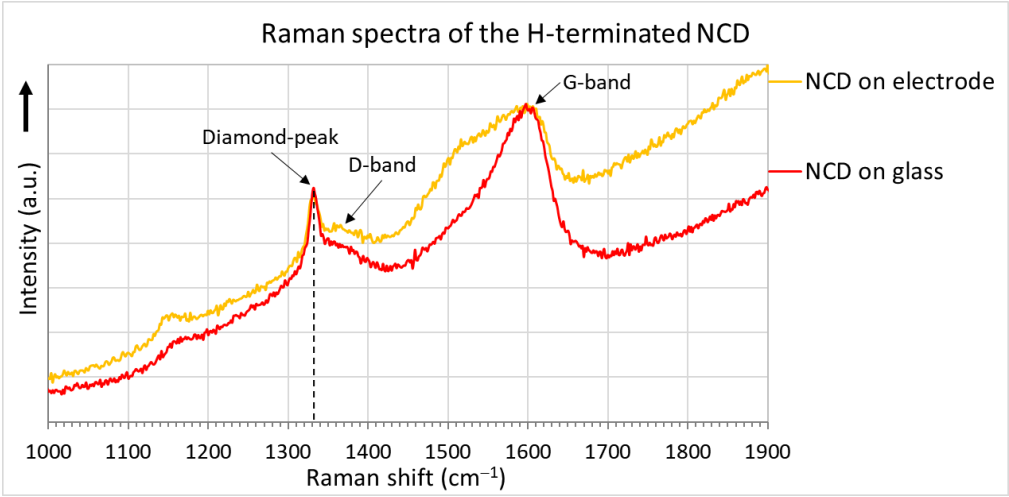

Figure 7. Raman spectra of the NCD layers.

2.3. Figaro TGS 826 Commercial Sensor

The commercially available conductivity sensor TGS 826 from Figaro (Figure 8) is designed for the detection of ammonia (reducing gas) with a concentration from 30 ppm to 300 ppm [14]. A larger test chamber with approximately 110 times the volume of the previously described test chamber is used, because the TGS 826 is larger than the diamond sensor. This sensor uses SnO_2 as an active material; it is currently the most widely used detection material due to its low cost, sufficient responsivity, and easy adjustment for a given gas [1,15]. According to the manufacturer's datasheet, the conductivity of the active material increases with increasing ammonia concentration. This conductivity sensor monitors a change in the conductivity of the active layer due to chemisorption, i.e., the binding (sorption) of gas molecules on a solid's surface by chemical bonding with electron transfer [15]. This sensor's advantages are reproducibility and a manufacturer-defined response. It is the most common type of gas sensor for ammonia.

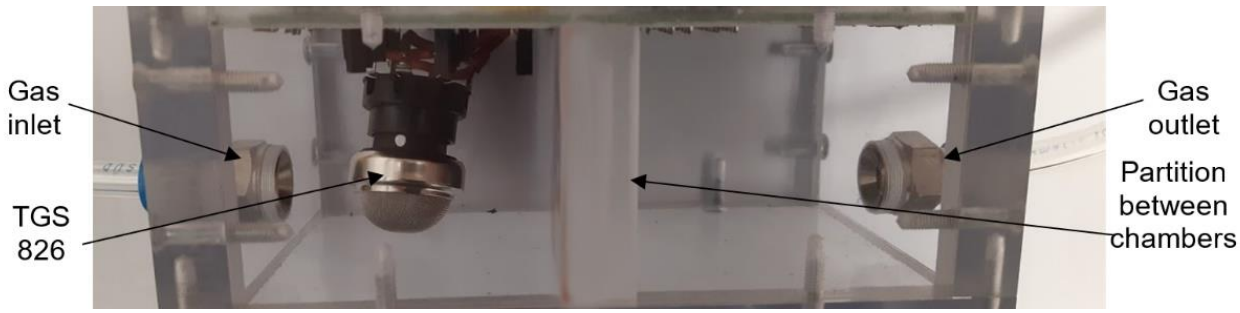

Figure 8. Photograph of conductivity sensor TGS 826 in test chamber.

2.4. Pyreos PY2055 Commercial Sensor

The infrared pyroelectric sensor PY2055 from Pyreos (Figure 9) is used to detect nitrogen dioxide (oxidizing gas) in the mixture [16]. For this sensor type, it is necessary to use a source of mid-wavelength infrared light. In this test, a tungsten filament lamp is used to cover wavelengths from 3.9 to 6.2 µm. A pulse voltage at 10 Hz powers the bulb. For this reason, a large testing chamber is used for measurement. The sensor consists of two pyroelectric elements. A special optical filter is placed in front of each element; there is one filter for the gas absorption spectrum (6.2 µm) and one for the reference measurement (3.9 µm). Infrared gas sensors use absorption spectrophotometry in the infrared region of the spectrum. This detection method can determine the composition of a gas mixture or detect a specific type of gas [15]. The sensor's output signals are represented by an alternating component of the output voltage modulated to half the supply voltage. The gas concentration is calculated as the AC component of Ch2 voltage divided by the AC component of Ch1 (REF) voltage [16]. The advantages of this sensor are the ability to take measurements without the active material coming into contact with the gas, accuracy, high selectivity using suitable filters, and a wide range of concentrations including up to almost 100% gas concentration.

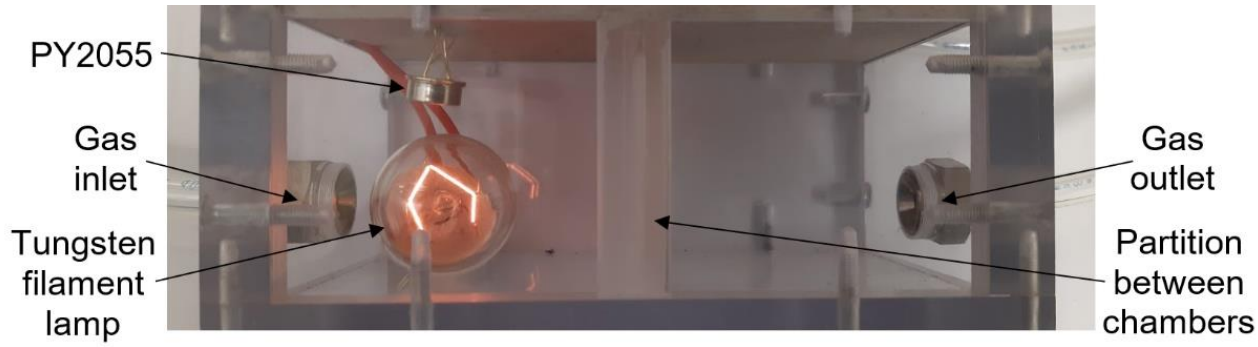

Figure 9. Photograph of infrared sensor PY2055 in test chamber.

3. Results

The responses of two H-terminated NCD conductivity sensors and two commercial sensors (TGS 826 and PY2055) are tested for sensitivity to ammonia and nitrogen dioxide gases.

3.1. H-Terminated NCD Conductivity Sensors

In the first measurement, the response of the H-terminated NCD conductivity sensor to two active gases, oxidizing and reducing, is measured in a test chamber at a temperature of 125 °C. Ammonia with a concentration of 96.6 ppm and nitrogen dioxide with a concentration of 99.6 ppm in a synthetic air mixture are used for testing. Figure 10 shows

the percentual dependence of the steady-state resistance on time. Changing the gas to nitrogen dioxide, the resistance decreases by 41% from a steady value resistance R_0 of 216 kΩ to 127 kΩ with a maximum speed of −0.998 kΩ/s. Changing the gas to ammonia caused an increase in the resistance of 39% from 216 kΩ to 302 kΩ, with a maximum speed of 0.908 kΩ/s. During the change of the gas from oxidizing to reducing, the resistance increases by 138%, from 127 kΩ to 303 kΩ. The maximum rate of change in resistance reaches 1.8 kΩ/s. The measurements show that the sample's responses to both gases are almost identical, with opposite changes in the conductivity in accordance with the theoretical expectation. The influence of the chamber's volume on the reaction time can be neglected because of its tiny volume and high gas flow of 100 sccm.

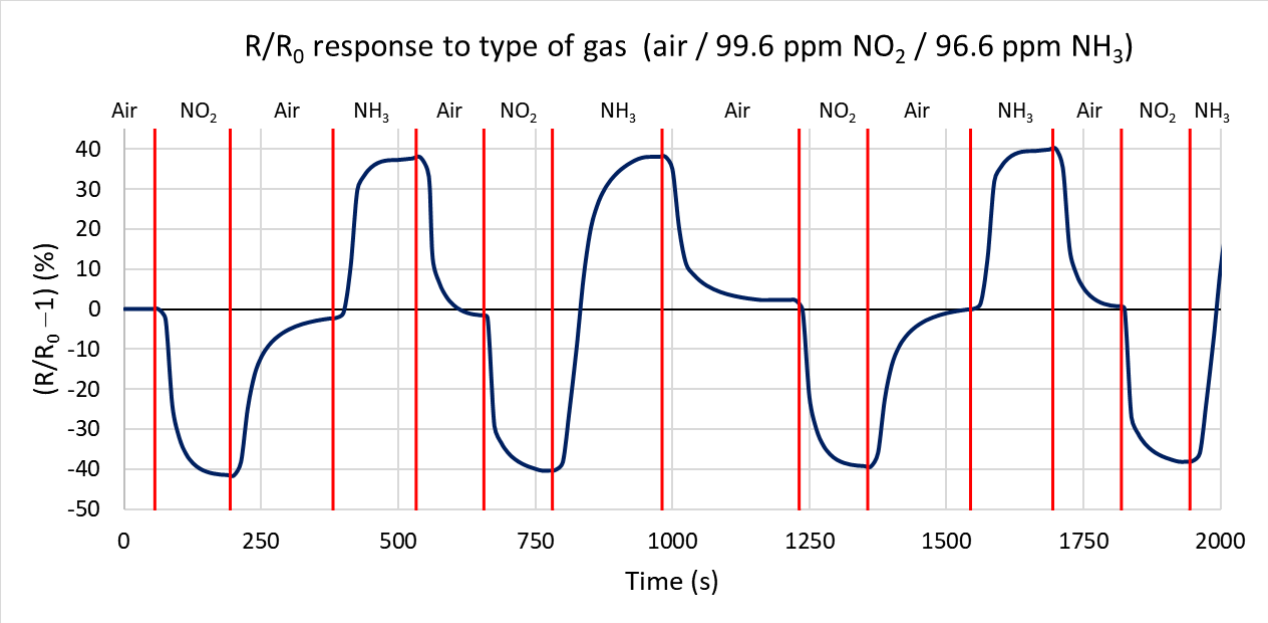

Figure 10. Time dependence of H-terminated NCD sensor's response to three types of gases (ammonia, nitrogen dioxide, and synthetic air) at 125 °C with a gas flow rate of 100 sccm.

Next, the response of the sensor to the reduction of the gas concentration at 125 °C is measured for ammonia concentrations of 96.6 ppm, 48.3 ppm, and 0 ppm (only synthetic air). Figure 11 shows the percentual dependence of the steady-state resistance on time. At a concentration of 96.6 ppm, the resistance increases by 38.5% from a steady value of 223 kΩ to 323 kΩ, in agreement with the first test. At a concentration of 48.3 ppm, the resistance decreases by 26% from a steady value of 224 kΩ to 294 kΩ. The difference of only 26% is caused by the non-linear sensitivity of NCD at a low concentration below 5 ppm. From these values, the calculated sensitivity is 0.26%/ppm, i.e., increasing the concentration by 1 ppm increases the resistance by 0.26%. The maximum rates of resistance change are very similar for repeated changes in the gas concentration (the sensor shows the repeatable dynamics of the response).

The response of the second sensor with an H-terminated NCD is measured with the same setup under the same conditions. The results are shown in Table 1. Subsequently, both sensors' responses are measured at temperatures of 75 °C and 40 °C using the same setup.

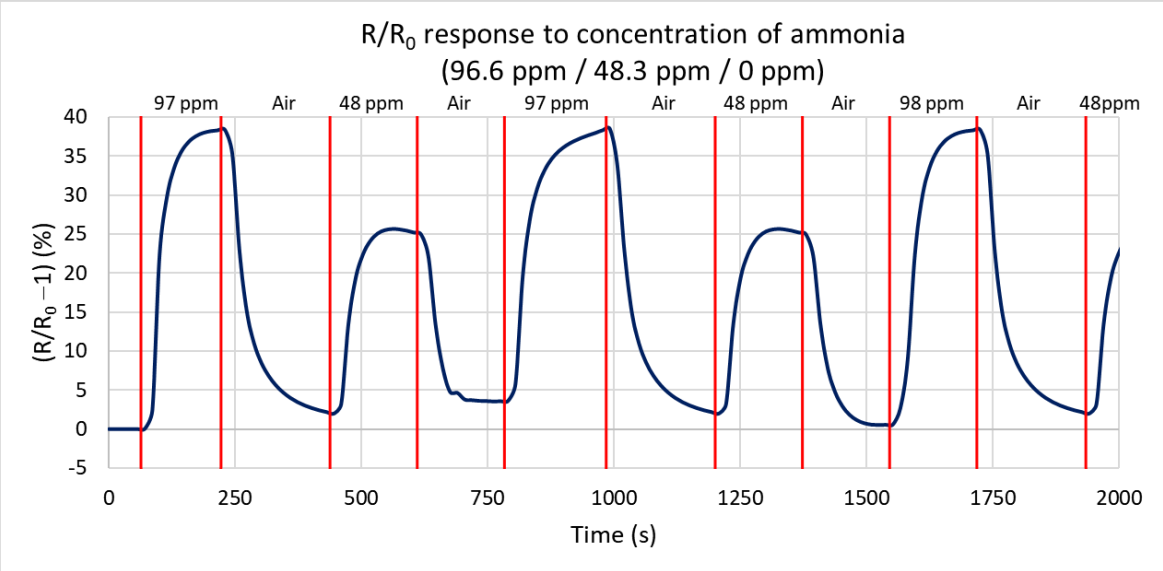

Figure 11. Time dependence of H-terminated NCD sensor's response to three concentrations of ammonia (96.6 ppm, 48.3 ppm, and 0 ppm (synthetic air)) at 125 °C with a gas flow rate of 100 sccm.

Table 1. Comparison of the responses and properties of the H-terminated NCD sensors with the TGS 826 and PY2055 commercial sensors.

	IDT Sensors with H-Terminated Diamond			**Commercial Sensors**	
	Temp. (°C)	**Sensor No. 1**	**Sensor No. 2**	**Figaro TGS 826 (SnO_2)**	**Pyreos PY2055 (IR Sensor)**
R_0 (kΩ)	125	216	111	52.9	0.12 (V)
	75	223	107		
	40	219	113		
$(R-R_0)/R_0$ response to 96.6 ppm NH_3 (%)	125	39	13	−16.9	N.A. $((U-U_0)/U_0)$
	75	4	5		
	40	N.A.	2.5		
$(R-R_0)/R_0$ response to 99.6 ppm NO_2 (%)	125	−41	−11	47.8	−46 $((U-U_0)/U_0)$
	75	−4.5	−7		
	40	N.A.	−5		
Time response to 96.6 ppm NH_3 (Ω/s)	125	908	183	−2238	N.A.
	75	84	123		
	40	N.A.	83		
Time response to 99.6 ppm NO_2 (Ω/s)	125	−998	−375	297	1.7 (%/s)
	75	−75	−214		
	40	N.A.	−102		
Sensitivity to NH_3 (%/ppm)	125	0.259	0.092	−0.135	N.A.
Sensitivity to NO_2 (%/ppm)	125	−0.161	−0.058	0.482	−0.315

3.2. TGS 826 SnO_2 Conductivity Sensor

In this test, the response of the TGS 826 commercial sensor is measured for both gas types, oxidizing and reducing. This sensor is one of the most used commercial sensors for detecting and sensing ammonia. The sensor responds to both testing gases by changing the conductivity. Figure 12 shows the percentual dependence of the steady-state resistance on time. The action of the reducing gas decreases the resistance of the active layer, and the oxidizing gas increases the resistance. The sensor responds faster to ammonia (the primary gas that the sensor should detect) than to the oxidizing gas. The values for this test range from −16.9% to 47.8%. For nitrogen dioxide, the maximum measured rate of change of the resistance is 0.297 kΩ/s. The lower value is probably due to the higher volume of the test chamber. For ammonia, this value reaches −2.238 kΩ/s.

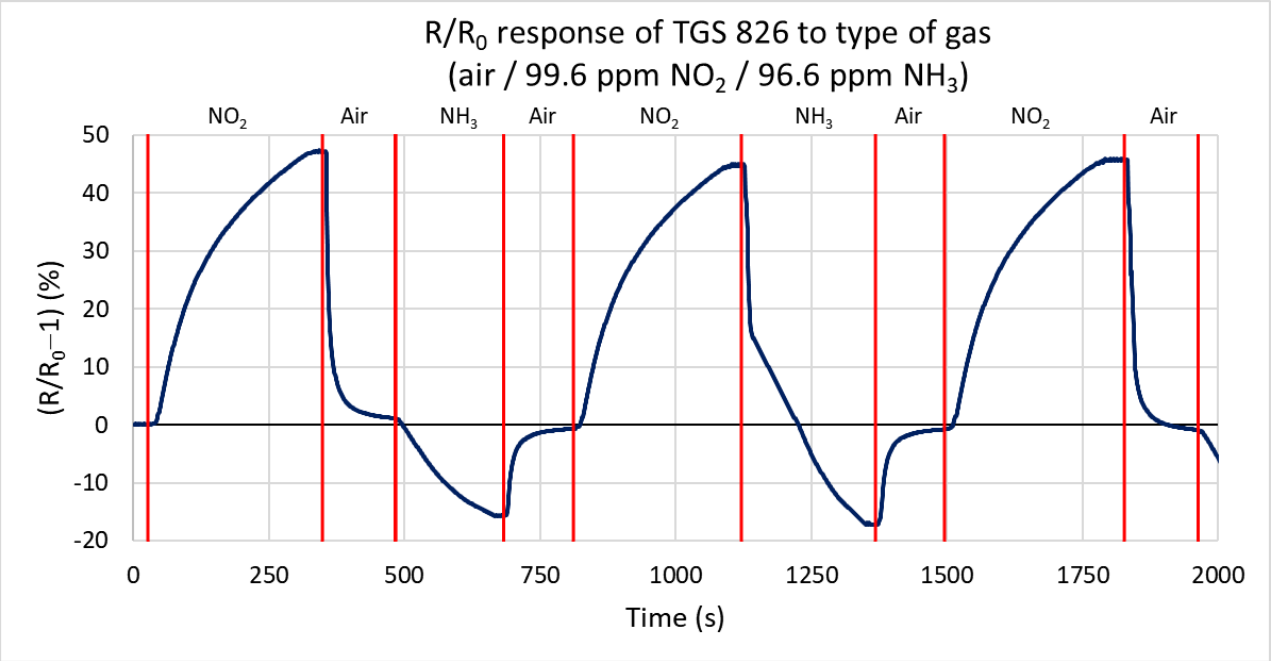

Figure 12. Response of TGS 826 sensor to three types of gases (ammonia, nitrogen dioxide, and synthetic air) at a gas flow rate of 100 sccm.

3.3. PY2055 Infrared Sensor

Ammonia and nitrogen dioxide with maximum concentrations of 99.6 ppm are used to test the infrared sensor's response. Figure 13 shows the percentual dependence of the output voltage's root mean square (RMS) value on the reference signal. Nitrogen dioxide (oxidizing gas) absorbs the IR radiation and decreases the effective value of the output signal. The ratio does not change under the action of ammonia. The range of response values is from 0% to −46%. At 99.6 ppm nitrogen dioxide, the ratio decreases by 46%, and at a concentration of 49.8 ppm, it decreases by 23%. The sensitivity is −0.3146%/ppm. For nitrogen dioxide, the rate of change is only 1.7%/s. The lower value of this rate is mostly due to the higher volume of the test chamber.

3.4. Comparison of Sensors

The electronic properties and responses of the sensors are summarized in Table 1. The table includes the measured data for two commercial sensors and two conductivity interdigital sensors with H-terminated diamond active layers, which were heated to three different temperatures, 125, 75, and 40 °C. Bold values indicate the best value from each row.

The time necessary to reach the operating temperature of H-terminated diamond active layers is one minute, and the power consumption for the first measurement (the

energy to heat up to operating temperature) is 125 W·s for 125 °C, 45 W·s for 75 °C, and only 20 W·s for 40 °C. Both sensor layers are created by the same technological process, but they exhibit different gas and temperature responses. These differences are most likely due to small differences in nucleation, deposition, and the structure of the thin layer (barriers between particles, etc.). The second sensor shows lower response to the gas at the temperature of 125 °C, but it can also be used at a low temperature of 40 °C, as shown in Table 1.

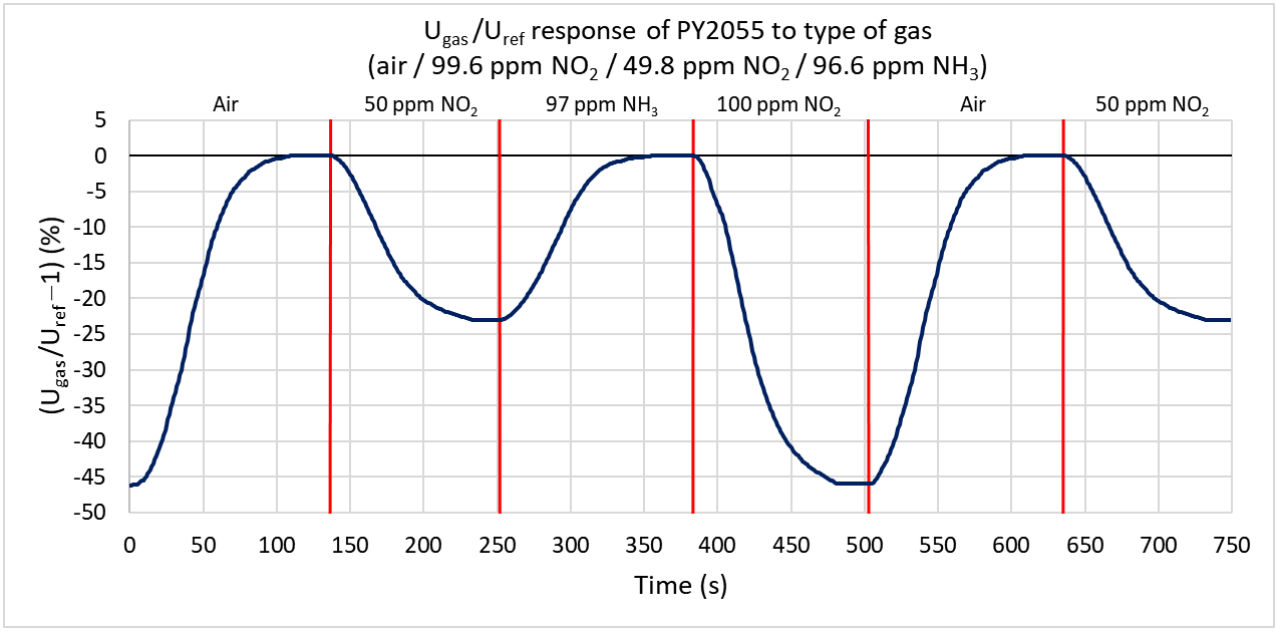

Figure 13. Response of PY2055 sensor to three types of gases (ammonia, nitrogen dioxide, and synthetic air) at a gas flow rate of 100 sccm.

The first commercial sensor is the Figaro TGS 826, which uses SnO_2 on the ceramic tube as an active material and a complementary principle similar to that of the diamond layer. The sensor consists of a 0.8 W heating element in the ceramic tube [14]. The total power consumption for one measurement is 240 W·s due to the 5 min of preheating necessary to reach the operating temperature of 300 °C [17]. The second sensor is the Pyreos PY2055: it uses absorption spectrophotometry in the infrared region of the spectrum, which is very selective. The total power consumption of this type of sensor depends on the IR radiation source used. A 1.2 W bulb with a 50% duty cycle was used in this case, and the total consumption is only 3 W·s.

4. Discussion

The designed and realized system is fully functional and suitable for testing sensors on two gas types, unlike most systems, which use only one active gas [6,9]. The selection valve allows fast switching between gases while keeping the flows constant, which allows a sufficiently continuous and defined measurement, minimizing peak-like events, in contrast to a system without a selection valve [6].

Experimental results show that the H-terminated NCD sensors are fully functional, with similar electrical characteristics to those of commercial sensors. However, the SnO_2-based sensor has a faster response than the diamond-based sensors. The differences in sensor characteristics may be due to differences in the active material volume and the sensing material's properties (i.e., surface morphology, etc.) [1,10]. The TGS 826 sensor consists of a ceramic tube with SnO_2 on the surface, conductive electrodes, and a heating element ensuring the correct temperature, which is almost 200 °C higher (300 °C total) than the temperature of the H-terminated NCD sensors [17]. This arrangement allows gas access

from all sides, unlike an interdigital structure with a thin layer. The other commercial sensor, PY2055, uses a different principle than the conductivity sensors. Infrared gas sensors use absorption spectrophotometry in the infrared region of the spectrum. This principle is suitable for gases formed by a more complex or asymmetric molecule; it shows a change in the molecule's energy state [15]. IR sensors are not suitable for detecting gases with a monoatomic or symmetric diatomic molecule, as these gases do not absorb radiation in the infrared [15]. This sensor also needs an IR source and evaluation electronic components to compare it to conductivity sensors, which require only an ohmmeter or SMU. However, this sensor is highly selective, as shown in experimental measurements [15].

Both sensors with an H-terminated NCD layer were prepared using the same technological process. At such a low film thickness, the polycrystalline film is dominated by grain boundaries and defects localized at these boundaries. As a result, it is still complicated to create two almost identical diamond samples. We propose that the observed response differences should be assigned to inhomogeneities in the diamond crystals and traps localized at the diamond sub-surface. Using larger IDT dimensions, such differences should be suppressed but at lowered sensitivity. The fabrication reproducibility can be improved by better controlling the fabrication steps, such as by ensuring a more densely packed nucleation density, the exact cooling of layers during switching off, etc. Similarly, commercial production also faces some reproducibility issues; for example, the TGS 826 conductivity sensors are produced in series and are subsequently tested and sorted into eighteen groups [14] by nominal resistance and sensitivity to ammonia.

In addition to the exposed gas type, the sensor conductivities are sensitive to other physical and material parameters, which can further increase or reduce the sensitivity of the sensors to the gas. Among the physical quantities by which the impedance sensor characteristics are determined, light, humidity, and temperature are the most important factors [7,18]. The H-terminated diamond gas sensor's temperature is crucial to its reaction dynamic because higher temperatures increase the reactivity with the gas and reduce the response to the intensity of light [18].

4.1. SnO_2 Surface Gas Interaction Model

The change in conductivity in SnO_2 is caused by chemisorption, reflecting the binding (sorption) of oxygen molecules on its solid surface by chemical bonding with electron transfer. Figure 14 depicts a schematic view of the time-sequenced set of interactions. The transfer of electrons between substances is called the oxidation-reduction process [1,15,19]. In the case of the oxidizing gas, NO_2 (Figure 14 left), free electrons are removed; thus, the conductivity of the n-type semiconductor is reduced. In Figure 14a, NO_2 gas molecules are adsorbed on the surface of the SnO_2 bulk; the gas attacks the available Sn sites and removes electrons from the conduction band, forming NO_2^-. This increases the barrier between particles and reduces conductivity. Subsequently, in Figure 14b, molecules of NO_2^- desorb as NO, leaving binding oxygen ions behind [19,20]. After exposure to a non-oxidizing gas (in Figure 14c), chemisorbed oxygen molecules with negative charges on the surface are released as O_2 with a neutral charge, and electrons are returned to SnO_2 [20]. This returns the conductivity to its previous value. Exposing the SnO_2 surface to the reducing gas NH_3 (Figure 14 right) transfers free electrons into the material and increases the conductivity of the n-type semiconductor. In Figure 14d, molecules of NH_4 are adsorbed, react with binding oxygen ions, and create charge-neutral NO and H_2O (air humidity) molecules. The excess electrons from the oxygen ions are transferred into semiconductors (in Figure 14e). This increases the conductivity and reduces the barrier between particles [20]. After exposure to a non-reducing (i.e., air) gas (in Figure 14f), the conductivity returns to the previous value due to the sorption of two oxygen ions from the neutral O_2 and the removal of free electrons [20].

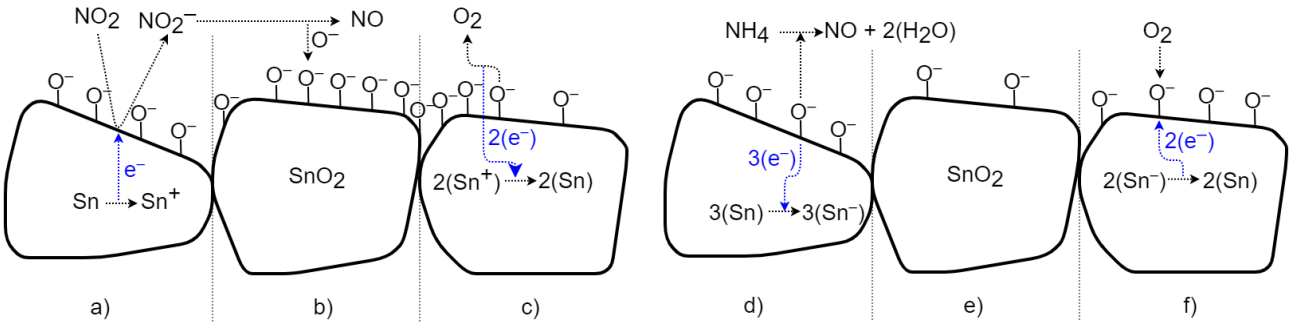

Figure 14. Schematic time process of gas interaction between the SnO_2 material and oxidizing and reducing gases.

4.2. H-Terminated NCD Surface Gas Interaction Model

H-terminated NCD reveals a similar detection principle to the surface of SnO_2 but with the opposite effect on its surface conductivity. The change in the NCD surface conductivity does not work on the gas sorption principle: it involves chemical reactions forming counter ions on its surface via an electron transfer model [7]. A widely established H-terminated diamond surface doping mechanism was used to explain the sensing mechanism. A thin layer of adsorbed water from the air is formed on the diamond surface [11]. The water molecule dissociates the ions H_3O^+ and OH^-. The H_3O^+ ions attract electrons from the diamond surface, so the p-type surface conductivity is formed on the H-terminated NCD (Figure 15a,d)). If oxidizing gas molecules (NO_2) are present (Figure 15b), the concentration of H_3O^+ ions rises due to a set of chemical reactions of the oxidizing gas with the adsorbed water monolayer. This causes a superiority of H_3O^+ molecules and creates a charge imbalance. Electrons are transferred from the diamond top surface to the direction of positive ions. Next, the resultant holes increase the 2DHG conductivity [2,10,11]. After exposure to a non-oxidizing (air) gas (Figure 15c), the number of H_3O^+ ions decreases and again H_3O^+ equilibrates with OH^-. The electrons return to the diamond, and conductivity reduces to its original value [10]. In the case of a reducing gas, such as NH_3 (Figure 15e), the concentration of OH^- ions increases due to the set of chemical reactions of the reducing gas with the adsorbed water monolayer. Due to the higher number of NH_4^+ ions, the concentration of the ions decreases, and electrons are shifted to the diamond and partially neutralize the 2DHG, which finally reduces the diamond's surface conductivity [10,12]. After exposure to a non-reducing (air) gas (Figure 15f), the number of OH^- ions decreases and OH^- equilibrates with H_3O^+ again. The electrons return from the diamond, and the conductivity increases to the original value.

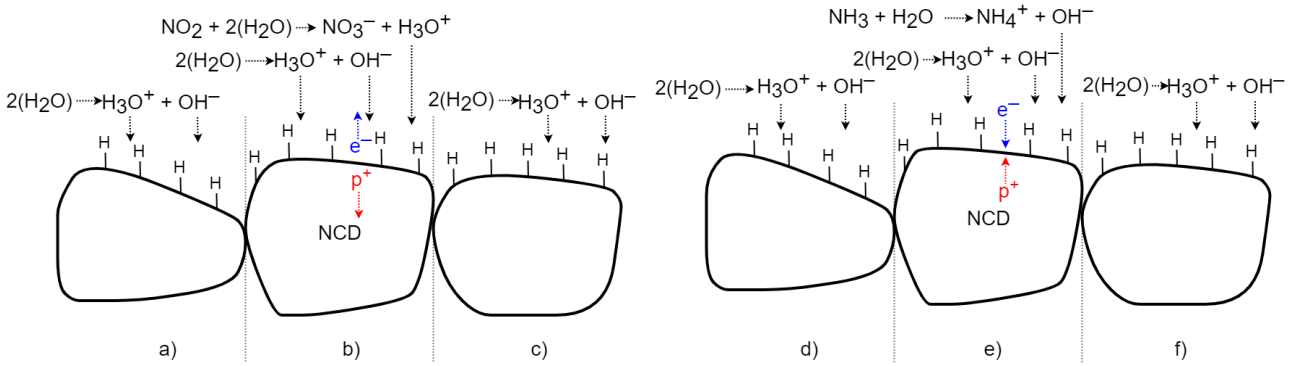

Figure 15. Schematic time process of gas interaction between the H-terminated NCD and oxidizing and reducing gases.

5. Conclusions

An NCD layer with H-termination was used as the active layer of the conductivity sensors. The crystallographic morphology of the prepared sensors with H-terminated NCD thin layers was confirmed by SEM and Raman spectroscopy. The SEM showed a continuous diamond layer on the electrode and glass, and the Raman spectra exhibit a sharp diamond peak for both parts. Fabricated H-terminated NCD sensors revealed sensor characteristics comparable to two commercial sensors in a similar testing setup after they were exposed to the reducing and oxidizing gases. The fabricated sensors have smaller dimensions and require a shorter amount of time for the first measurement, and thus they require less energy than the commercial TGS 826. Still, the TGS 826 sensor had a faster response to ammonia, due to a larger active surface area and a geometrical arrangement that allowed the gas access from all sides [17]. The infrared PY2055 sensor exhibits the highest selectivity, but it requires an IR source, which increases the consumption of electrical energy and demands on the size of the sensor system. It reacts only to nitrogen dioxide (selective gas), as declared in the manufacturer's datasheet [16]; this was confirmed by measurements. The lower value of the time response is due to the higher volume of the test chamber. Overall, it is possible to conclude that hydrogen-terminated diamond expands the family of wide-bandgap semiconductors, where gas detection is possible even at temperatures of 100 °C. Moreover, its surface sensitivity can be enhanced not only by geometrical design (IDT distance) or surface morphology (nanorods) but also by using diamond-based composites, metal oxides, or transition metal dichalcogenide monolayers operated at low temperatures, with a reliable, reproducible response tuned to specific gas sensing applications.

Author Contributions: Conceptualization, M.K., A.B. and A.K.; methodology, M.K. and A.K.; software, M.K.; investigation, M.K., O.S. and A.K.; experiments, M.K. and O.S.; data curation, M.K.; writing—original draft preparation, M.K. and O.S.; writing—review and editing, A.B., O.S., M.H. and A.K.; supervision, M.H. and A.K. All authors have read and agreed to the published version of the manuscript.

Funding: This research was funded by the bilateral GAAV project no. SAV-21-10 and by the Operational Program Research, Development and Education, financed by European Structural and Investment Funds and the Czech Ministry of Education, Youth and Sports (Project No. SOLID21-CZ.02.1.01/0.0/0.0/16_019/0000760). This work used the large research infrastructure CzechNanoLab supported by the LM2018110 project and partially by CTU project No. SGS20/175/OHK3/3T/13 Integrated and phonic circuits and microstructures.

Institutional Review Board Statement: Not applicable.

Informed Consent Statement: Not applicable.

Data Availability Statement: The data presented in this study are available on request from the corresponding author.

Acknowledgments: The authors kindly acknowledge R. Jackivová for the SEM and E. Shagieva for the Raman measurements.

Conflicts of Interest: The authors declare no conflict of interest.

References

1. Wang, C.; Yin, L.; Zhang, L.; Xiang, D.; Gao, R. Metal Oxide Gas Sensors: Sensitivity and Influencing Factors. *Sensors* **2010**, *10*, 2088–2106. [CrossRef] [PubMed]
2. Helwig, A.; Mueller, G.; Garrido, J.A.; Eickhoff, M. Gas Sensing Properties of Hydrogen-Terminated Diamond. *Sens. Actuators B Chem.* **2008**, *133*, 156–165. [CrossRef]
3. Liao, M.; Shen, B.; Wang, Z. *Ultra-Wide Bandgap Semiconductor Materials*; Elsevier: Amsterdam, The Netherlands, 2019; ISBN 9780128172568.
4. Sze, S.M.; Ng, K.K. *Physics of Semiconductor Devices*, 3rd, ed.; Wiley: Hoboken, NJ, USA, 2007; ISBN 0471143235.
5. Adachi, S. *Properties of Group-IV, III-V and II-VI Semiconductors*; Wiley: Hoboken, NJ, USA, 2005; ISBN 9780470090343.
6. Joshi, R.K.; Weber, J.E.; Hu, Q.; Johnson, B.; Zimmer, J.W.; Kumar, A. Carbon Monoxide Sensing at Room Temperature via Electron Donation in Boron Doped Diamond Films. *Sens. Actuators B Chem.* **2010**, *145*, 527–532. [CrossRef]

7. Gurbuz, Y.; Kang, W.P.; Davidson, J.L.; Kinser, D.L.; Kerns, D.V. Diamond Microelectronic Gas Sensors. *Sens. Actuators B Chem.* **1996**, *33*, 100–104. [CrossRef]
8. Sato, H.; Kasu, M. Electronic Properties of H-terminated Diamond during NO2 and O3 Adsorption and Desorption. *Diam. Relat. Mater.* **2012**, *24*, 99–103. [CrossRef]
9. Laposa, A.; Kroutil, J.; Davydova, M.; Taylor, A.; Voves, J.; Klimsa, L.; Kopecek, J.; Husak, M. Inkjet Seeded CVD-Grown Hydrogenated Diamond Gas Sensor Under UV-LED Illumination. *IEEE Sens. J.* **2020**, *20*, 1158–1165. [CrossRef]
10. Davydova, M.; Kulha, P.; Laposa, A.; Hruska, K.; Demo, P.; Kromka, A. Gas Sensing Properties of Nanocrystalline Diamond at Room Temperature. *Beilstein J. Nanotechnol.* **2014**, *5*, 2339–2345. [CrossRef] [PubMed]
11. Davydova, M.; Stuchlik, M.; Rezek, B.; Larsson, K.; Kromka, A. Sensing of Phosgene by a Porous-Like Nanocrystalline Diamond Layer with Buried Metallic Electrodes. *Sens. Actuators B Chem.* **2013**, *188*, 675–680. [CrossRef]
12. Mueller, G.; Krstev, I.; Maier, K.; Helwig, A.; Stutzmann, M.; Garrido, J. Resettable, Low-Temperature Accumulation Gas Sensors Based on Hydrogenated Diamond Transducers. *Eurosensors* **2015**, *120*, 590–593. [CrossRef]
13. Kromka, A.; Davydova, M.; Rezek, B.; Vanecek, M.; Stuchlik, M.; Exnar, P.; Kalbac, M. Gas Sensing Properties of Nanocrystalline Diamond Films. *Diam. Relat. Mater.* **2010**, *19*, 196–200. [CrossRef]
14. FIGARO USA, INC. TGS 826—For the Detection of Ammonia: Product Information. Available online: https://www.figarosensor.com/product/docs/TGS%20826%20%2805_04%29.pdf (accessed on 22 December 2020).
15. Štulík, K.; Barek, J.; Janata, J.; Král, V.; Krond'ák, M.; Šťastný, M. *Sensors: General Aspects of Chemical Sensing*; VŠCHT: Prague, Czech Republic, 2007; ISBN 9788086238203.
16. Pyreos Limited, Thin Film Pyroelectric Dual Channel Sensor: Product Information. Available online: https://pyreos.com/wp-content/uploads/2020/11/Pyreos-Analog-TO-Two-Channels.pdf (accessed on 22 December 2020).
17. FIGARO USA, INC. FIGARO GAS SENSORS: 1-Series and 8-Series: Product Catalogue. Available online: https://www.figarosensor.com/product/docs/figaro_tgs_serien.pdf (accessed on 1 February 2020).
18. Nahlik, J.; Laposa, A.; Voves, J.; Kroutil, J.; Drahokoupil, J.; Davydova, M. A High Sensitivity UV Photodetector with Inkjet Printed ZnO/Nanodiamond Active Layers. *IEEE Sens. J.* **2019**, *19*, 5587–5593. [CrossRef]
19. Sharma, A.; Tomar, M.; Gupta, V. SnO2 Thin Film Sensor with Enhanced Response for NO2 Gas at Lower Temperatures. *Sens. Actuators B Chem.* **2011**, *156*, 743–752. [CrossRef]
20. Wang, Y.; Zhao, Z.; Sun, Y.; Li, P.; Ji, J.; Chen, Y.; Zhang, W.; Hu, J. Fabrication and Gas Sensing Properties of Au-loaded SnO2 Composite Nanoparticles for Highly Sensitive Hydrogen Detection. *Sens. Actuators B Chem.* **2017**, *240*, 664–673. [CrossRef]

II. Enhanced gas sensing capabilities of diamond layers using Au nanoparticles

Authors: Michal Kočí, Ondrej Szabó, Gabriel Vanko, Miroslav Husák, Alexander Kromka

Diamond & Related Materials 138 (2023) 110218

Contents lists available at ScienceDirect

Diamond & Related Materials

journal homepage: www.elsevier.com/locate/diamond

Enhanced gas sensing capabilities of diamond layers using Au nanoparticles

Michal Kočí [a,b,*], Ondrej Szabó [a], Gabriel Vanko [c], Miroslav Husák [b], Alexander Kromka [a]

[a] Department of Semiconductors, Institute of Physics of the Czech Academy of Sciences, Prague 162 00, Czech Republic
[b] Department of Microelectronics, Faculty of Electrical Engineering, Czech Technical University in Prague, Prague 166 27, Czech Republic
[c] Department of Microelectronics and Sensors, Institute of Electrical Engineering, Slovak Academy of Sciences, Dúbravská Cesta 9, Bratislava 841 04, Slovak Republic

ARTICLE INFO

Keywords:
Gas sensors
H-terminated NCD (H-NCD)
O-terminated NCD (O-NCD)
Gold nanoparticles (Au NPs)

ABSTRACT

The nanocrystalline diamond (NCD) film reveals a unique combination of physical, chemical, and optoelectronic properties, which makes it a promising material for various sensing applications. To improve a gas sensor's response, selectivity, or reproducibility, its surface is often modified with specific terminations, functional groups or (bio)molecules, thin films, etc. In this work, the NCD surface modification was achieved by a) layer morphology variation using two different types of chemical vapor deposition (CVD) systems, b) top surface termination (H-NCD and O-NCD), and c) Au nanoparticles (Au NPs). The properties of each structure are measured, compared and subsequently evaluated. The electrical properties (resistance changes) are measured for two types of active gas (oxidizing gas NO_2 and reducing gas NH_3) in a temperature range from 22 °C to 125 °C. Neutral synthetic air (80 % nitrogen and 20 % oxygen) was applied for flushing and resetting the sensors. Thin film fabrication, surface analysis (scanning electron microscopy and Raman spectroscopy), and measurement of electrical properties are described. Surface morphology greatly influences gas response because a large active surface area (higher roughness or 3D-like surface) enhances interaction with gas molecules. While the termination of the NCD with hydrogen is essential for the functionality of the gas sensor, the Au NPs further enhanced the dynamic response of the sensor and magnitude.

1. Introduction

The growing number of dangerous substances released into the air (mainly by heavy industry) reduces the overall quality of life. A strong emphasis is placed on monitoring the concentration of toxic pollutants (NH_3 or NO_2) with a significant impact on human health. Therefore, gas sensors are almost an integral part of industry and everyday life. In the last 20 years, one can observe an increasing interest in air quality monitoring with a focus on harmful pollutant detection [1].

Currently, the most used gas sensors use the conductivity principle and metal oxide (MO_X) material, especially SnO_2. MO_X is used for its low price and flexible production [1,2]. On the other hand, the high operating temperature (over 300 °C) and the relatively large dimensions are limiting factors that prevent applications as sensor nodes for Internet-of-Things with integrated energy harvesting supply [1,2]. The main requirements are related to the optimized battery capacity and energy transfer to enhance sensor nodes with the long-life operation. The development of sensors working at a lower temperature (100 °C and lower) is very important due to reducing consumption and reducing dimensions. Among the carbon-based gas sensors, reduced graphene oxide (rGO) with sensitivity 0.004 %•ppm^{-1} [3] and carbon nanotubes (CNT) [4] are mainly considered for gas sensors operating at room temperature. Considering that the electronic properties of CNTs are highly sensitive toward any change in their chemical environment, several exciting works on pristine CNTs as chemoresistive sensors have been widely explored, where their sensitivity is affected by the number of walls, i.e., SWCNT-based sensors have higher sensitivity than MWCNTs for NO_2 sensing even at a low operating temperature. In this case, Naje et al. [5] investigated SWCNTs and MWCNTs for sensing 3 % NO_2 gas and observed 79.81 % and 59.61 % sensitivity, respectively. Due to the lower sensitivity of pristine CNTs, functionalized CNTs have also been studied to enhance the selectivity toward specific analytes. In addition, various metallic nanoparticles and metal oxides have been incorporated into CNTs to achieve specificity to different analytes. In this case, ZnO-doped SWCNTs [6] and ZnO-doped MWCNTs [7] were investigated for NO_2 sensing, which exhibited the highest sensitivity at operating temperatures of 150 °C and 300 °C, respectively. The NO_2 sensing mechanism of monolayer, bilayer and multilayer graphene gas sensors has been presented in [8]. They have measured gas response (Δ_R/R) of layered graphene gas sensors as a function of NO_2

* Corresponding author at: Department of Semiconductors, Institute of Physics of the Czech Academy of Sciences, Prague 162 00, Czech Republic.
E-mail addresses: kocim@fzu.cz, kocimic1@fel.cvut.cz (M. Kočí).

https://doi.org/10.1016/j.diamond.2023.110218
Received 11 January 2023; Received in revised form 21 June 2023; Accepted 16 July 2023
Available online 19 July 2023

concentration up to 35 % with a considerable selectivity to various gases at room temperature. Further, for bendable NO_2 sensors, various CNT-polymer hybrids have been explored. In 2019, Kumar et al. [9] reported NO_2 sensing using a polyethyleneimine (PEI)-functionalized SWCNT sensor. The as-made sensor showed high sensitivity (37 %) for 50 ppm NO_2 at room temperature with recovery time (240 s). A comparison of NO_2 sensing at room temperature is given in Table 3 within the reference [10].

For those reasons, high demands are placed on developing new high-accuracy sensors for detecting various kinds of gases, which must show excellent reproducibility, sensitivity, and stability. Smaller, more accurate, and cheaper sensors with a lower production cost are being developed utilizing new materials and processing. It needs to use novel sensing materials, surface modification, or new fabrication processes to increase the sensor's performance [11–17]. In accordance with that, great attention is focused on new materials suitable for conductivity gas sensors. Gas sensors with Wide BandGap semiconductors (exceptionally diamond thin layers) have immense potential due to possible miniaturization and modification, e.g., material science or technology progress [16–19].

The method of improving gas response by reducing the resistance with a more conductive material is well-known and used. This principle is used for carbon-based gas sensors [20–22] or MO_X gas sensors [23–25], which is a more common material for gas sensing applications [1,25]. These pristine materials exhibit unsatisfactory responses to gases and high working temperatures, which might limit their applications. Samples treated with this method, adding more conductive material, show a better response to gases than pure materials, especially at room temperature [20,21,23]. But the response is still low at room temperature [20], or layer preparation is very complex (nanotubes, etc.) [22,23].

This work presents an NCD film decorated with Au as the active layer for gas sensing applications. Microwave plasma-enhanced CVD formed the NCD film, and the gas-sensitive conductive layer was induced by the hydrogen termination (H-NCD). The H-NCD films with the best morphology for sensors were also coated with Au NPs. Then the gas sensing capabilities of the H-NCD + Au NPs hybrid system in oxidizing and reducing gas mixtures were studied, and results were compared and discussed.

2. Experimental

2.1. H-NCD and H-NCD + Au NPs layers preparation

The fabrication and measuring of four types of sensors with NCD active layer are described in the following chapter. The interdigital (IDT) structures from Micrux Technologies with 90 pairs of 10/10/0.2 μm Au electrodes (10 μm width and 10 μm gap between electrodes with thickness of 200 nm) were used as a substrate for diamond growth. This structure shows very good adhesion of the diamond layer and good stability during deposition. The NCD layers were prepared by microwave plasma-enhanced chemical vapor deposition (MWPECVD). After separating technological steps, the fabricated sensor is depicted in Fig. 1.

First, the IDT Au electrodes were ultrasonic cleaned in acetone, isopropylalcohol, deionized water for 10 min and dried by nitrogen flow.

In all cases, the diamond nucleation layer was prepared by the substrate treatment in the ultrasound bath in water-based nanodiamond powder suspension (NanoAmando, with nominal particle size 5 nm) for 40 min.

The first prepared layer was made in a focused MW plasma system (Aixtron P6 deposition device). This system is characterized by a high-density plasma resulting in high diamond growth rates at higher temperatures (>450 °C). During the diamond layer growth on glass substrates with IDT electrodes, a technological limitation in layer inhomogeneity and peeling due to high temperature in the focused plasma system was observed. The reduced adhesion of diamond layers on glass substrates with IDT electrodes was probably due to the stress between the crystallographic structure of the diamond and substrate and the different thermal expansion of the different materials. The improvement of the homogeneity and adhesion of diamond on IDT electrodes was achieved by using an adhesive interlayer, also diamond, but deposited in a different deposition system with linear antennas. The deposition system where the adhesive diamond layer was prepared is characterized by two linear microwave antennas (Roth&Rau AK 400 deposition device) where diamond deposition takes place under low-temperature loading of the substrates (temperatures <350 °C), leading to low growth rates. The process parameters of the system with linear antennas are as follows: power of MW generators 1700 W, working pressure 0.15 mbar of gas mixture 150 sccm H_2, 5 sccm CH_4 (3.3 %), 20 sccm CO_2 (13.3 %), deposition time 20 h, heating of the substrate holder to 300 °C (during deposition did not exceed 325 °C). The diamond layer was prepared at a thickness of 100 nm (a deposition rate of about 5 nm/h). The H-NCD diamond layer was realized in the focused plasma system Aixtron P6. The process parameters of the system with focused plasma are as follows: power of MW generators 1500 W, working pressure 30 mbar of gas mixture 300 sccm H_2, 3 sccm CH_4 (1 %), deposition time 3 h, during the deposition the temperature did not exceed 520 °C. The diamond layer was prepared at a thickness of 120 nm (a deposition rate of about 40 nm/h). It was necessary to functionalize the diamond layer by H-termination in hydrogen MW plasma. Immediately after the diamond deposition, the CH_4 flow was turned off and the surface was terminated with hydrogen for 10 min under the same power, temperature, and hydrogen flow conditions.

The second prepared layer was made in the same system as the adhesive diamond layer at the same conditions. Similar to the previous sensor, the H-termination was necessary for the diamond surface conductivity. Immediately after the diamond deposition, the CH_4 and CO_2 flow was turned off and the surface was terminated with hydrogen for 10 min under the same power, temperature, and hydrogen flow conditions.

The third type of sensor was the O-termination (O-NCD) prepared using the same procedure as the second sample, but instead of hydrogen plasma, oxygen plasma was used for O-NCD. First, the sample was

Fig. 1. Photographs of a) Au IDT structure on a glass substrate, b) H-NCD from focused plasma system, c) H-NCD from linear plasma system, d) O-NCD from linear plasma system, and e) H-NCD + Au NPs from linear plasma system.

placed in the chamber of the Tesla VT 214 followed by pumping until the air pressure in the chamber was about 22 Pa. Next, the chamber was filled with oxygen (50 sccm), and the pressure in the chamber increased to 60 Pa. After that, the plasma modification process was initiated. The plasma was generated by a radio frequency source with 100 W input power for 1 min. Finally, after the plasma modification process, the chamber was filled with air to atmospheric pressure and the sample was removed.

The fourth type of sensor was prepared as the second sample, and its surface was additionally coated with Au NPs. The Au NPs were prepared by evaporating a thin Au layer (thickness 3 nm) on the H-NCD, which was further annealed in hydrogen microwave plasma (H_2, 500 °C for 10 min). This treatment resulted in the formation of nano-sized particles (droplets) on the diamond surface. The Au NPs were chosen due to chemical stability and preparation that hardly affects the active H-NCD layer.

The evolution process and the applied layers are schematically shown in Fig. 2. After sample preparation, all were let to stabilize for 48 h before gas characterization.

2.2. Surface characterization

The surface morphology of prepared samples was measured by a scanning electron microscope (SEM) Tescan MAIA 3. The first sample prepared by a focused plasma system (Fig. 3a) had the same morphology on the whole substrate (on the gold and glass areas). The second sample prepared by linear plasma system (Fig. 3b) revealed different morphologies on gold and glass, as seen in SEM. The NCD had higher roughness on the glass, further enhancing the contact area between gas and NCD and increasing the response size. In the case of the third sample (Fig. 3c), the surface morphology did not change compared to the second sample because the termination had no impact. The last sample with Au NPs has similar morphology of NCD to the previous two samples. The morphology of the Au NPs layer is shown in Fig. 3d, and their size and concentration were measured and calculated. The chemical composition of the prepared samples was measured with a Renishaw inVia Reflex Confocal Raman microscope with a 442 nm laser. Raman spectra of samples are illustrated in Fig. 4. The samples exhibit a typical Raman spectrum for NCD. In this spectrum, there is a representative narrow peak at 1331 cm^{-1} attributed to the first-order diamond peak and two broad bands labeled as D and G at 1362 cm^{-1} and 1595 cm^{-1} recognized as disordered sp^2 carbon phases and graphitic phases [12,16].

Using an SEM image, the diameters and density of Au NPs were analyzed from backscattered electrons (BSE) (Fig. 5a). BSE showed a contrast between diverse materials (carbon and gold) used for computer post-processing (Fig. 5b). Fig. 5c plots the calculated probability density as a function of particle diameter from the program ImageJ. ImageJ is a public-domain Java image processing and analysis program inspired by NIH Image. It can calculate the statistics of user-defined selections based on area and pixel values and can measure distances and angles to create density histograms and line profile plots. It supports standard image processing functions such as contrast manipulation, sharpening, smoothing, edge detection, and median filtering.

The diameter of Au NPs was found to vary between 7.5 and 40 nm with Log-normal distribution with the modus d_M 17.5 nm. It has been previously shown that by using a linear antenna system with CO_2 in the feed gas, the formation of nanoparticles from the underlying Au layer can occur, and need to be suppressed [26]. Contrary to this work, we provided experiment at different parameters (MW power, gas composition, different adhesion layer - Ti instead of Cr) which did not result in the formation of Au NPs from IDT metallization. In addition, we mainly focused on the formation and use of Au NPs formed on the diamond layer.

2.3. Experimental setup for gas sensors testing

A homemade computer-controlled system was used to measure the responses of prepared sensors. The system prepared two independent gas mixtures of oxidizing NO_2 and reducing NH_3 gases with concentrations of 100 ppm. Synthetic air (80 % of N_2 and 20 % of O_2) is used for flushing and resetting the sensors. The resistance changes are measured using a source measure unit (SMU) Keithley SourceMeter 2401 with four-wire DC resistance measurement (Kelvin resistance measurement). The fabricated sensors were measured with a nominal voltage value of 0.1 V. The temperature sensor PT1000 measures the temperature in the chamber via a standard Ohmmeter. The sensors were placed in a gas chamber with a total volume of 20 mm^3, allowing a quick ambient change around the sensors.

3. Results

The responses and properties were measured at three selected values of temperature (125 °C, 75 °C, and room temperature about 22 °C) for two types of active gas with the same concentration of 100 ppm: reducing (NH_3) and oxidizing (NO_2) gas. First, the steady-state resistance R_0 values of the active layers on the different sensors were measured (Fig. 6a). The gas-sensitive layer changed the resistance from steady-state R_0 to actual resistance R_G in the presence of the tested gas. The resistance changes Δ_R in the presence of active gas were calculated by Eq. (1). The calculated responses are shown in Fig. 6b and c for NH_3 and NO_2, respectively. The steady-state resistance decreased slightly with increasing temperature, but the change was <5 % for a temperature change above 100 °C. The main reason for the small change is subsurface 2DHG. The bulk resistance is very high and the 2DHG has very little change in resistance with increasing temperature [27].

$$\Delta_R = \left(\frac{R_G}{R_0} - 1\right)\cdot 100 = \left(\frac{R_G - R_0}{R_0}\right)\cdot 100\ (\%) \quad (1)$$

Fig. 7 shows the percentage change dependence over time of all tested samples. The sequence of the gases was as follows: NO_2 for 3 min, followed by synthetic air (+3 min), then the gas was switched to NH_3 for another 3 min followed by synthetic air and synthetic air with 90 % humidity (+3 min), finished by synthetic air again.

The H-NCD prepared in a focused plasma system (the first type) had the lowest resistance value and gas response smaller than 5 %. The small response was probably due to the a) high-temperature deposition system

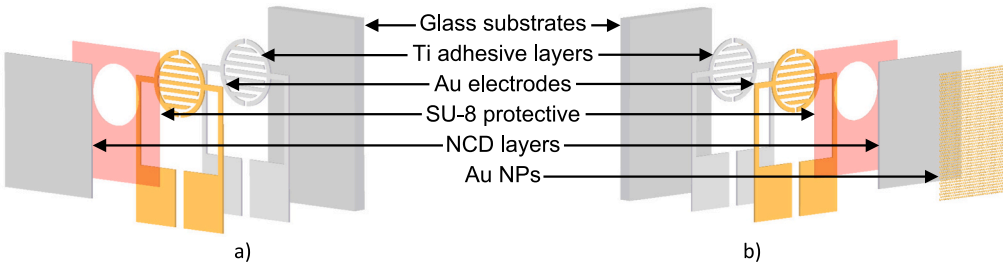

Fig. 2. Exploded schematic views of prepared sensors a) without and b) with Au NPs.

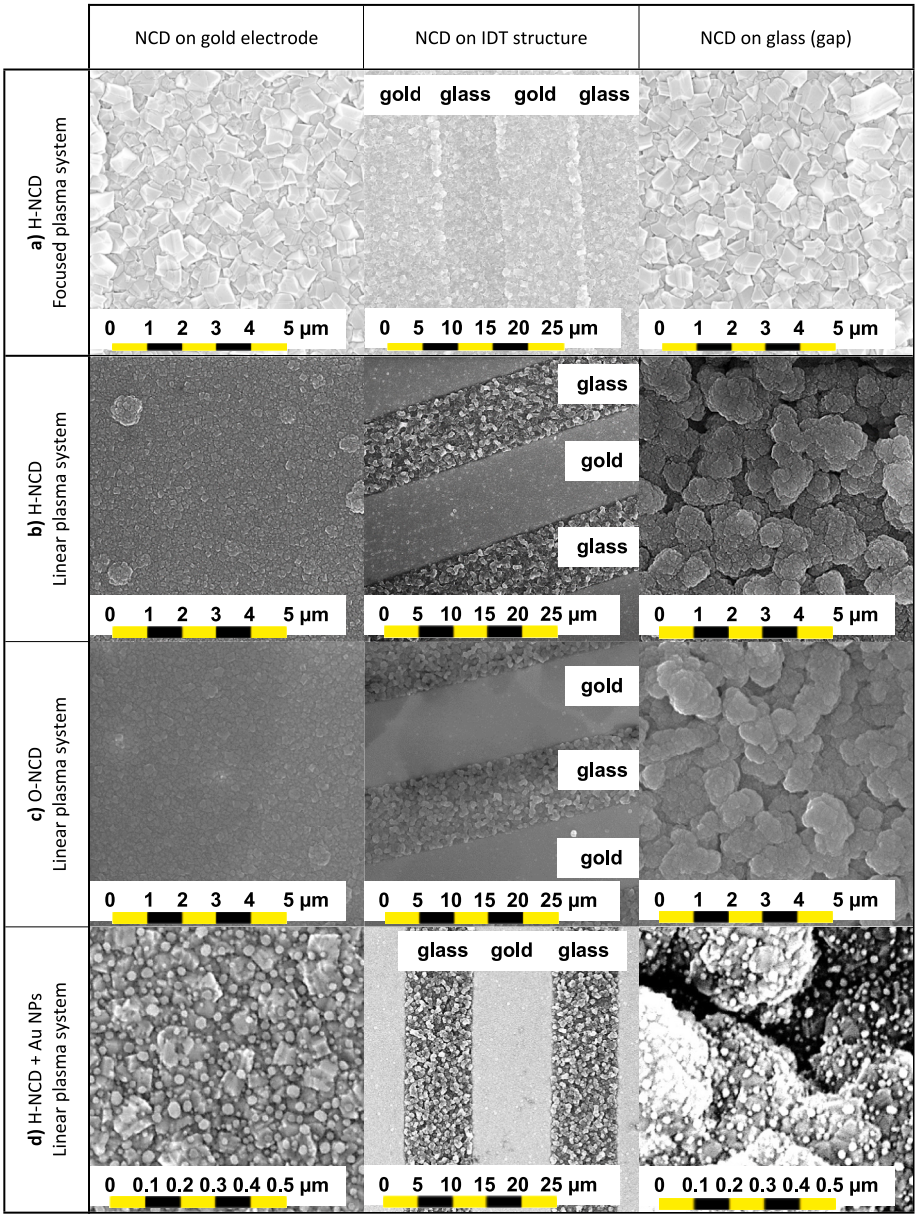

Fig. 3. SEM images of prepared samples.

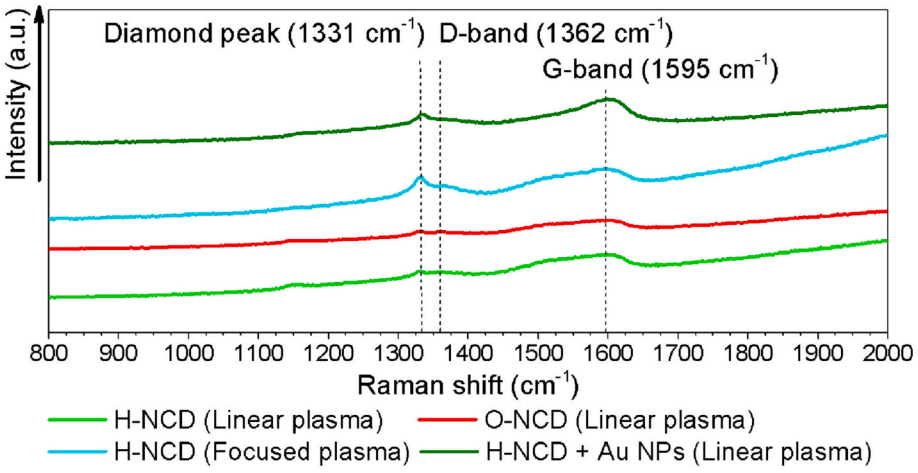

Fig. 4. Raman spectra of prepared samples.

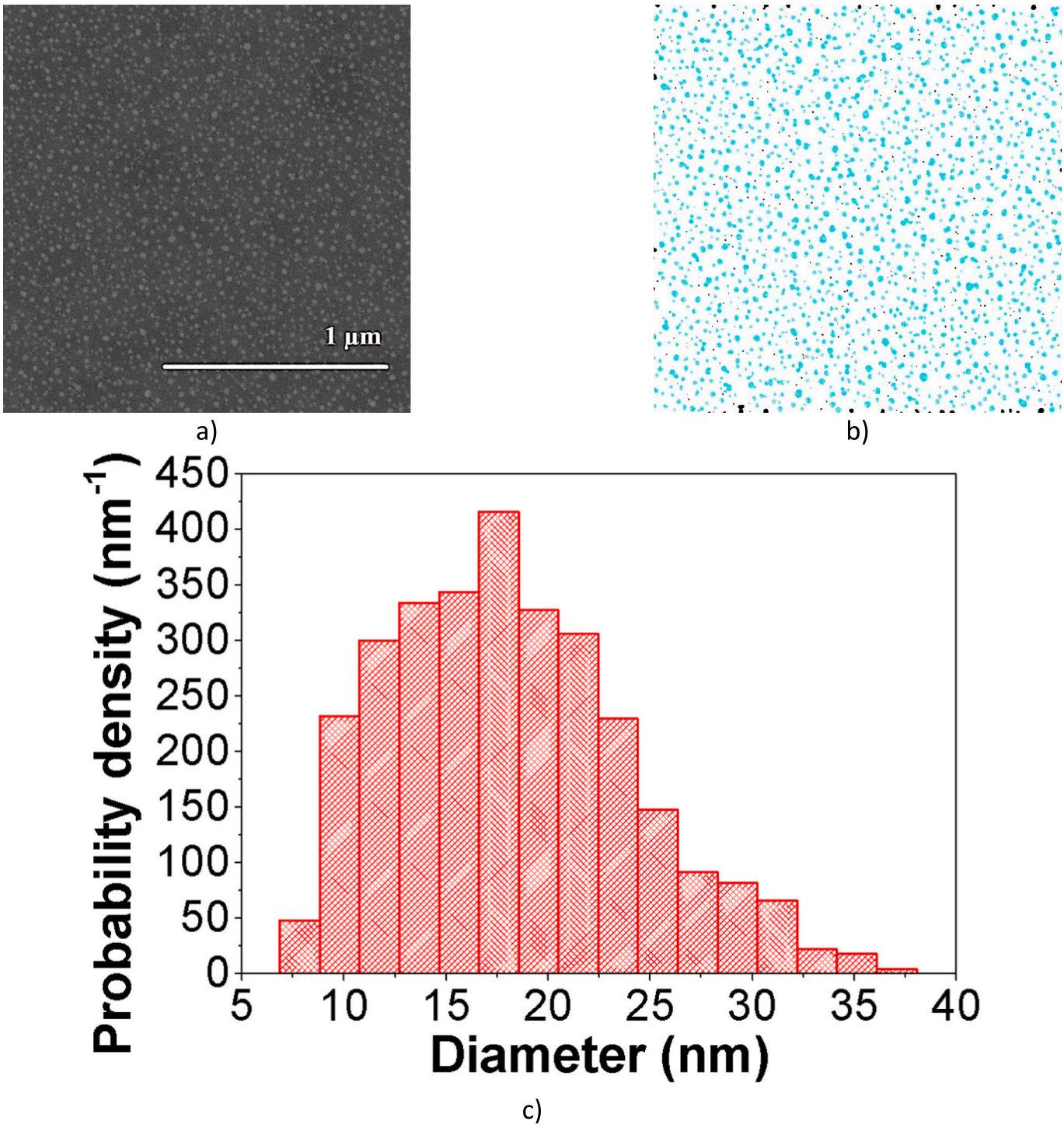

Fig. 5. a) BSE in SEM image of H-NCD + Au NPs, b) post-processing of image and highlighting conductive (Au) particles, and c) probability density plot as a function of particle diameter.

(i.e., lower quality of termination) and b) the same surface morphology over the entire surface of the NCD layer. The higher temperature during deposition causes a lower quality of hydrogen termination in comparison with a low-temperature system [15,27,28]. The same non-porous surface on both parts of the sensor (on glass and gold electrodes) does not increase the effective area (the total area of the surface with which the gas is in direct contact and where reactions between the sensor and the gas occur) between active material and gases [1,2,28]. The second sensor type (H-NCD prepared in the linear plasma system at a lower temperature) initially revealed higher resistance and good response, about 40 % at 125 °C, for both testing gas types. This response improvement should be attributed to the specific surface morphology on the glass, which reveals not only higher surface roughness, and thus larger effective active area, but also the compact 3D-like active surface area. For the first and second sample types, the sensor response to the exposed gases is attributed to the modulation of 2D hole gas (2DHG) induced by the hydrogen termination on the intrinsic diamond layer (i.e., high bulk resistivity). The 2DHG top layer is known to be sensitive to exposed gas or organic molecules [12,15,16,27], which also agrees with our observation. Moreover, the trend of response change reflects the

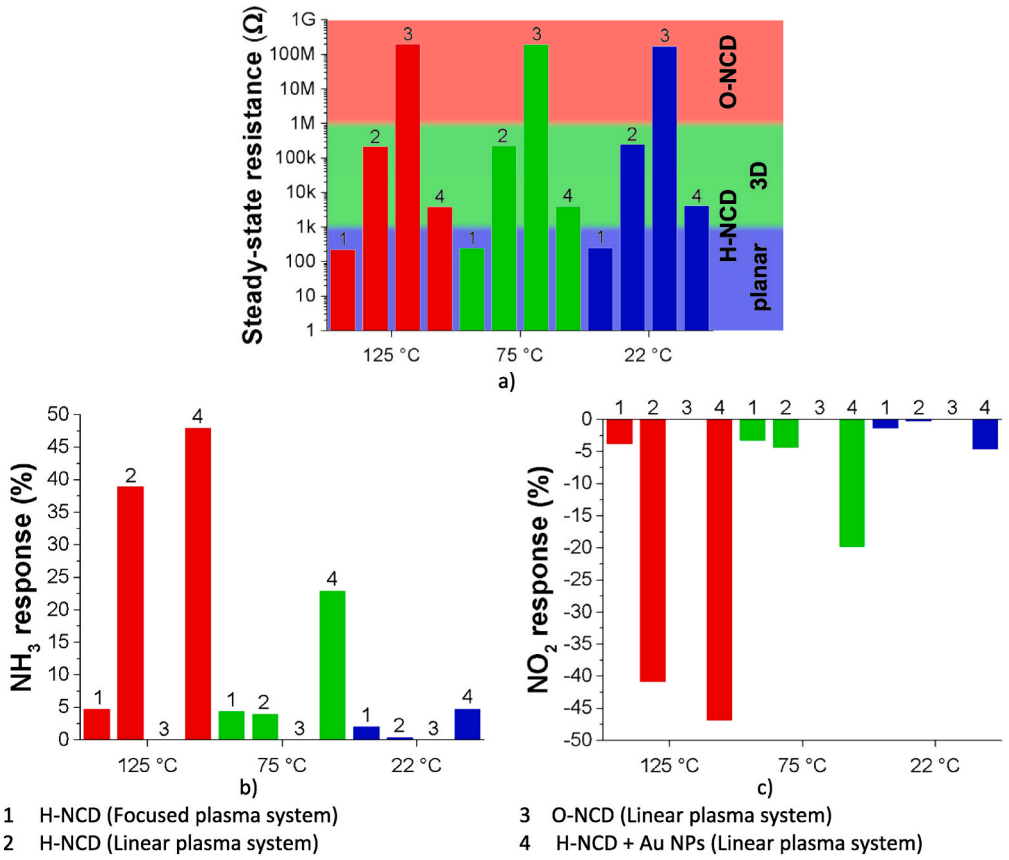

Fig. 6. Measured data depending on the temperature (125 °C, 75 °C, and room temperature 22 °C) of a) steady-state resistance, b) response to 100 ppm NH_3, and c) response to 100 ppm NO_2.

type of tested gas, i.e., it is negative/positive for oxidizing/reducing gas atmosphere, respectively. The third type (O-NCD prepared in a linear plasma system) had the highest resistance due to the oxygen termination, which didn't induce subsurface conductivity. The diamond layer remained highly resistive (about 200 MΩ), and the gas sensing response was almost unmeasurable (lower than 0.01 %). For these reasons, the calculated value of the response is equal to noise. The fourth sample with Au NPs reduced the resistance value by 98.3 % compared to the second sample (from 250 kΩ to 4.15 kΩ). Moreover, this surface coated with Au NPs achieved the best gas response for all sensor types and all temperatures tested (about 50 % for 125 °C and about 5 % for room temperature) while still keeping gas sensing selectivity to oxidizing/reducing gas type. The Au NPs also improved the time characteristic, as shown in Fig. 7. The response to gases and recovery time is fast, and in the case of H-NCD + Au NPs, there is no shift in the steady-state resistance due to the permanent absorption of molecules on the surface. H-NCD + Au NPs at 125 °C has a response time of 60 s for NH_3 and only 15 s for recovery. The measured properties and responses are shown in following Table 1. Time stability (in the order of months) is the subject of further research and measurement.

4. Discussion

Gas sensing experimental measurements showed that Au NPs enhanced the gas sensing characteristic of H-NCD at room temperature. The linear plasma system synthesized a rougher surface on the glass and thus increased the active contact area between the gas and sensing layer. A smaller diamond crystal size and higher roughness also increase the steady-state resistance of the sensors and thereby reduce the percentual gas response, as shown in Eq. (1). The Au NPs decrease the steady-state resistance and increase the percentual responses to oxidizing and reducing gases. The Au NPs were used for several reasons. The first reason is the chemical stability of Au NPs compared to other materials (does not oxidize, does not react with other materials used in production, etc.). Furthermore, Au has very good adhesion for preparing Au NPs. The last reason is the simple preparation of Au NPs, which hardly affect the H-NCD layer.

The increasing temperature increases the response to both gases for all sensors, except the O-NCD, which has no response to these gases. The increasing temperature enhances chemical reactions and thus the size of the responses [1,17,19]. On the other hand, a higher temperature requires heating and increases energy consumption. For this reason, room temperature gas sensors are more required and used. The H-NCD with Au NPs achieves the best response at room temperature (22 °C), but the response is still about 5 % for both gases. This value is more than twice higher than standard H-NCD. The higher temperature enhances all H-NCD samples' responses, especially 3D H-NCD. The 3D H-NCD samples achieve a response of around 40 % for H-NCD, respectively 50 % for H-NCD with Au NPs.

4.1. Surface gas interaction model

The surface of NCD behaves as the p-type semiconductor due to p-type induced subsurface conductivity, also known as 2DHG [16,17,27]. This subsurface layer is sensitive to the environment, such as humidity, temperature, or organic/inorganic molecules. The change in the resistance of the H-NCD subsurface layer is caused by chemical reactions in which counter ions are formed on its surface and explained by the electron transfer model [17]. The gas interaction with the H-NCD surface has been described and explained in previous work [27]. Only briefly, the air humidity molecules H_2O dissociate to H_3O^+ and OH^- above the surface (Fig. 8a). The H_3O^+ ions react with the surface and

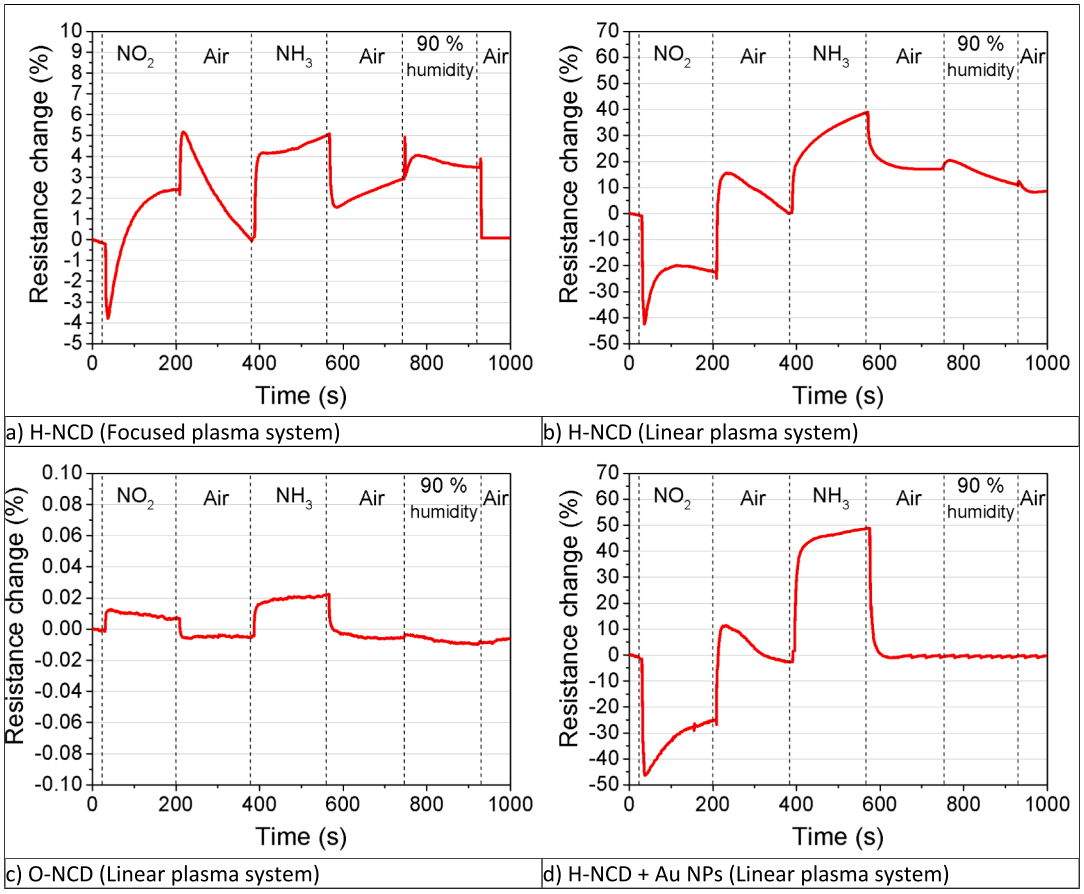

Fig. 7. Measured gas responses at 125 °C for NO_2, NH_3 and 90 % humidity of all tested samples.

Table 1
Comparison of the steady-state resistance and responses of the NCD samples at three temperatures[a].

	Temperature (°C)	R_0 (kΩ)	NH_3 response (%)	NO_2 response (%)
H-NCD Focused plasma system	125	0.228	4.8	-3.9
	75	0.247	4.5	-3.4
	(RT) 22	0.262	2.1	-1.5
H-NCD Linear plasma system	125	216	39	-41
	75	227	4	-4.5
	(RT) 22	250	0.5	-0.4
O-NCD Linear plasma system	125	204 692	0.02	0.01
	75	198 354	0.02	0.02
	(RT) 22	177 594	0.01	0.01
H-NCD + Au NPs Linear plasma system	125	4	48	-47
	75	4.1	23	-20
	(RT) 22	4.15	4.8	-4.7

[a] Highlighted values show the best achieved values

attract the electron from the diamond bulk, which creates the p-type subsurface conductivity channel 2DHG. The presence of gasses near the surface causes an imbalance in the number of ions. The imbalance of ions changes the number of free charge carriers and, thus, the resistance. The substitute electrical circuit diagram is shown in Fig. 8b and is represented by the total electric resistance divided into two resistors: the resistance of 2DHG and the barrier resistance. The barrier resistance includes several factors. The most crucial is a) the resistance between diamond (nano) particles or b) the resistance between 2DHG conductive areas (i.e., not ideally terminated diamond surface).

The detection principle of H-NCD with Au NPs is based on the same gas interaction model mentioned above. The H-NCD reacts with gas molecules and changes the resistance. However, the Au NPs represent local electrically conductive islands (shortcuts) for the resistive barrier and decrease the steady-state resistance to 4.15 kΩ. More free charge carriers tunnel through the Au NPs instead of the barriers, as is shown in

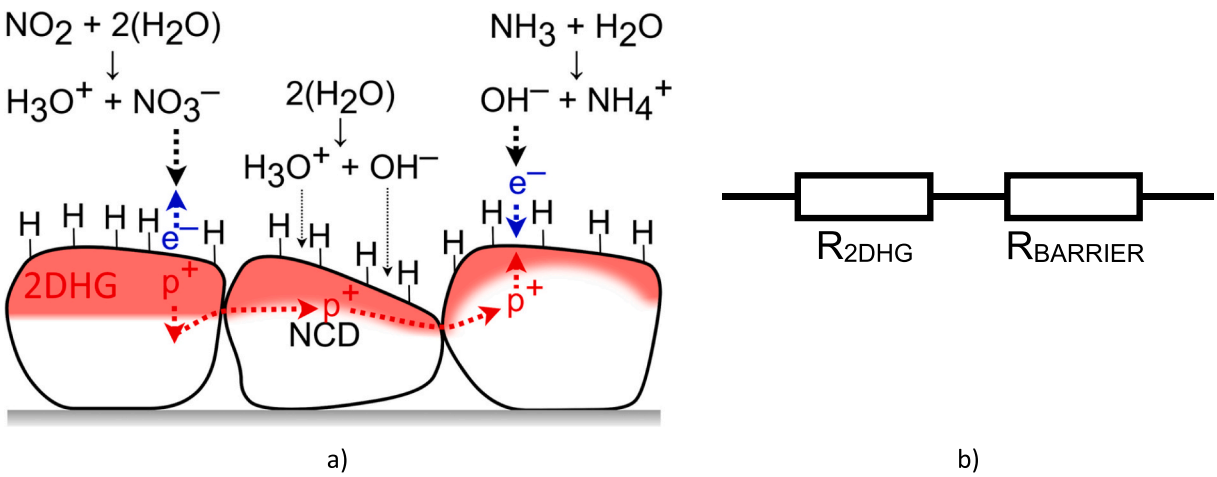

Fig. 8. a) Gas interaction model and b) substitute circuit diagram of the H-NCD layer.

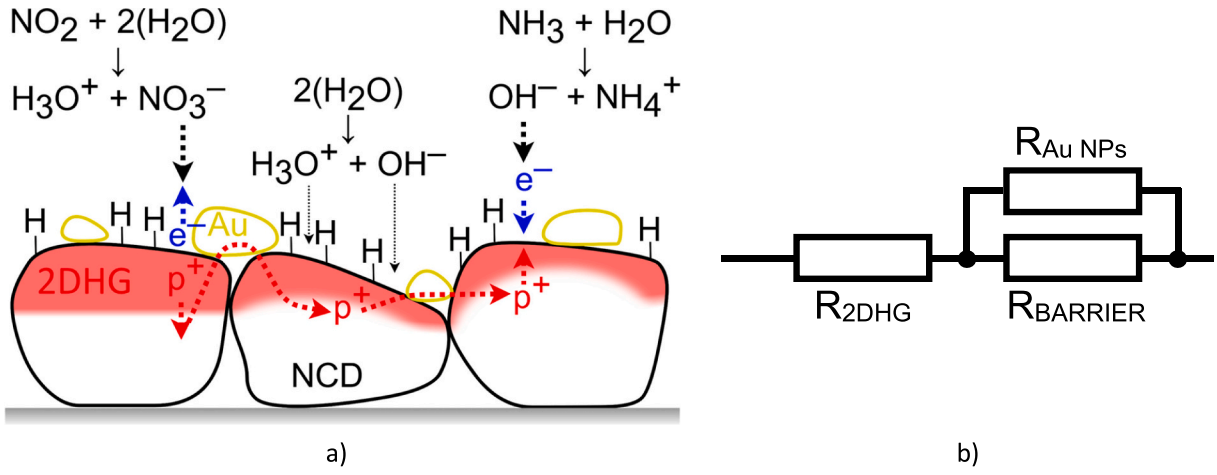

Fig. 9. a) Gas interaction model and b) substitute circuit diagram of the H-NCD layer with Au NPs.

Fig. 9a. In the substitute circuit diagram (Fig. 9b), the Au NPs are represented by a resistor parallelly connected to the barrier resistor. Thus, the final resistance has a lower value than the NCD layer. In this meaning, the H-NCD + Au NPs hybrid structure reduces the steady-state resistance value by utilizing conductive Au NPs and preserving the functionality of the H-NCD gas sensing layer. If these two parameters are well combined, the final percentage value, calculated by Eq. (1), relative to primary resistance, is higher. However, the Au NPs reduce the total response of the diamond surface due to the partial overcoating of the H-NCD functional layer. Finally, the higher concentration of Au NPs also increases power consumption for sensor measurement because a higher current is required for the same voltage. Therefore, the optimal concentration on NPs has to be experimentally determined to achieve the best possible gas sensing result by compromising response vs. power consumption. Similar to concentration, the ideal size of NPs can be found. This size should be small enough to not cover a large area of the active layer and thus decrease the response to gases. But it must be large enough to cause a shortcut between the two NCD grains.

5. Conclusion

The four active layers were designed, prepared and measured at three different temperatures for two active gases. The H-NCD active layers were prepared by two different systems (linear and focused plasma systems). A linear plasma system prepared H-NCD, O-NCD, and H-NCD + Au NPs hybrid structures. The measurements revealed that the hybrid structure exhibits preferable responses to exposed gas compared with H-NCD without Au NPs at all measured temperatures. The O-NCD had an almost unmeasurable response to both gases due to the absence of subsurface conductivity and is not appropriate for gas sensing applications. The H-NCD prepared in a focused plasma system can be grown quickly due to a high growth rate at a higher temperature. It was highly conductive, but the planar-like surface morphology revealed a smaller active area and thus a smaller reaction to gases. The H-NCD prepared in a linear plasma system produced bottom-up porous-like 3D diamond layers [29], which had sufficient gas responses. The response of 3D H-NCD was about 40 % for both gases at 125 °C but <1 % for lower temperatures. The Au NPs enhanced the responses at all temperatures by decreasing the steady-state resistance value. The response was about 50 % at 125 °C and about 5 % at 22 °C (room temperature). This hybrid structure allows a reduction in the working temperature and thus power consumption for heating. Although the current for measuring the structure will increase, but it is negligible compared to the heating power. Our findings represent a promising alternative solution to the new class of gas sensors due to miniaturization and low power consumption compared to commercial MO_X gas sensors. Overall, one can conclude that the H-NCD + Au NPs hybrid structure enhances the gas responses at high and room temperatures. However, the optimum concentration of Au NPs for these conditions has to be found.

CRediT authorship contribution statement

We confirm that all figures/photographs (including the graphical abstract) appearing in this manuscript were created by the authors of this manuscript.

Michal Kočí: Conceptualization, Methodology, Software, Investigation, Writing - Original Draft

Ondrej Szabó: Methodology, Software, Investigation, Writing - Original Draft

Gabriel Vanko: Methodology, Resources, Writing - Review & Editing

Miroslav Husák: Validation, Writing - Review & Editing

Alexander Kromka: Conceptualization, Methodology, Validation, Resources, Writing - Review & Editing, Project administration

Declaration of competing interest

The authors declare that they have no known competing financial interests or personal relationships that could have appeared to influence the work reported in this paper.

Data availability

Data will be made available on request.

Acknowledgments

The authors kindly acknowledge R. Jackivová and K. Hruška for SEM measurements. This work was supported by the bilateral projects GAAV grant no. SAV-AV ČR-23-11 and MEYS grant no. LU-ASK22147 (SK no. SK-CZ-RD-21-0116). This work used the large research infrastructure Czech NanoLab supported by the LM2023051 project and partially by CTU project No. SGS23/181/OHK3/3T/13 Materials and structures for sensors, integrated and photonic circuits.

References

[1] J. Fraden, Handbook of Modern Sensors: Physics, Designs, and Applications, 5th ed., Springer International Publishing, Cham, 2016. Imprint: Springer. (ISBN: 9783319193038).

[2] K. Štulík, J. Barek, J. Janata, V. Král, M. Kronďák, M. Šťastný, SENZORY: General Aspects of Chemical Sensing, VŠCHT Praha, 2007 (ISBN: 978-80-86238-20-3).

[3] L. Ding, Z. Qin, Z. Dou, Y. Shen, Y. Cai, Y. Zhang, Y. Zhou, Morphology-promoted synergistic effects on the sensing properties of polyaniline ultrathin layers on reduced graphene oxide sheets for ammonia and formaldehyde detection, J. Mater. Sci. 53 (10) (2018) 7595–7608, https://doi.org/10.1007/s10853-018-2109-7.

[4] J. Hur, S. Park, J.H. Kim, J.Y. Cho, B. Kwon, J.H. Lee, G.Y. Bae, H. Kim, J.T. Han, W.H. Lee, Ultrasensitive, transparent, flexible, and ecofriendly NO2 gas sensors enabled by oxidized single-walled carbon nanotube bundles on cellulose with engineered surface roughness, ACS Sustain. Chem. Eng. 10 (10) (2022) 3227–3235, https://doi.org/10.1021/acssuschemeng.1c07559.

[5] A.N. Naje, R.R. Ibraheem, F.T. Ibrahim, Parametric analysis of NO2 gas sensor based on carbon nanotubes, Photonic Sens. 6 (2) (2016) 153–157, https://doi.org/10.1007/s13320-016-0304-1.

[6] S. Barthwal, B. Singh, N.B. Singh, ZnO-SWCNT nanocomposite as NO2 gas sensor, Mater. Today Proc. 5 (7) (2018) 15439–15444, https://doi.org/10.1016/j.matpr.2018.05.030.

[7] Y.J. Kwon, A. Mirzaei, S.Y. Kang, M.S. Choi, J.H. Bang, S.S. Kim, H.W. Kim, Synthesis, characterization and gas sensing properties of ZnO-decorated MWCNTs, Appl. Surf. Sci. 413 (2017) 242–252, https://doi.org/10.1016/j.apsusc.2017.03.290.

[8] Y. Seekaew, D. Phokharatkul, A. Wisitsoraat, C. Wongchoosuk, Highly sensitive and selective room-temperature NO2 gas sensor based on bilayer transferred chemical vapor deposited graphene, Appl. Surf. Sci. 404 (2017) 357–363, https://doi.org/10.1016/j.apsusc.2017.01.286.

[9] S. Kumar, V. Pavelyev, P. Mishra, N. Tripathi, Thin film chemiresistive gas sensor on single-walled carbon nanotubes-functionalized with polyethylenimine (PEI) for $${\hbox {NO}}_{2}$$ gas sensing, Bull. Mater. Sci. 43 (1) (2020), https://doi.org/10.1007/s12034-020-2043-6.

[10] P. Dariyal, S. Sharma, G.S. Chauhan, B.P. Singh, S.R. Dhakate, Recent trends in gas sensing via carbon nanomaterials: outlook and challenges, Nanoscale Adv. 3 (23) (2021) 6514–6544, https://doi.org/10.1039/D1NA00707F.

[11] G. Mueller, I. Krstev, K. Maier, A. Helwig, M. Stutzmann, J. Garrido, Resettable, low-temperature accumulation gas sensors based on hydrogenated diamond transducers, EUROSENSORS 120 (2015) 590–593, 2015, https://doi.org/10.1016/j.proeng.2015.08.733.

[12] M. Davydova, P. Kulha, A. Laposa, K. Hruska, P. Demo, A. Kromka, Gas sensing properties of nanocrystalline diamond at room temperature, Beilstein J. Nanotechnol. 5 (2014) 2339–2345, https://doi.org/10.3762/bjnano.5.243.

[13] R.K. Joshi, J.E. Weber, Q. Hu, B. Johnson, J.W. Zimmer, A. Kumar, Carbon monoxide sensing at room temperature via electron donation in boron doped diamond films, Sensors Actuators B-Chemical 145 (1) (2010) 527–532, https://doi.org/10.1016/j.snb.2009.12.070.

[14] H. Sato, M. Kasu, Electronic properties of H-terminated diamond during NO2 and O-3 adsorption and desorption, Diam. Relat. Mater. 24 (2012) 99–103, https://doi.org/10.1016/j.diamond.2011.12.004.

[15] A. Kromka, M. Davydova, B. Rezek, M. Vanecek, M. Stuchlik, P. Exnar, M. Kalbac, Gas sensing properties of nanocrystalline diamond films, Diam. Relat. Mater. 19 (2–3) (2010) 196–200, https://doi.org/10.1016/j.diamond.2009.10.006.

[16] A. Helwig, G. Mueller, J.A. Garrido, M. Eickhoff, Gas sensing properties of hydrogen-terminated diamond, Sensors Actuators B-Chem. 133 (1) (2008) 156–165, https://doi.org/10.1016/j.snb.2008.02.007.

[17] Y. Gurbuz, W.P. Kang, J.L. Davidson, D.L. Kinser, D.V. Kerns, Diamond microelectronic gas sensors, Sensors Actuators B Chem. 33 (1–3) (1996) 100–104.

[18] S.M. Sze, K.K. Ng, Physics of Semiconductor Devices, 3rd ed., Wiley, Hoboken, 2007 (ISBN: 0-471-14323-5).

[19] S. Adachi, Properties of Group-IV, III-V and II-VI Semiconductors 2005, John Wiley & Sons Ltd, Chichester West Sussex England, 2006 (ISBN: 0470090324).

[20] 4th International Conference nanoFIS 2020 - Functional Integrated nanoSystems. Basel Switzerland: MDPI.

[21] A. Saravanan, B.-R. Huang, J.P. Chu, A. Prasannan, H.-C. Tsai, Interface engineering of ultrananocrystalline diamond/MoS2-ZnO heterostructures and its highly enhanced hydrogen gas sensing properties, Sensors Actuators B Chem. 292 (2019) 70–79, https://doi.org/10.1016/j.snb.2019.04.108.

[22] E. Dilonardo, M. Penza, M. Alvisi, C. Di Franco, R. Rossi, F. Palmisano, L. Torsi, N. Cioffi, Electrophoretic deposition of Au NPs on MWCNT-based gas sensor for tailored gas detection with enhanced sensing properties, Sensors Actuators B Chem. 223 (2016) 417–428, https://doi.org/10.1016/j.snb.2015.09.112.

[23] A. Liu, S. Lv, L. Jiang, F. Liu, L. Zhao, J. Wang, X. Hu, Z. Yang, J. He, C. Wang, X. Yan, P. Sun, K. Shimanoe, G. Lu, The gas sensor utilizing polyaniline/ MoS2 nanosheets/SnO2 nanotubes for the room temperature detection of ammonia, Sensors Actuators B Chem. 332 (2021), 129444, https://doi.org/10.1016/j.snb.2021.129444.

[24] Y. Wang, Z. Zhao, Y. Sun, P. Li, J. Ji, Y. Chen, W. Zhang, J. Hu, Fabrication and gas sensing properties of Au-loaded SnO2 composite nanoparticles for highly sensitive hydrogen detection, Sensors Actuators B Chem. 240 (2017) 664–673, https://doi.org/10.1016/j.snb.2016.09.024.

[25] C. Wang, L. Yin, L. Zhang, D. Xiang, R. Gao, Metal oxide gas sensors: sensitivity and influencing factors, Sensors (Basel, Switzerland) 10 (3) (2010) 2088–2106, https://doi.org/10.3390/s100302088.

[26] S.S. Nicley, S. Drijkoningen, P. Pobedinskas, J. Raymakers, W. Maes, K. Haenen, Growth of boron-doped diamond films on gold-coated substrates with and without gold nanoparticle formation, Cryst. Growth Des. 19 (6) (2019) 3567–3575, https://doi.org/10.1021/acs.cgd.9b00488.

[27] M. Koci, A. Kromka, A. Boura, O. Szabo, M. Husak, Hydrogen-terminated diamond surface as a gas sensor: a comparative study of its sensitivities, SENSORS 21 (16) (2021), https://doi.org/10.3390/s21165390.

[28] P. Hubík, J.J. Mareš, H. Kozak, A. Kromka, B. Rezek, J. Krištofik, D. Kindl, Transport properties of hydrogen-terminated nanocrystalline diamond films, Diam. Relat. Mater. 24 (2012) 63–68, https://doi.org/10.1016/j.diamond.2011.10.021.

[29] M. Varga, Š. Potocký, M. Domonkos, T. Ižák, O. Babčenko, A. Kromka, Great variety of man-made porous diamond structures: pulsed microwave cold plasma system with a linear antenna arrangement, ACS Omega 4 (5) (2019) 8441–8450, https://doi.org/10.1021/acsomega.9b00323.

III. Improved Gas Sensing Capabilities of MoS_2/Diamond Heterostructures at Room Temperature

Authors: Michal Kočí, Tibor Izsák, Gabriel Vanko, Michaela Sojková, Jana Hrdá, Ondrej Szabó, Miroslav Husák, Karol Végsö, Marian Varga, and Alexander Kromka

ACS APPLIED MATERIALS & INTERFACES

www.acsami.org

Research Article

Improved Gas Sensing Capabilities of MoS_2/Diamond Heterostructures at Room Temperature

Michal Kočí,* Tibor Izsák, Gabriel Vanko, Michaela Sojková, Jana Hrdá, Ondrej Szabó, Miroslav Husák, Karol Végsö, Marian Varga, and Alexander Kromka

Cite This: *ACS Appl. Mater. Interfaces* 2023, 15, 34206−34214

Read Online

ACCESS | Metrics & More | Article Recommendations | Supporting Information

ABSTRACT: Molybdenum disulfide (MoS_2) and nanocrystalline diamond (NCD) have attracted considerable attention due to their unique electronic structure and extraordinary physical and chemical properties in many applications, including sensor devices in gas sensing applications. Combining MoS_2 and H-terminated NCD (H-NCD) in a heterostructure design can improve the sensing performance due to their mutual advantages. In this study, the synthesis of MoS_2 and H-NCD thin films using appropriate physical/chemical deposition methods and their analysis in terms of gas sensing properties in their individual and combined forms are demonstrated. The sensitivity and time domain characteristics of the sensors were investigated for three gases: oxidizing NO_2, reducing NH_3, and neutral synthetic air. It was observed that the MoS_2/H-NCD heterostructure-based gas sensor exhibits improved sensitivity to oxidizing NO_2 ($0.157\%{\cdot}ppm^{-1}$) and reducing NH_3 ($0.188\%{\cdot}ppm^{-1}$) gases compared to pure active materials (pure MoS_2 achieves responses of $0.018\%{\cdot}ppm^{-1}$ for NO_2 and $-0.0072\%{\cdot}ppm^{-1}$ for NH_3, respectively, and almost no response for pure H-NCD at room temperature). Different gas interaction model pathways were developed to describe the current flow mechanism through the sensing area with/without the heterostructure. The gas interaction model independently considers the influence of each material (chemisorption for MoS_2 and surface doping mechanism for H-NCD) as well as the current flow mechanism through the formed P−N heterojunction.

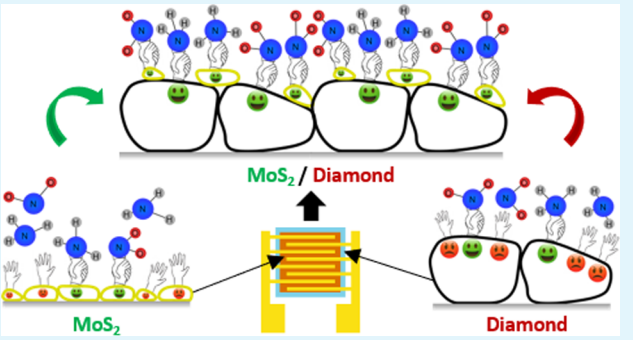

KEYWORDS: *gas sensors, H-terminated diamond, MoS_2, MoS_2/H-NCD heterostructure, room temperature, P−N junction, sensitivity, gas interaction model*

1. INTRODUCTION

Gas sensors are essential for industry, healthcare, and almost everyday life, with an increasing emphasis on detecting hazardous substances and improving air quality.[1] The development of sensors based on new materials with high sensitivity, stability, and reproducibility for the detection of various gases is therefore subject to high demands.[2−6] Researchers are currently focusing on emerging two-dimensional (2D) materials, such as transition-metal dichalcogenides (TMDs), for use as active layers in gas sensing applications.

TMDs are a group of compounds with the chemical formula MX_2, where M is a transition-metal atom and X is a chalcogen atom. Their structure consists of an atomic layer of transition metals sandwiched between two chalcogen layers.[7] TMDs exhibit unique electronic structures and extraordinary physical and chemical properties for many applications.[3,7] For example, TMDs are featured by a thickness-dependent electronic band structure,[8] high charge carrier mobility,[9] and in general a high surface-to-volume ratio, which is a natural asset for applications such as chemical sensors.[10] Their properties, especially semiconductor properties, depend on the thickness of the layer; e.g., the band gap of MoS_2 changes its value and type from direct (∼1.8 eV) to indirect (∼1.2 eV) as the number of layers increases.[7,11,12] Therefore, TMDs could be bulk types, such as MoS_2 grains or a film of nanoflakes. TMDs have several sensing applications.[11−13] Although TMDs have excellent sensitivity at high temperatures (above 100 °C), bare layers have poor sensing properties at room temperature.[7] Increasing temperature, UV illumination, or combination with other materials can improve these limitations as reported in the literature.[7,14] For example, carbon-based materials,[15−17] graphene,[18] reduced graphene oxide,[2] or metal oxides (ZnO_2,[19] SnO_2,[20,21] or TiO_2[22]), have been proven to improve sensing characteristics. The NCD surface consists of sp^3-hybridized carbon bonds that are chemically and mechanically

Received: March 28, 2023
Accepted: June 20, 2023
Published: July 3, 2023

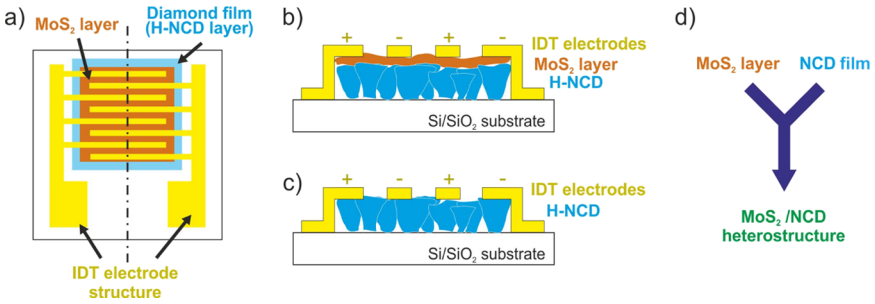

Figure 1. Schematic top (a) and cross-sectional views of MoS_2/H-NCD/SiO_2/Si (b), cross-sectional view of H-NCD/SiO_2/Si (c) sensors, and schematic illustration of the combination of both materials in a heterostructure (d). In the case of the MoS_2/SiO_2/Si sensor, the MoS_2 layer was prepared directly on the SiO_2/Si substrate, and no diamond deposition was performed (not illustrated in this figure).

stable. Surface-grafting specific atoms and functional chemical groups, such as oxygen, hydrogen, and amine groups, can tailor the wettability and influence the surface energy of NCD films, making the surface properties hydrophobic for hydrogen-terminated and hydrophilic for oxygen-terminated surfaces.[23] It has already been shown that hydrogen-terminated nanocrystalline diamond (H-NCD) films, which exhibit P-type subsurface conductivity, reliably detect oxidizing and reducing gases.[24−26]

The solid-state resistive gas sensors can be manufactured from any material that reacts to the presence of gases.[1] This type of sensor is most commonly used to detect oxidizing or reducing gases. Nowadays, gas sensors based on MO_X materials, which are heated to higher temperatures, are being studied intensively.[27] The development of sensors working at room temperature is very demanding from the point of reduced consumption, reduced dimensions, and the possibility of use in hazardous areas. Among the carbon-based gas sensors, reduced graphene oxide (rGO)[28] with a sensitivity of 0.004%·ppm^{-1}[29] and carbon nanotubes (CNTs)[30,31] are mainly considered for gas sensors operating at room temperature. The second group that is intensively researched is represented by 2D materials. From this group, TMDs (MoS_2, $PtSe_2$, etc.)[2−7] with a sensitivity of 0.3%·ppm^{-1} for MoS_2 nanoworm films after 90 days at 150 °C[3] and 2D MO_X[27] were presented. Furthermore, to improve the performance of the gas sensors, several strategies can be used. For example, in the case of carbon-based gas sensors, the performance was improved by fabricating heterostructures that consisted of carbon nanostructures with polymers,[29,32] ceramic nanoparticles,[33] or other suitable materials.

Similarly, mesoporous In_2O_3 nanocrystals for the detection of NO_X at room temperature have been recently published by Gao et al.[34] Due to the synergistic effect between its mesoporous and highly crystalline nature, the detection limit from 1000 ppb to 100 ppm was achieved.[35] Shaik et al.[36] have introduced a NO_2 sensor with a detection limit of 5 ppm at room temperature by using N-doped reduced graphene oxide (rGO). Moreover, the composites of carbon nanotubes combined with hexagonal WO_3 are shown to detect low concentrations (100 ppb) of NO_2 at room temperature.[37]

Here, we present a novel MoS_2/H-NCD heterostructure as a prospective gas sensor with improved gas sensing parameters (response and recovery time) even at room temperature due to the synergistic effect of both materials. This improvement is compared and described within the proposed gas interaction model of the sensing principles of individual MoS_2 and H-NCD materials and their heterostructure. The sensitivity and time domain characteristics of the sensors were investigated for two active gases: oxidizing NO_2 and reducing NH_3. They were chosen as representative gases largely produced by industries, worsening the air quality in the environment and hazardous to health in higher concentrations.[1,27]

2. EXPERIMENTAL SECTION

2.1. Active Layer Preparation. Thin MoS_2 layers were prepared on three substrates—bare Si, SiO_2/Si, and diamond-coated SiO_2/Si (H-NCD/SiO_2/Si). First, 4 in. SiO_2/Si and Si wafers were ultrasonically cleaned in acetone, isopropyl alcohol, and deionized water for 10 min and dried by nitrogen flow. Subsequently, the MoS_2 layers were prepared in a two-step process. In the first step, a 4 nm thin Mo layer was deposited using DC magnetron sputtering in an Ar atmosphere (10^{-3} mbar) from a Mo target at room temperature (about 22 °C). The DC power and emission current were 460 W and 0.3 A, respectively. The rotation speed of the sample holder controlled the thickness of the prepared Mo films. Next, the predeposited Mo layers were sulfurized in a custom-designed CVD chamber. The Mo layer was annealed in sulfur vapors at a high temperature of 800 °C in a N_2 atmosphere at ambient pressure. The substrate was placed together with the sulfur powder in the center of the furnace so that the temperature of the substrate and the powder were the same during the growth,[38,39] unlike the standard CVD method, which uses a two-zone furnace with different temperatures for the sulfur powder and the Mo substrate.

In the case of NCD film growth, a clean SiO_2/Si wafer was first treated by applying ultrasonic agitation in a water-based diamond powder suspension (~5 nm particles) for 40 min, followed by the growth in a linear antenna microwave plasma CVD system (Roth&Rau AK400) consisting of two linear antennas. The NCD was grown at a low deposition rate (about 15 nm/h) to a thickness of 450 nm (evaluated from the interference fringes of the reflectance spectra measured in the vis−NIR region). The process parameters of the linear antenna system are as follows: the power of the microwave generators was 2 kW, the pressure of the gas mixture was 0.15 mbar (200 sccm H_2, 5 sccm CH_4, and 20 sccm CO_2), the deposition time was 30 h, and the substrate temperature was 550 °C. The surface of the as-grown NCD films was treated in hydrogen plasma to obtain hydrophobic properties. Surface functionalization by hydrogen was performed in a focused MW plasma CVD chamber (Aixtron P6 system, 1500 W, 30 mbar, 300 sccm of H_2, 20 min, 500 °C). These layers are further referred to as H-NCD.

Finally, the deposited MoS_2, H-NCD layers, and their heterostructure MoS_2/H-NCD were coated with a 120 nm-thick Ti/Au (20 nm of Ti and 100 nm of Au) interdigitated electrode (IDT) structure for electrical connection on the top layer (Figure 1). The IDT was connected with measurement pins using a wire bonding technique for better electrical contact and handling. Metal contact pads were fabricated by a combination of electron beam evaporation and a consequent lift-off technique.

2.2. Characterization of MoS_2 and Diamond Films. The surface morphology of the prepared samples was measured using a

https://doi.org/10.1021/acsami.3c04438
ACS Appl. Mater. Interfaces 2023, 15, 34206−34214

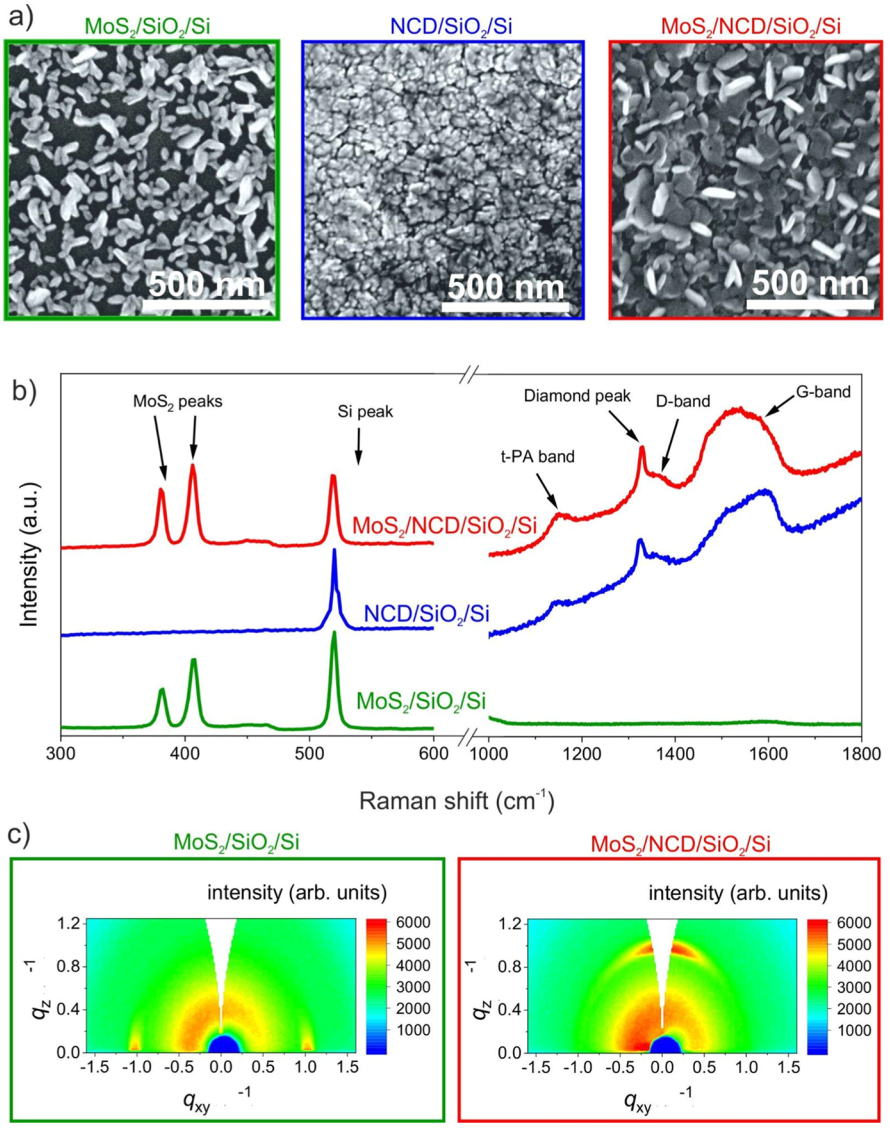

Figure 2. (a) Top-view SEM images of samples $MoS_2/SiO_2/Si$, H-NCD/SiO_2/Si, and MoS_2/H-NCD/SiO_2/Si and (b) corresponding Raman spectra of samples taken at a 442 nm excitation wavelength; (c) GIWAXS reciprocal space maps of the $MoS_2/SiO_2/Si$ and MoS_2/H-NCD/SiO_2/Si samples.

Tescan MAIA 3 scanning electron microscope at a 10 keV electron gun energy. The surface morphology of the samples is shown in Figure 2a. As shown in Figure 2a, the SiO_2/Si substrate was covered with a completely closed H-NCD film. In contrast to SiO_2, the surface coverage by MoS_2 nanoflakes (flake size in the range of 50−100 nm) was lower for MoS_2/H-NCD, probably due to the higher surface roughness. The MoS_2 layer was also prepared on the reference Si substrate (the SEM image is shown in Figure S1 in the Supporting Information).

The chemical composition of the prepared samples was measured using a Renishaw inVia Reflex Confocal Raman microscope with a 442 nm excitation wavelength. As shown in Figure 2b, the H-NCD/SiO_2/Si sample exhibits a typical Raman spectrum for NCD. In this spectrum, there is a representative peak of the Si substrate at 520 cm^{-1}, a narrow peak at 1331 cm^{-1} attributed to the first-order diamond peak, and two broad bands labeled as D and G at 1350 and 1595 cm^{-1} and recognized as disordered sp^2 carbon and graphitic phases, respectively.[24,26] The $MoS_2/SiO_2/Si$ sample is characterized by a Si peak at 520 cm^{-1} and two narrow peaks at 381 and 406 cm^{-1} attributed to MoS_2.[7,40] The Raman spectrum of MoS_2/H-NCD/SiO_2/Si combines all the peaks described above.

Grazing-incidence wide-angle X-ray scattering (GIWAXS) measurements were performed with a home-built system based on a microfocus X-ray source (Cu Kα, IμS, Incoatec) and a 2D X-ray detector (Pilatus 100K, Dectris). The angle of incidence on the sample was set to 0.2°. The sample−detector distance was 90 mm, as validated by a calibration standard (corundum). The collected GIWAXS patterns provided structural information about the prepared samples. Figure 2c shows reciprocal space maps of the as-prepared MoS_2 films on the SiO_2 and NCD films, respectively. The GIWAXS of the MoS_2 film prepared on the reference Si substrate is shown in the Supporting Information (Figure S2a). The appearance of two symmetrical 002 diffraction spots at $q_{xy} \sim \pm 1$ $Å^{-1}$ for Si and SiO_2/Si substrate means the vertical alignment of MoS_2. It means that the *c*-axis is parallel to the substrate surface. Horizontal alignment was observed with the *c*-axis perpendicular to H-NCD/SiO_2/Si, as confirmed by the position of the 002 diffractions at $q_z \sim 1$ $Å^{-1}$.

The wetting properties of the diamond film surfaces (H-termination and O-termination) were determined by contact angle measurements at room temperature using a static method in a material−water droplet system. The contact angle (wetting angle) was obtained by dropwise addition of a liquid onto the surface of a material. The surface tension of the liquid causes the drop to form a

https://doi.org/10.1021/acsami.3c04438
ACS Appl. Mater. Interfaces 2023, 15, 34206−34214

dome shape. 3 μL-volume water was added dropwise onto the diamond surface and captured by a digital CCD camera. The contact angles were calculated by a multipoint fitting of the drop profile using Surface Energy Evaluation software (Advex Instruments, Czechia). The H-terminated NCD is hydrophobic. A higher contact angle means more terminated hydrogen on the surface and thus a better response to the exposed gas. It should be noted that the optimal contact angle for a good H-termination is at least 90°.[26,39,41] The contact angle of the prepared H-NCD/SiO_2/Si samples was evaluated to be greater than 100°. The photographs of the measured contact angles are given in the Supporting Information (Table S1).

2.3. Experimental Setup for Gas Sensor Testing. A custom-built computer-controlled system was used for the characterization of the gas sensors. The creation of two independent gas mixtures (NH_3 and NO_2) with different concentrations and humidity is a major advantage of this experimental setup. The accuracy of this system is less than 1 ppm (measured by commercial gas sensors). However, the accuracy also depends on the purity of the delivered gases in the cylinder (the accuracy of the gas concentration in bottles is less than 0.1 ppm). The electrical characteristic (resistance change) was measured using a sensor holder with spring pins (Figure S3) and a source measure unit (SMU) Keithley SourceMeter 2401 with four-wire DC resistance measurement (Kelvin resistance measurement). The prepared sensors were measured with a voltage source with a nominal value of 0.1 V. A PC with a LabVIEW program was used to acquire the data from the SMU and ohmmeter. The four-input selection valve selects one input to the first output and three others to the second output (exhaust). The gas sensors were placed in the polycarbonate test chamber with two sections in series. The volume of one section was 22 cm^3. The sensors were measured in the first section to minimize the time delay due to the gas exchanges in the chamber. The PT1000 sensor measures the temperature in the chamber throughout the measurement of the gas sensors. A photo of the experimental setup is shown in Figure S3.

3. MEASUREMENTS AND RESULTS

Characterization of materials using SEM, Raman spectroscopy, and GIWAXS measurements is described in the previous chapter. In this part of the paper, we focus on the detailed characterization of the sensing properties of the prepared samples. First, the time-relative responses (i.e., response curves) of the fabricated conductivity gas sensors were measured for NH_3 and NO_2 gases at room temperature. The measured temperature was relatively stable, fluctuating between 21.8 and 22.5 °C, with an average of 22 °C. Active gases were used directly from gas bottles with the concentration and humidity defined and verified by the manufacturer (99.6 ppm in synthetic air (80% of N_2 and 20% of O_2) and <5% humidity for NO_2 and 96.6 ppm in synthetic air and <5% humidity for NH_3). In addition, 90% humid synthetic air without active gas was used at the end of the cycle to verify the effect of humidity on the sensors. The impact of increased humidity on the sensor's response properties for NO_2 and NH_3 was not investigated. Gas humidity was measured with a commercial hydrometer at the same temperature as in the gas sensor measurements. Mixtures of active gases and synthetic dry air for measuring the response to different concentrations were used to create the appropriate concentration. The resistance change Δ_R was calculated by eq 1, where R represents resistance measured for selected gas and R_0 is the initial resistance.

$$\Delta_R = \left(\frac{R}{R_0} - 1\right) \times 100 = \left(\frac{R - R_0}{R_0}\right) \times 100\ (\%) \qquad (1)$$

Four sensing layers were tested: reference H-NCD/SiO_2/Si, reference MoS_2/Si, MoS_2/SiO_2/Si, and heterostructure MoS_2/H-NCD/SiO_2/Si. The measured responses of the H-NCD/SiO_2/Si reference sample are given in the Supporting Information (Chapter 3).

3.1. Gas Response of MoS_2 on SiO_2. The first type of structure combines thin layers of MoS_2 and SiO_2. Figure 3a shows the absolute and relative change in resistance over time. The initial resistance (R_0) is 19.6 kΩ, increasing by 1.8% to 20 kΩ for NO_2. For NH_3 the resistance decreases from 19.9 to 19.7 kΩ (−0.7%). From the measured gas responses, the calculated sensitivity of the MoS_2/SiO_2/Si sample is 0.018%·ppm^{-1} (3.53 Ω·ppm^{-1}) for NO_2 and −0.0072%·ppm^{-1} (1.41 Ω·ppm^{-1}) for NH_3.

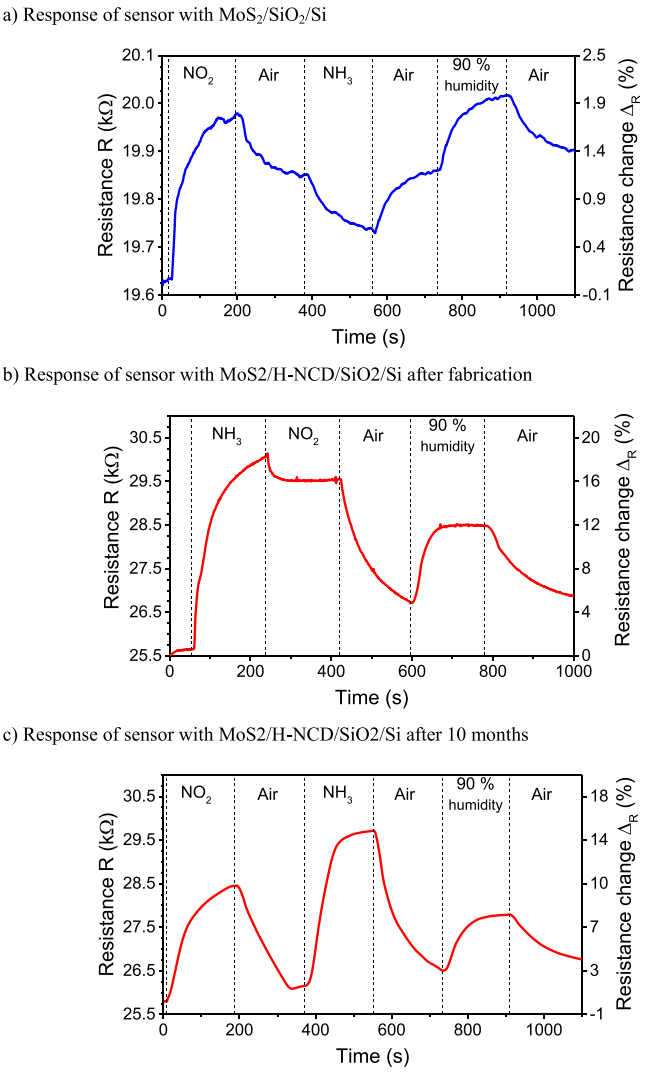

Figure 3. Time response of the sensor with MoS_2/SiO_2/Si (a), MoS_2/H-NCD/SiO_2/Si after fabrication (b), and MoS_2/H-NCD/SiO_2/Si after 10 months (c) to three gases (ammonia, nitrogen dioxide, and 90% humidity).

3.2. Gas Response of MoS_2 on Diamond. The time response of the MoS_2/H-NCD heterostructure on the SiO_2/Si substrate to three gases was measured at room temperature (22 °C) as in the previous measurement. Figure 3b shows the absolute and relative change in resistance over time. The resistance increases by 17.8% from 25.5 to 30 kΩ for NH_3.

https://doi.org/10.1021/acsami.3c04438
ACS Appl. Mater. Interfaces 2023, 15, 34206−34214

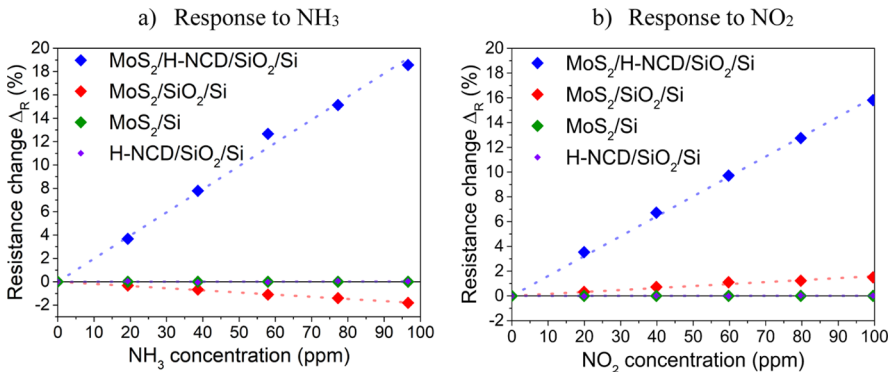

Figure 4. Relative resistance change of sensors with MoS_2/H-NCD/SiO_2/Si, MoS_2/SiO_2/Si, MoS_2/Si, and H-NCD/SiO_2/Si to six different concentrations of ammonia (a) and nitrogen dioxide (b).

Table 1. Comparison of Response and Characteristics of Different Sensor Types

	MoS_2 on Si	diamond on SiO_2	MoS_2 on SiO_2	MoS_2 on diamond	
				at 0 day	after 10 months
R_0 (kΩ) (source: 0.1 V)	0.006	17.8	19.6	25.5	25.8
$(R - R_0)\cdot R_0^{-1}$ response to 96.6 ppm NH_3 (%)	<0.01	<0.01	−0.7	17.8	15.2
$(R - R_0)\cdot R_0^{-1}$ response to 99.6 ppm NO_2 (%)	<0.01	<0.01	1.8	15.7	10.5
time response to 96.6 ppm NH_3 ($\Omega\cdot s^{-1}$)	0	0	−3.18	179	103
time response to 99.6 ppm NO_2 ($\Omega\cdot s^{-1}$)	0	0	9.26	181	63
sensitivity to NH_3 (%·ppm^{-1})	<0.0001	<0.0001	−0.0072	0.1884	0.1573
sensitivity to NO_2 (%·ppm^{-1})	<0.0001	<0.0001	0.0180	0.1572	0.1054

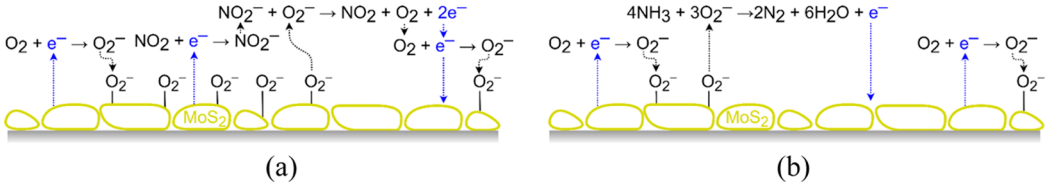

Figure 5. Schematic illustration of the gas sensing mechanism between a layer of MoS_2 nanoflakes and (a) oxidizing and (b) reducing gases.

This value is more than 25 times higher than that for MoS_2/SiO_2/Si. After this, NO_2 is released into the test chamber. The resistance changes the value to 29.5 kΩ, and the percentual change is 15.7%. This value is approximately 9 times higher than that of the MoS_2/SiO_2/Si sample. The calculated sensitivity is 0.1884%·ppm^{-1} (48 Ω·ppm^{-1}) for NH_3 and 0.1572%·ppm^{-1} (40 Ω·ppm^{-1}) for NO_2.

Figure 3c shows the absolute and relative change in resistance over time measured after 10 months of sample storage in air. This measurement examined the time stability (i.e., aging) of the heterostructure to NH_3 and NO_2. The response decreases by only 2.6% for NH_3 and by 5.2% for NO_2. The average monthly fluctuations of the gas responses are 0.26%·$months^{-1}$ for NH_3 and 0.52%·$months^{-1}$ for NO_2.

3.3. Comparison of Sensors. A comparison of the relative changes in resistance of all sensor types is plotted in Figure 4a for different NH_3 concentrations and in Figure 4b for NO_2 at room temperature (22 °C). The Δ_R value (i.e., the response) increases/decreases linearly with an active gas concentration in all cases. The values have a small deviation (max. 1.8%) from linear interpolation.

The electronic characteristics and responses for all sensors are summarized in Table 1. The table includes the measured data for all sensors. It can be concluded that the MoS_2/Si and H-NCD/SiO_2/Si samples are not suitable for gas sensing at room temperature. The MoS_2/SiO_2/Si sample slightly increased the gas response and the initial resistance. However, the resistance change of the active layer is still low. The MoS_2/H-NCD/SiO_2/Si structure does not increase the initial resistance but improves the gas response on the active layer. Compared to previous types of sensors, MoS_2/H-NCD/SiO_2/Si exhibited improved resistance change for both oxidizing and reducing gases. Unfortunately, this heterostructure has lost its selectivity for the recognition of oxidizing and reducing gases as it increases resistance to both types of gas. For the MoS_2/H-NCD/SiO_2/Si heterostructure, the minimal detection concentration for the change of 1% is 7 ppm and 5 ppm for NO_2 and NH_3, respectively.

4. DISCUSSION

Experimental gas sensing measurements show that the MoS_2/H-NCD/SiO_2/Si heterostructure is fully functional and enhances the gas sensing characteristics at room temperature. Both materials exhibit different types of conductivity. The MoS_2 nanoflakes represent an N-type semiconductor (excess negative charge carriers), and the H-NCD forms a two-dimensional subsurface hole gas (2DHG) with P-type conductivity (excess positive charge carriers). Different conductivity types cause opposite responses (and reactions) when exposed to reducing and oxidizing gases. The following subsections describe the interaction of gas molecules at the active layers of the fabricated sensors.

https://doi.org/10.1021/acsami.3c04438
ACS Appl. Mater. Interfaces 2023, 15, 34206−34214

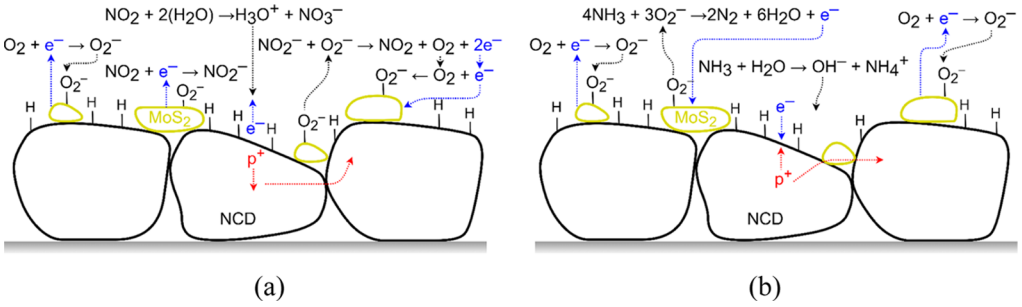

Figure 6. Schematic illustration of the gas sensing mechanism and charge transport for two parallel connected layers represented by MoS_2 nanoflakes and H-NCD exposed to the (a) oxidizing and (b) reducing gas.

4.1. Gas Interaction Model. MoS_2 generally behaves as an N-type semiconductor.[7] The change in resistance in MoS_2 nanoflakes is caused by chemisorption, reflecting the sorption of oxygen molecules on its solid surface by chemical bonding with electron transfer. Defects in MoS_2, such as flake edges and sulfur vacancies, serve as active sites for the gas molecules under investigation. Gas sensing properties depend on the charge transfer between the gas molecules and defects in MoS_2.[2,3,40] Figure 5 shows a schematic illustration of the gas sensing mechanism based on already published works.[2−5] First, the O_2 molecule from the air chemisorbs to the surface of MoS_2 and forms a native oxide. These molecules act as electron trap centers, extracting electrons from MoS_2 and generating O_2^-.[2,3] As a result, the concentration of free electrons decreases, and consequently, the conductivity decreases too. The chemisorbed oxygen sets the baseline resistance of the sensing layer. For the oxidizing gas NO_2 (Figure 5a), the gas molecules form NO_2^- ions,[2−4] which increase the resistivity of the layer. After switching the oxidizing gas to synthetic air, NO_2^- ions react with chemisorbed O_2^- to form NO_2 and O_2. The two remaining electrons from the chemical reaction are released back into the conduction band of MoS_2 or form new O_2^- ions with O_2.[2,4,6,22,40] On the other hand, the reducing gas NH_3 (Figure 5b) reacts with chemisorbed O_2^- ions and creates H_2O and N_2.[5] The remaining electron from the reaction is released into MoS_2 and reduces the resistivity of the sensing layer.[3,20] During the recovery process, i.e., after the change of the reducing gas to synthetic air, O_2 is chemisorbed from the atmosphere onto the surface of MoS_2.[5,6,14,20,40]

On the other hand, H-NCD reveals unique properties of P-type induced subsurface conductivity, also known as 2DHG, which is sensitive to exposed gas or organic molecules.[25,26] The change in resistance of H-NCD is caused by chemical reactions forming counterions on its surface via the electron transfer model.[25] The gas interaction model with the widely established H-NCD subsurface doping mechanism is described in ref.[41] The water molecule from the air humidity dissociates the ions H_3O^+ and OH^-. The H_3O^+ ions attract electrons from the diamond surface, leading to P-type subsurface conductivity.

Thus, the MoS_2/H-NCD/SiO_2/Si heterostructure shows two types of conductivity: P-type H-NCD[26] and N-type MoS_2.[3] This combination provides a unique material platform in which different conductivity types react oppositely to reducing and oxidizing gases.[17] The gas interaction could be influenced by several factors, such as surface-controlled charge injection into/out of the depletion region, surface shortcuts from diamond or MoS_2 layers, modulation of the P-type diamond subsurface conductivity by MoS_2 (the gating-like effect), and the gradual degradation of the P-type diamond subsurface conductivity due to the deposition of MoS_2 and others. Although the primary origin is still under investigation, the simplified model should be based on the coupling of two conduction paths via H-NCD or MoS_2 layers. The change in resistance of the MoS_2/H-NCD sensor is caused by (1) chemical reactions forming counterions on H-NCD and (2) chemisorption of oxygen molecules on the solid surface of MoS_2 by chemical bonding with electron transfer. Its gas-sensing properties further depend on the charge carrier concentrations for both materials. Figure 6 gives a schematic illustration of the gas sensing mechanism for two layers coupled in parallel. Suppose there are oxidizing gas molecules in their vicinity (Figure 6a). In this case, the number of charge carriers increases for H-NCD and decreases for MoS_2. Thus, the charge carrier transport mainly prevails through the diamond layer rather than through the MoS_2 layer, while this charge carrier transport is scattered at the diamond grain boundaries. The reducing gas (Figure 6b) causes a decrease in the number of charge carriers for H-NCD and an increase for MoS_2. As a result, the resistance of the MoS_2 nanoflakes decreases and more charge carriers flow through these nanoflakes with lower resistance than through the potential barriers between individual diamond grains. However, H-NCD blocks the final charge transport due to its total area coverage. The total resistance is therefore higher for NH_3 than for NO_2 because the surface coverage of the MoS_2 nanoflakes is low and H-NCD has a more pronounced effect on the change in resistance for reducing gases.

Reducing and oxidizing gases contribute to the increased resistance of the MoS_2/H-NCD heterostructure. In addition to the mechanisms described above, two effects of the resistance change are also manifested. The current flow and the subsequent resistance change consist of mutually constrained components:I. the horizontal one representing the current through the H-NCD and II. the vertical one representing the current through the MoS_2/H-NCD. The schematic illustration is shown in Figure 7. The current flowing through the P−N junction must tunnel through the space charge region (SCR). When the gas is applied, the width of the SCR (w_{SCR}) increases, and thus, the resistance increases too. The w_{SCR} can be calculated from the concentrations of free charge carriers injected into the semiconductors by the gases according to formula 2. The concentration of free charge carriers in H-NCD (N_A) increases for the oxidizing gas (NO_2) and decreases for the reducing gas (NH_3), as described in the previous model. For N-type MoS_2, the concentration has the opposite effect. So, the concentration (N_D) decreases for NO_2 and increases for NH_3. The formula shows that the SCR width increases for

https://doi.org/10.1021/acsami.3c04438
ACS Appl. Mater. Interfaces 2023, 15, 34206−34214

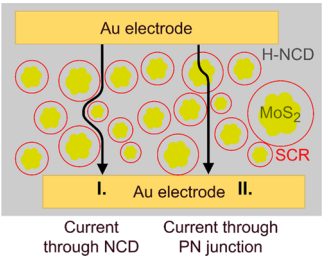

Figure 7. Schematic illustration of two ways (I and II) for the current flow between IDT electrodes, I—horizontal flow through H-NCD and II—combined horizontal/vertical flow, i.e., horizontal through H-NCD and MoS_2 and vertical through the MoS_2/H-NCD heterostructure.

both types of gas. As the width of the SCR increases, the number of charge carriers tunneling through the SCR decreases; thus, the total resistance is increased. In the case of the current flowing through H-NCD, formula 3 can be considered. The deposited interdigital electrodes measure this current component, while the additional resistance includes the distance between adjacent fingers. In the presence of the oxidizing or reducing gas, the geometric dimensions of the 2DHG change due to the increase in the width of the SCR, and thus, the total length l is increased, and the cross-section S is reduced. The total resistance therefore increases.

$$w_{SCR} = x_N + x_P = \sqrt{\frac{2\varepsilon_S V_D}{e}\left(\frac{N_A + N_D}{N_A N_D}\right)}(m) \quad (2)$$

$$\text{Resistance } R = \rho \cdot \frac{l}{S}(\Omega) \quad (3)$$

In addition, to support the importance of our model, we also investigated the role of H-NCD in the MoS_2/H-NCD/SiO_2/Si sensor. The measured responses and contact angles are given in the Supporting Information (Tables S1 and S2).

4.2. Effect of Oxidizing vs Reducing Gases. As described above, individual MoS_2 and hydrogen-terminated diamonds are capable of recognizing oxidizing/reducing gases but with opposite signs of resistance change as illustrated in Figure 8. Here, the Y-axis represents only qualitative information and not quantitative. Unfortunately, the H-NCD did not reveal any response to exposed gases at room temperature, but the illustrative behavior was achieved for temperatures higher than 40 °C (see S5), which is in good agreement with our previous work.[41] The MoS_2/H-NCD heterostructure has a different response to gases as it increases resistance to both types of gases (i.e., it loses selectivity to oxidizing/reducing gas). The magnitude of the change also depends on the gas type; i.e., it is lower for the oxidizing gas than for the reducing gas, which can be attributed to the dominance of H-NCD in the MoS_2/H-NCD heterostructure. However, heterostructures prepared with different ratios of diamond to MoS_2 can further tailor the response to oxidizing and reducing gases.

5. CONCLUSIONS

MoS_2/Si, MoS_2/SiO_2/Si, H-NCD/SiO_2/Si, and MoS_2/H-NCD/SiO_2/Si structures were used to fabricate conductivity gas sensors and tested at room temperature (22 °C). The active layers of MoS_2 and H-NCD were analyzed by SEM, Raman spectroscopy, contact angle, and GIWAXS measurements in their individual and combined forms. In terms of gas sensing properties, MoS_2 and H-NCD showed poor responses at room temperature. However, by combining them into a MoS_2/H-NCD heterostructure, the gas sensing parameters were significantly improved. The formed heterostructure, consisting of the P-type subsurface conductive H-NCD layer and the N-type conductive MoS_2 nanoflakes, resulted in a synergistic effect that enhanced the gas response. While well-established interactions of gas molecules were experimentally validated for the particular form of MoS_2 and H-NCD layers, the MoS_2/H-NCD heterostructure did not reveal such a specific behavior. The presented model pointed out the influence of the P−N junction, especially the geometrical variation of the SCR, after its exposure to the tested gases. Unfortunately, this heterostructure abolishes the selectivity; i.e., increased resistance was observed for oxidizing and reducing gases with different responses. However, the combination of a MoS_2/H-NCD heterostructure with a single MoS_2 layer within one sensor chip seems to be a promising solution to overcome this limitation. This sensor can select the gas type on the MoS_2 according to a mark of resistance change and the gas concentration by the size resistance change of the MoS_2/H-NCD. In conclusion, this article introduces a new class of conductivity gas sensors that can provide miniaturization and reduction of power consumption compared to commercial sensors. The presented TMD/diamond heterostructures could be very suitable for portable devices or energy-harvesting applications.

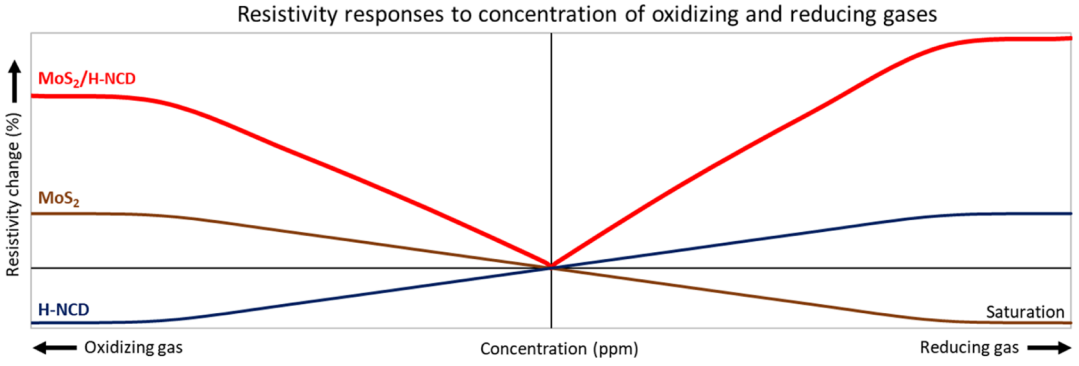

Figure 8. Qualitative illustration of the relative responses of MoS_2, H-NCD, and MoS_2/H-NCD sensor devices to different concentrations of oxidizing and reducing gases based on gas interaction models.

https://doi.org/10.1021/acsami.3c04438
ACS Appl. Mater. Interfaces 2023, 15, 34206−34214

■ ASSOCIATED CONTENT

Supporting Information

The Supporting Information is available free of charge at https://pubs.acs.org/doi/10.1021/acsami.3c04438.

Surface morphology of all samples, photo of the sensor testing setup, gas responses of reference samples, verification of the synergy effect between MoS_2 and H-NCD via the O-term NCD, and water contact angle measurements (PDF)

■ AUTHOR INFORMATION

Corresponding Author

Michal Kočí − *Department of Semiconductors, Institute of Physics of the Czech Academy of Sciences, Prague 6 162 00, Czech Republic; Department of Microelectronics, Faculty of Electrical Engineering, Czech Technical University in Prague, Prague 6 166 27, Czech Republic;* orcid.org/0000-0003-0715-8639; Email: kocim@fzu.cz, kocimic1@fel.cvut.cz

Authors

Tibor Izsák − *Department of Microelectronics and Sensors, Institute of Electrical Engineering, Slovak Academy of Sciences, Bratislava 841 04, Slovak Republic;* orcid.org/0000-0002-0411-7279

Gabriel Vanko − *Department of Microelectronics and Sensors, Institute of Electrical Engineering, Slovak Academy of Sciences, Bratislava 841 04, Slovak Republic*

Michaela Sojková − *Department of Microelectronics and Sensors, Institute of Electrical Engineering, Slovak Academy of Sciences, Bratislava 841 04, Slovak Republic;* orcid.org/0000-0002-7490-3240

Jana Hrdá − *Department of Microelectronics and Sensors, Institute of Electrical Engineering, Slovak Academy of Sciences, Bratislava 841 04, Slovak Republic;* orcid.org/0000-0002-4492-9415

Ondrej Szabó − *Department of Semiconductors, Institute of Physics of the Czech Academy of Sciences, Prague 6 162 00, Czech Republic;* orcid.org/0000-0001-7784-9780

Miroslav Husák − *Department of Microelectronics, Faculty of Electrical Engineering, Czech Technical University in Prague, Prague 6 166 27, Czech Republic;* orcid.org/0000-0001-9102-9818

Karol Végsö − *Department of Multilayers and Nanostructures, Institute of Physics, Slovak Academy of Sciences, Bratislava 845 11, Slovak Republic; Centre for Advanced Materials Application (CEMEA), Slovak Academy of Sciences, Bratislava 845 11, Slovak Republic*

Marian Varga − *Department of Semiconductors, Institute of Physics of the Czech Academy of Sciences, Prague 6 162 00, Czech Republic; Department of Microelectronics and Sensors, Institute of Electrical Engineering, Slovak Academy of Sciences, Bratislava 841 04, Slovak Republic;* orcid.org/0000-0002-9613-4614

Alexander Kromka − *Department of Semiconductors, Institute of Physics of the Czech Academy of Sciences, Prague 6 162 00, Czech Republic*

Complete contact information is available at: https://pubs.acs.org/10.1021/acsami.3c04438

Notes

The authors declare no competing financial interest.

■ ACKNOWLEDGMENTS

The authors kindly acknowledge R. Jackivová for SEM measurements and E. Shagieva for Raman measurements. This work was supported by GACR bilateral project no. 23-04322L and GAAV project no. SAV-AV ČR-23-11. M.V. acknowledges project no. 19MRP0010 financed from the MoRePro Programme and the Slovak Academy of Sciences funding. This work used the research infrastructure Czech NanoLab supported by the LM2023051 project and partially by CTU project no. SGS23/181/OHK3/3T/13 Materials and structures for sensors, integrated, and photonic circuits.

■ REFERENCES

(1) Dhall, S.; Mehta, B. R.; Tyagi, A. K.; Sood, K. A review on environmental gas sensors: Materials and technologies. *Sens. Int.* **2021**, *2*, 100116.

(2) Zhou, Y.; Liu, G.; Zhu, X.; Guo, Y. Ultrasensitive NO2 gas sensing based on rGO/MoS2 nanocomposite film at low temperature. *Sens. Actuators, B* **2017**, *251*, 280−290.

(3) Neetika; Kumar, A.; Chandra, R.; Malik, V. K. MoS2 nanoworm thin films for NO2 gas sensing application. *Thin Solid Films* **2021**, *725*, 138625.

(4) Reddeppa, M.; Park, B.-G.; Murali, G.; Choi, S. H.; Chinh, N. D.; Kim, D.; Yang, W.; Kim, M.-D. NOx gas sensors based on layer-transferred n-MoS2/p-GaN heterojunction at room temperature: Study of UV light illuminations and humidity. *Sens. Actuators, B* **2020**, *308*, 127700.

(5) Yan, H.; Song, P.; Zhang, S.; Zhang, J.; Yang, Z.; Wang, Q. A low temperature gas sensor based on Au-loaded MoS2 hierarchical nanostructures for detecting ammonia. *Ceram. Int.* **2016**, *42*, 9327−9331.

(6) Luo, H.; Cao, Y.; Zhou, J.; Feng, J.; Cao, J.; Guo, H. Adsorption of NO2, NH3 on monolayer MoS2 doped with Al, Si, and P: A first-principles study. *Chem. Phys. Lett.* **2016**, *643*, 27−33.

(7) Akbari, E.; Jahanbin, K.; Afroozeh, A.; Yupapin, P.; Buntat, Z. Brief review of monolayer molybdenum disulfide application in gas sensor. *Phys. B* **2018**, *545*, 510−518.

(8) Mak, K. F.; Lee, C.; Hone, J.; Shan, J.; Heinz, T. F. Atomically thin MoS_2: a new direct-gap semiconductor. *Phys. Rev. Lett.* **2010**, *105*, 136805.

(9) Kim, S.; Konar, A.; Hwang, W.-S.; Lee, J. H.; Lee, J.; Yang, J.; Jung, C.; Kim, H.; Yoo, J.-B.; Choi, J.-Y.; et al. High-mobility and low-power thin-film transistors based on multilayer MoS2 crystals. *Nat. Commun.* **2012**, *3*, 1011.

(10) Lee, E.; Yoon, Y. S.; Kim, D.-J. Two-Dimensional Transition Metal Dichalcogenides and Metal Oxide Hybrids for Gas Sensing. *ACS Sens.* **2018**, *3*, 2045−2060.

(11) Chromik, Š.; Sojková, M.; Vretenár, V.; Rosová, A.; Dobročka, E.; Hulman, M. Influence of GaN/AlGaN/GaN (0001) and Si (100) substrates on structural properties of extremely thin MoS 2 films grown by pulsed laser deposition. *Appl. Surf. Sci.* **2017**, *395*, 232−236.

(12) Kannan, P. K.; Late, D. J.; Morgan, H.; Rout, C. S. Recent developments in 2D layered inorganic nanomaterials for sensing. *Nanoscale* **2015**, *7*, 13293−13312.

(13) Sojkova, M.; Vegso, K.; Mrkyvkova, N.; Hagara, J.; Hutar, P.; Rosova, A.; Caplovicova, M.; Ludacka, U.; Skakalova, V.; Majkova, E.; et al. Tuning the orientation of few-layer MoS2 films using one-zone sulfurization. *RSC Adv.* **2019**, *9*, 29645−29651.

(14) Shokri, A.; Salami, N. Gas sensor based on MoS2 monolayer. *Sens. Actuators, B* **2016**, *236*, 378−385.

(15) Yu, X.; Chen, X.; Ding, X.; Yu, X.; Zhao, X.; Chen, X. Facile fabrication of flower-like MoS2/nanodiamond nanocomposite toward high-performance humidity detection. *Sens. Actuators, B* **2020**, *317*, 128168.

(16) Saravanan, A.; Huang, B.-R.; Chu, J. P.; Prasannan, A.; Tsai, H.-C. Interface engineering of ultrananocrystalline diamond/MoS2-ZnO

heterostructures and its highly enhanced hydrogen gas sensing properties. *Sens. Actuators, B* **2019**, *292*, 70−79.
(17) Petit-Domínguez, M. D.; Quintana, C.; Vazquez, L.; Del Pozo, M.; Cuadrado, I.; Maria Parra-Alfambra, A.; Casero, E. Synergistic effect of MoS2 and diamond nanoparticles in electrochemical sensors: determination of the anticonvulsant drug valproic acid. *Microchim. Acta* **2018**, *185*, 334.
(18) Niu, Y.; Wang, R.; Jiao, W.; Ding, G.; Hao, L.; Yang, F.; He, X. MoS2 graphene fiber based gas sensing devices. *Carbon* **2015**, *95*, 34−41.
(19) Yan, H.; Song, P.; Zhang, S.; Yang, Z.; Wang, Q. Facile synthesis, characterization and gas sensing performance of ZnO nanoparticles-coated MoS2 nanosheets. *J. Alloys Compd.* **2016**, *662*, 118−125.
(20) Liu, A.; Lv, S.; Jiang, L.; Liu, F.; Zhao, L.; Wang, J.; Hu, X.; Yang, Z.; He, J.; Wang, C.; et al. The gas sensor utilizing polyaniline/MoS2 nanosheets/SnO2 nanotubes for the room temperature detection of ammonia. *Sens. Actuators, B* **2021**, *332*, 129444.
(21) Wang, F.; Liu, H.; Hu, K.; Li, Y.; Zeng, W.; Zeng, L. Hierarchical composites of MoS2 nanoflower anchored on SnO2 nanofiber for methane sensing. *RSC Adv.* **2019**, *45*, 22981−22986.
(22) Luo, Y.; Zhang, C. Pt-activated TiO2-MoS2 nanocomposites for H2 detection at low temperature. *J. Alloys Compd.* **2018**, *747*, 550−557.
(23) Liskova, J.; Babchenko, O.; Varga, M.; Kromka, A.; Hadraba, D.; Svindrych, Z.; Burdikova, Z.; Bacakova, L. Osteogenic cell differentiation on H-terminated and O-terminated nanocrystalline diamond films. *Int. J. Nanomed.* **2015**, *10*, 869−884.
(24) Davydova, M.; Kulha, P.; Laposa, A.; Hruska, K.; Demo, P.; Kromka, A. Gas sensing properties of nanocrystalline diamond at room temperature. *Beilstein J. Nanotechnol.* **2014**, *5*, 2339−2345.
(25) Gurbuz, Y.; Kang, W. P.; Davidson, J. L.; Kinser, D. L.; Kerns, D. V. Diamond microelectronic gas sensors. *Sens. Actuators, B* **1996**, *33*, 100−104.
(26) Helwig, A.; Müller, G.; Garrido, J. A.; Eickhoff, M. Gas sensing properties of hydrogen-terminated diamond. *Sens. Actuators, B* **2008**, *133*, 156−165.
(27) Raju, P.; Li, Q. Review—Semiconductor Materials and Devices for Gas Sensors. *J. Electrochem. Soc.* **2022**, *169*, 057518.
(28) Kumar, R.; Avasthi, D. K.; Kaur, A. Fabrication of chemiresistive gas sensors based on multistep reduced graphene oxide for low parts per million monitoring of sulfur dioxide at room temperature. *Sens. Actuators, B* **2017**, *242*, 461−468.
(29) Ding, L.; Qin, Z.; Dou, Z.; Shen, Y.; Cai, Y.; Zhang, Y.; Zhou, Y. Morphology-promoted synergistic effects on the sensing properties of polyaniline ultrathin layers on reduced graphene oxide sheets for ammonia and formaldehyde detection. *J. Mater. Sci.* **2018**, *53*, 7595−7608.
(30) Hur, J.; Park, S.; Kim, J. H.; Cho, J. Y.; Kwon, B.; Lee, J. H.; Bae, G. Y.; Kim, H.; Han, J. T.; Lee, W. H. Ultrasensitive, Transparent, Flexible, and Ecofriendly NO 2 Gas Sensors Enabled by Oxidized Single-Walled Carbon Nanotube Bundles on Cellulose with Engineered Surface Roughness. *ACS Sustainable Chem. Eng.* **2022**, *10*, 3227−3235.
(31) Shooshtari, M.; Salehi, A. An electronic nose based on carbon nanotube -titanium dioxide hybrid nanostructures for detection and discrimination of volatile organic compounds. *Sens. Actuators, B* **2022**, *357*, 131418.
(32) Gavgani, J. N.; Hasani, A.; Nouri, M.; Mahyari, M.; Salehi, A. Highly sensitive and flexible ammonia sensor based on S and N co-doped graphene quantum dots/polyaniline hybrid at room temperature. *Sens. Actuators, B* **2016**, *229*, 239−248.
(33) Seekaew, Y.; Wisitsoraat, A.; Wongchoosuk, C. ZnO quantum dots decorated carbon nanotubes-based sensors for methanol detection at room temperature. *Diamond Relat. Mater.* **2023**, *132*, 109630.
(34) Gao, J.; Wu, H.; Zhou, J.; Yao, L.; Zhang, G.; Xu, S.; Xie, Y.; Li, L.; Shi, K. Mesoporous In 2 O 3 nanocrystals: synthesis, characterization and NO x gas sensor at room temperature. *New J. Chem.* **2016**, *40*, 1306−1311.
(35) Qu, F.; Liu, H.; Guarecuco, R.; Jiao, Y.; Yang, M. Mesoporous InN/In2O3 heterojunction with improved sensitivity and selectivity for room temperature NO2 gas sensing. *Nanotechnology* **2016**, *27*, 385501.
(36) Shaik, M.; Rao, V. K.; Gupta, M.; Murthy, K. S. R. C.; Jain, R. Chemiresistive gas sensor for the sensitive detection of nitrogen dioxide based on nitrogen doped graphene nanosheets. *RSC Adv.* **2016**, *6*, 1527−1534.
(37) Wang, S.-C.; Shaikh, M. O. A Room Temperature H2 Sensor Fabricated Using High Performance Pt-Loaded SnO2 Nanoparticles. *Sensors* **2015**, *15*, 14286−14297.
(38) Sojkova, M.; Siffalovic, P.; Babchenko, O.; Vanko, G.; Dobrocka, E.; Hagara, J.; Mrkyvkova, N.; Majkova, E.; Izak, T.; Kromka, A.; et al. Carbide-free one-zone sulfurization method grows thin MoS2 layers on polycrystalline CVD diamond. *Sci. Rep.* **2019**, *9*, 2001.
(39) Chromik, S.; Rosová, A.; Dobročka, E.; Kobzev, A. P.; Hulman, M.; Sojkova, M.; Hutár, P.; Machajdík, D. MoS2 thin films prepared by sulfurization. In *Nanoengineering: Fabrication, Properties, Optics, and Devices XIV*; Campo, E. M., Dobisz, E. A., Eldada, L. A., Eds.; SPIE, 2017; p 56.
(40) Barzegar, M.; Iraji zad, A.; Tiwari, A. On the performance of vertical MoS2 nanoflakes as a gas sensor. *Vacuum* **2019**, *167*, 90−97.
(41) Koci, M.; Kromka, A.; Boura, A.; Szabo, O.; Husak, M. Hydrogen-Terminated Diamond Surface as a Gas Sensor: A Comparative Study of Its Sensitivities. *Sensors* **2021**, *21*, 5390.

https://doi.org/10.1021/acsami.3c04438
ACS Appl. Mater. Interfaces 2023, 15, 34206−34214

IV. Gas sensors based on diamond heterostructures for air quality monitoring

Authors: Michal Kočí, Ondrej Szabó, Tibor Izsák, Michaela Sojková, Marcin Godzierz, Paweł Wróbel, Miroslav Husák, Alexander Kromka

Gas sensors based on diamond heterostructures for air quality monitoring

[1,2] Michal KOČÍ, [1] Ondrej SZABÓ, [3] Tibor IZSÁK, [3] Michaela SOJKOVÁ, [4] Marcin GODZIERZ, [4] Paweł WRÓBEL, [2] Miroslav HUSÁK, [1] Alexander KROMKA

[1]*Institute of Physics of the Czech Academy of Sciences, Prague, Czech Republic, EU, kocim@fzu.cz*

[2]*Faculty of Electrical Engineering, Czech Technical University in Prague, Czech Republic, EU*

[3]*Institute of Electrical Engineering, Slovak Academy of Sciences, Bratislava, Slovak Republic, EU*

[4]*Centre of Polymer and Carbon Materials of the Polish Academy of Sciences, Zabrze, Poland, EU*

https://doi.org/10.37904/nanocon.2023.4785

Abstract

Currently, great emphasis is placed on air quality and the presence of pollutants, whether on toxic substances (NH_3 or CO), substances that reduce the quality of life (CO_2) or chemical vapors from industries (acetone or ethanol). Attention is therefore focused on new gas-sensing materials enabling detection even at low (up to room) temperatures with sufficient response and short reaction time.

Here, we investigate the suitability of hydrogen-terminated nanocrystalline diamond (H-NCD) films and their heterostructures with molybdenum disulfide (MoS_2), graphene oxide (GO), reduced GO (rGO), thiol-functionalized GO (SH-GO), or gold nanoparticles (Au NPs) for gas sensing applications. Electrical properties are measured for oxidizing gas NO_2, reducing gas NH_3, and chemical vapor of ethanol (C_2H_5OH), and at temperatures varied from room temperature to 125 °C. All tested gases were used with a concentration of up to 100 ppm. Synthetic air is used as the flushing gas. The measured parameters of the tested sensors are compared, both with each other and with commercial sensors, and subsequently evaluated. In contrast to the individual forms of employed materials with limited response to the exposed gases, the H-NCD heterostructures revealed better sensing properties. In particular, the Au NPs/H-NCD heterostructures revealed a higher response at 125 °C in contrast to H-NCD, MoS_2/H-NCD had quite good response even at room temperature and GO/H-NCD revealed high sensitivity to chemical vapor, which further improved for the SH-GO/H-NCD.

Keywords: Gas sensors, nanocrystalline diamond, heterostructures, air quality monitoring

1. INTRODUCTION

Air quality is essential, especially regarding hazardous substances like ammonia (NH_3), as well as those that reduce our overall quality of life, such as nitrogen dioxide (NO_2) or carbon oxide (CO_2). The release of an increasing number of harmful substances into the air, mainly by industry, significantly threatens the quality of our lives. Nowadays, air quality monitoring and pollutant detection are significant issues. As a result, gas sensors have become almost indispensable parts of industrial processes and everyday life. Currently, the most used gas sensor that uses the conductivity principle is metal oxide (MO_X) material, especially SnO_2 [1, 2]. MO_X sensors are used for their low price and flexible production. On the other hand, these sensors need a very high operating temperature, and the dimensions cannot be reduced too much [3, 4]. The high energy consumption and large dimensions prevent applications as sensor nodes in IoT (Internet of Things) applications with Energy Harvesting supply. Therefore, developing devices that work at room temperature (about 22 °C) with low cost and high sensitivity is still challenging. For this reason, high demands are placed on developing new types of sensors [1, 2]. With new materials and processing, smaller, more accurate, and cheaper sensors with lower power consumption are being developed. Following that, great attention is focused on new materials suitable for gas sensors. Gas sensors with wide bandgap semiconductors (exceptionally diamond-thin layers) [5, 6, 7]

or 2D materials (e.g., TMDs [8, 9, 10] or GOs [11, 12]) active layers have great potential due to possible miniaturization and modification, e.g., material science or technology progress [2]. Here, a miniaturized conductivity gas sensor is realized with H-NCD films and their heterostructures with MoS_2, GOs (GO, rGO, and SH-GO), and Au NPs, which revealed enhanced gas-sensing parameters.

2. EXPERIMENTAL

The fabrication of active layers for gas sensors (pure materials and heterostructures) is described in the following chapters. The glass substrate with an interdigital (IDT) structure from Micrux was used instead of MoS_2 layers, which were prepared on Si substrate. The IDT structure from Micrux contains 90 pairs of 10 μm width gold electrodes with 200 nm thickness and 10 μm gap between electrodes. The Au/Ti IDT structures with a 120 nm thick were evaporated on the top of MoS_2 layers. Then, the substrates were ultrasonically cleaned in acetone, subsequently in isopropyl alcohol, and finally in deionized water for 10 minutes. All fabricated sensors, the distinct materials and their heterostructures are depicted in **Figure 1**.

2.1 H-NCD

The H-NCD layers were grown by microwave plasma-enhanced chemical vapor deposition (MW-PECVD) technology. A four-step process was used - 1) preparation of a diamond nucleation layer on the substrate by treatment in an ultrasonic bath in a water-based nanodiamond powder suspension, 2) growth of the adhesion NCD layer in a linear antenna MW-PECVD system consisting of two linear antennas for better adhesion between the substrate and functional NCD layer, 3) growth of the functional NCD layer in a focused MW-PECVD chamber, and 4) surface functionalization of the NCD layer by hydrogen termination (H-NCD) realized in hydrogen plasma [13].

2.2 MoS_2

The MoS_2 layers were prepared as follows. Firstly, a 4 nm thin Mo layer was deposited using DC magnetron sputtering in an Ar atmosphere from a Mo target at room temperature (about 22 °C). The rotation speed of the sample holder controlled the thickness of the prepared Mo films. Next, the pre-deposited Mo layers were sulfurized in a custom-designed CVD chamber. The Mo layer was annealed in sulfur vapors at a high temperature of 800 °C in an N_2 atmosphere at ambient pressure. The substrate was placed together with the sulfur powder in the center of the furnace so that the temperature of the substrate and the powder were the same during the growth, unlike the standard CVD method, which uses a two-zone furnace with different temperatures for the sulfur powder and the Mo substrate [14].

2.3 GOs

GO was prepared using a modified Hummers method from graphite powder. rGO was made from GO dispersion, evaporating in a water bath to yield a mud-like residue. The sample was treated in ascorbic acid solution and sonicated. SH-GO arose from GO. GO was refluxed and stirred in a toluene/P_4S_{10} solution for 7 days. All active layers were prepared by drop-casting of 20 μl acetone suspension (ratio of 1 g in 25 ml).

2.4 Au NPs

The Au NPs were prepared by evaporating a thin Au layer (thickness of about 3 nm), which was further annealed in hydrogen microwave plasma. This treatment resulted in the formation of nano-sized Au particles (droplets) on the H-NCD surface. The Au was chosen due to its chemical stability and simple preparation [15].

2.5 Heterostructures

The preparation of heterostructures combined previous technological steps to prepare active layers for gas sensors. The first layer is, in most cases, H-NCD and the second material is prepared on it. The prepared heterostructures were kept for a week to stabilize the sensor surface [14, 15].

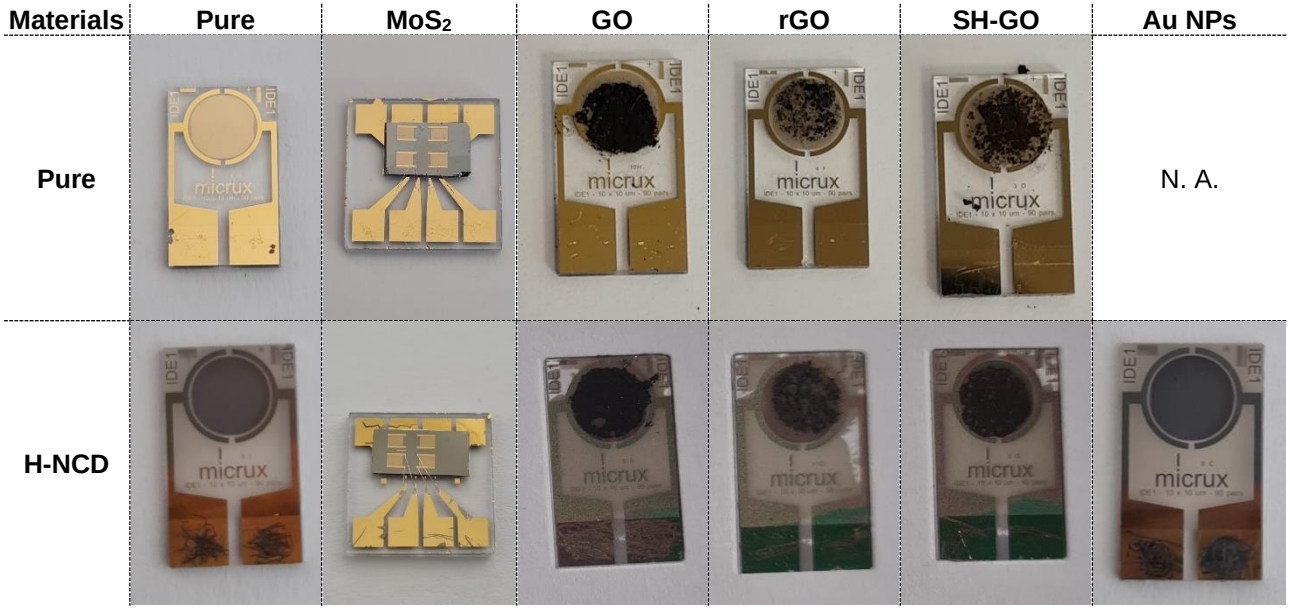

Figure 1 Photographs of all fabricated and tested sensors with pure materials and heterostructures

3. RESULTS AND DISCUSSION

The gas responses of these sensors were measured at a high temperature of 125 °C and room temperature (about 22 °C) for three testing gases concentrated at 100 ppm: ethanol vapor, NH_3, and NO_2. The gas-sensitive layer changed the resistance from steady-state R_0 to actual resistance R_G in the presence of the tested gas. The resistance changes Δ_R in the presence of active gas were calculated using equation (1). **Table 1** and **Table 2** show the responses achieved for individual sensors.

$$\Delta_R = \left(\frac{R_G}{R_0} - 1\right) \cdot 100 = \left(\frac{R_G - R_0}{R_0}\right) \cdot 100\ (\%) \quad (1)$$

Where:

Δ_R – Resistance change (%)

R_G – Resistance in the presence of the tested gas (Ω)

R_0 – Steady-state resistance (Ω)

Table 1 Responses of sensors at 125 °C exposed to 100 ppm ethanol vapor, 100 ppm NH_3 and 100 ppm NO_2. In the table, the best and the second-best values are highlighted in dark green and light green.

125 °C	Pure			H-NCD		
	100 ppm Ethanol	100 ppm NH_3	100 ppm NO_2	100 ppm Ethanol	100 ppm NH_3	100 ppm NO_2
Pure [13]	No response			98	39	-13
MoS_2	Unmeasured					
GO	352	28	-39	498	69	-40
rGO	148	-11	17	254	72	-39
SH-GO	46	8	-5	554	76	-47
Au NPs [15]	Unmeasured			587	48	-47

Table 2 Responses of sensors at 22 °C exposed to 100 ppm ethanol vapor, 100 ppm NH_3 and 100 ppm NO_2. In the table, the best and the second-best values are highlighted in dark green and light green.

RT (22 °C)	Pure			H-NCD		
	100 ppm Ethanol	100 ppm NH_3	100 ppm NO_2	100 ppm Ethanol	100 ppm NH_3	100 ppm NO_2
Pure [13]	No response			3	0.5	-0.7
MoS_2 [14]	35	-0.7	1.8	248	17.8	15.7
GO	301	5.2	-7.9	153	2.1	-7.2
rGO	130	-2	1.8	195	7.1	-2.2
SH-GO	16	0.6	-0.2	634	41	-19
Au NPs [15]	Unmeasured			164	4.8	-4.7

The responses are summarized and compared in **Figures 2**, **3**, and **4**. Compared to pure materials, their combination in heterostructure significantly enhanced the gas responses. The best response to gases exhibited SH-GO/H-NCD and Au NPs/H-NCD heterostructures at 125 °C, respectively SH-GO/H-NCD at room temperature. The SH-GO/H-NCD sensor exposed to 100 ppm ethanol achieved the most significant response of 634 % and 554 % at 22 °C and 125 °C, respectively. The second-best ethanol sensor is a heterostructure of Au NPs/H-NCD with a response of 587 % at 125 °C. The pure materials revealed a low response (<2 %) at room temperature, except for GO, with very high steady-state resistance. The higher temperature enhanced the response of almost all sensors. The only exception is the ethanol response of SH-GO/H-NCD. In this case, the response decreased from 634 % to 554 %.

The measured response to NH_3 is -16.9 % and 47.8 % to NO_2 [13]. A similar response to NO_2 had an IR gas sensor PY2055 from Pyreos, which is designed to detect NO_2 [17]. This sensor uses the absorption of IR light by gas. The disadvantage is the need to use an IR light source and as long as possible interaction path where the light will be absorbed. The total response to NO_2 is -46 %. This sensor had no response to NH_3, because this type has very high selectivity [13]. All prepared heterostructures have comparable responses at 125 °C to gases with these commercial sensors. In addition, the SH-GO/H-NCD and MoS_2/H-NCD have good responses comparable with commercial sensors at room temperature.

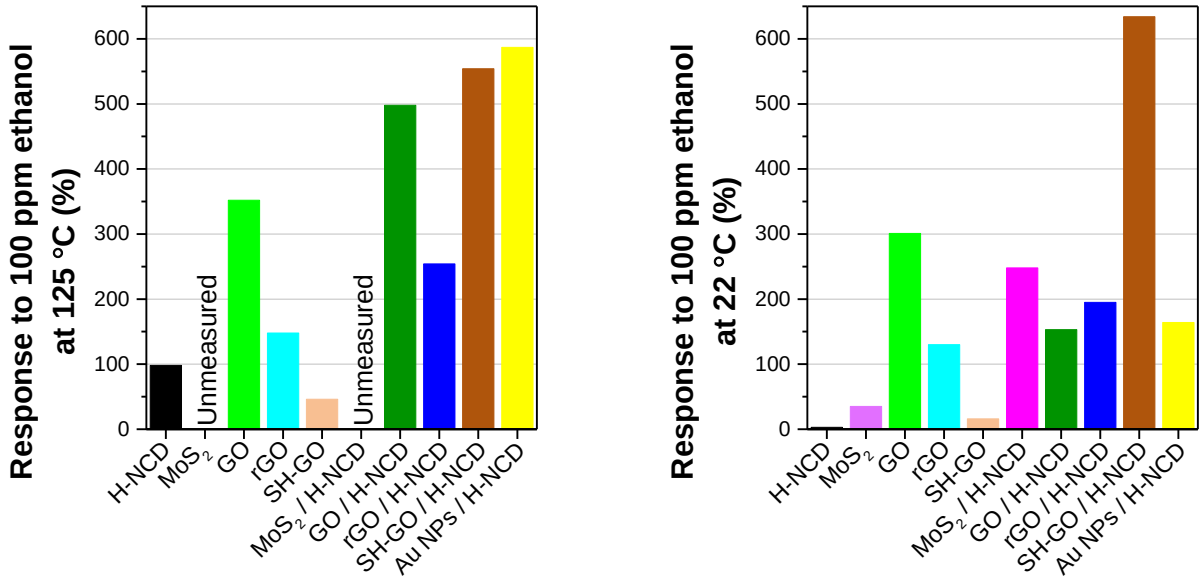

Figure 2 Responses of fabricated sensors to 100 ppm ethanol vapor at 125 °C and 22 °C (room temperature)

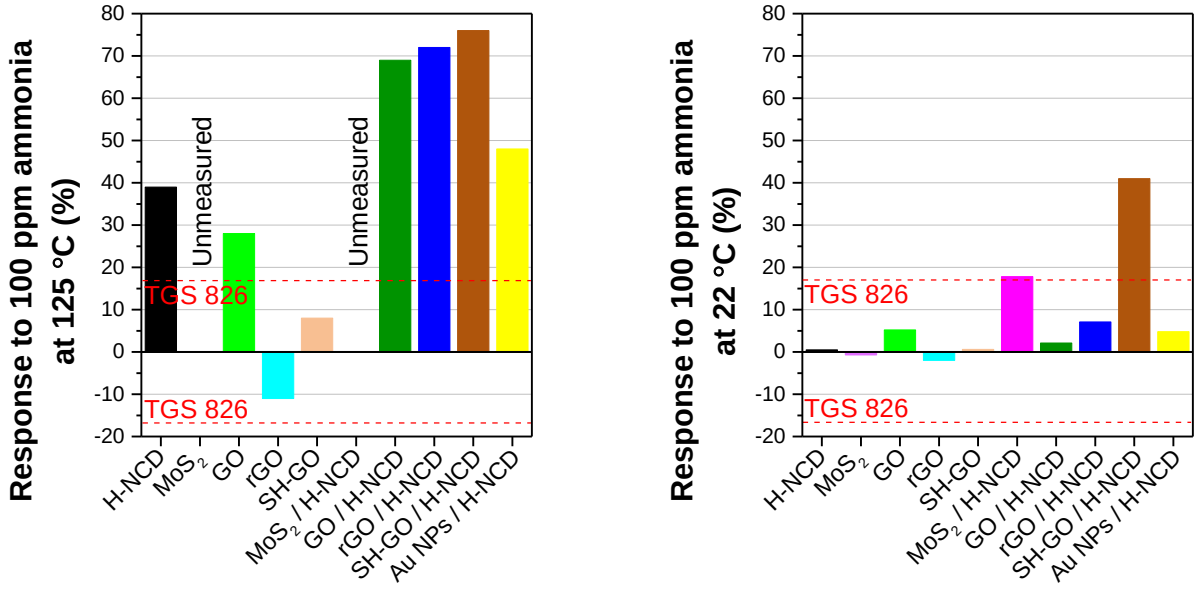

Figure 3 Responses of fabricated sensors to 100 ppm NH_3 at 125 °C and 22 °C (room temperature)

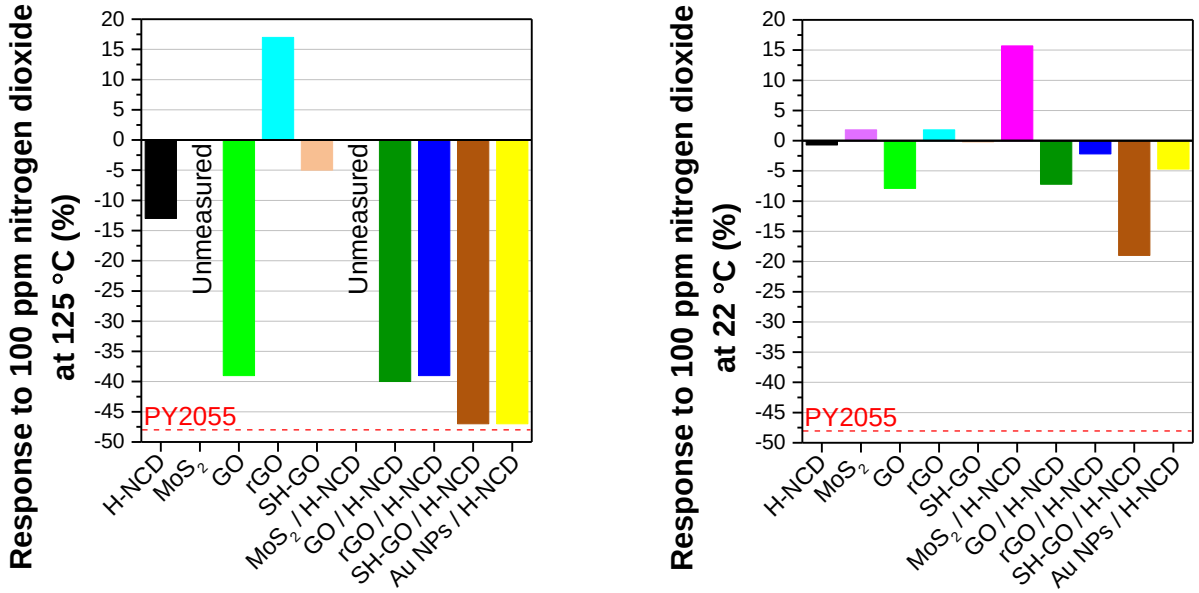

Figure 4 Responses of measured sensors to 100 ppm NO_2 at 125 °C and 22 °C (room temperature)

4. CONCLUSION

The newly introduced heterostructures H-NCD and the second material (MoS_2, GO, rGO, SH-GO or Au NPs) were designed, fabricated, and tested. The measurements revealed that most heterostructures exhibit preferable responses to exposed gas compared with pure materials at high and room temperatures. Even, the responses of some heterostructures are comparable with commercial gas sensors at 22 °C.

At a high temperature of 125 °C, all heterostructures and pure materials respond very well. At these conditions, the best responses exhibited SH-GO/H-NCD and Au NPs/H-NCD heterostructures with responses over 47 % for all tested gases, which are well comparable with commercial sensors. The power consumption for our heater should be still optimized, but it is much lower than the power needed for commercial sensors. For room temperature applications, pure materials and some heterostructures have very low, almost immeasurable, responses. The best combination of materials with good responses is SH-GO/H-NCD and MoS_2/H-NCD. These sensors have a response of over 15 % for all tested gases. These high responses are attributed to the optimum steady-state resistance, further enhanced by the synergistic effect at the interface of active materials.

In conclusion, our findings represent a promising alternative solution as the new class of gas sensors suitable for portable or energy-harvesting applications due to miniaturization and low power consumption. For now, however, the reproducibility of sensor production technology needs to be scaled up and optimized to meet industrial uses.

ACKNOWLEDGEMENTS

This research was funded by the mobility projects CSIR-23-05 and PAN 20 21 of the Czech Academy of Sciences. This work used the research infrastructure CzechNanoLab supported by the LM2023051 project and partially by CTU University project No. SGS23/181/OHK3/3T/13 Materials and structures for sensors, integrated and photonic circuits.

REFERENCES

[1] FRADEN, J. Handbook of modern sensors: Physics, designs, and applications, 3rd ed. New York: Springer. 2003. ISBN: 0-387-00750-4.

[2] DHALL, S., MEHTA, B. R., TYAGI, A. K., SOOD, K. A review on environmental gas sensors: Materials and technologies. Sensors International. 2021, 2, 100116. doi: 10.1016/j.sintl.2021.100116

[3] ŠTULÍK, K., BAREK, J., JANATA, J., KRÁL, V., KRONĎÁK, M., ŠŤASTNÝ, M. SENZORY: General Aspects of Chemical Sensing. VŠCHT Praha, 2007, ISBN: 978-80-86238-20-3.

[4] WANG, C., YIN, L., ZHANG, L., XIAND, D., GAO, R. Metal Oxide Gas Sensors: Sensitivity and Influencing Factors. Sensors. 2010. doi: 10.3390/s100302088.

[5] HELWIG, A., MUELLER, G., GARRIDO, J. A., EICKHOFF, M. Gas sensing properties of hydrogen-terminated diamond. Sensors and Actuators B: Chemical. 2008. doi: 10.1016/j.snb.2008.02.007.

[6] GURBUZ, Y., KANG, W. P., DAVIDSON, J. L., KINSER, D. L., KERNS, D.V. Diamond microelectronic gas sensors. Sensors and Actuators B: Chemical. 1996. doi: 10.1016/0925-4005(96)01839-4.

[7] MÜELLER, G., KRSTEV, I., MAIER, K., HELWIG, A., STUTZMANN, M., GARRIDO, J. Resettable, low-temperature accumulation gas sensors based on hydrogenated diamond transducers. *EUROSENSORS 2015*. 2015, doi: 10.1016/j.proeng.2015.08.733.

[8] NEETIKA, KUMAR, A., CHANDRA, R., MALIK, V. K. MoS2 nanoworm thin films for NO2 gas sensing application. Thin Solid Films. 2021. doi: 10.1016/j.tsf.2021.138625.

[9] LUO, H., CAO, Y., ZHOU, J., FENG, J., CAO, J., GUO, H. Adsorption of NO2, NH3 on monolayer MoS2 doped with Al, Si, and P: A first-principles study. Chemical Physics Letters. 2016. doi: 10.1016/j.cplett.2015.10.077.

[10] SHOKRI, A., SALAMI, N. Gas sensor based on MoS2 monolayer. Sensors and Actuators B: Chemical. 2016. doi: 10.1016/j.snb.2016.06.033.

[11] KUMAR, R., AVASTHI, D. K., KAUR, A. Fabrication of chemoresistive gas sensors based on multistep reduced graphene oxide for low parts per million monitoring of sulfur dioxide at room temperature. Sensors and Actuators B: Chemical. 2017. doi: 10.1016/j.snb.2016.11.018.

[12] DING, L., QIN, Z., DOU, Z., SHEN, Y., CAI, Y., ZHANG, Y., ZHOU, Y. Morphology-promoted synergistic effects on the sensing properties of polyaniline ultrathin layers on reduced graphene oxide sheets for ammonia and formaldehyde detection. J Mater Sci. 2018. doi: 10.1007/s10853-018-2109-7.

[13] KOČÍ, M., KROMKA, A., BOUŘA, A., SZABÓ, O., HUSÁK, M. Hydrogen-Terminated Diamond Surface as a Gas Sensor: A Comparative Study of Its Sensitivities. Sensors (Basel, Switzerland). 2021, 21, 16. doi: 10.3390/s21165390.

[14] KOČÍ, M., IZSÁK, T., VANKO, G., SOJKOVÁ, M., HRDÁ, J., SZABÓ, O., HUSÁK, M., VÉGSÖ, K., VARGA, M., KROMKA, A. Improved Gas Sensing Capabilities of MoS2/Diamond Heterostructures at Room Temperature. ACS applied materials & interfaces. 2023. doi: 10.1021/acsami.3c04438.

[15] KOČÍ, M., SZABÓ, O., VANKO, G., HUSÁK, M., KROMKA, A. Enhanced gas sensing capabilities of diamond layers using Au nanoparticles. Diamond and Related Materials. 2023. doi: 10.1016/j.diamond.2023.110218.

[16] FIGARO USA, INC. *TGS 826 - for the Detection of Ammonia: Product Information*. Available online: https://www.figarosensor.com/product/docs/TGS%20826%20%2805_04%29.pdf.

[17] Pyreos Limited. *Thin Film Pyroelectric Dual Channel Sensor: Product Information*. Available online: https://pyreos.com/wp-content/uploads/2020/11/Pyreos-Analog-TO-Two-Channels.pdf